AN ABSTRACT OF THE DISSERTATION OF

Sasidhar N. Nirudodhi for the degree of Doctor of Philosophy in Chemistry presented on November 13, 2013.

Title: Hydrogen/Deuterium Exchange Mass Spectrometry as a Technology Platform for Studying Conformational Dynamics in Large Protein Complexes

Abstract approved:

Claudia S. Maier

Proteins are essential to all biological systems. Proteins participate in numerous cellular processes by interacting with other proteins, other metabolites and membranes in a dynamic environment. Studying the structural and conformational properties of proteins in the solution phase is necessary to understand their protein folding and interaction dynamics. This research project focused on the development and application of hydrogen deuterium exchange mass spectrometry (HDX-MS) technology for studying the conformational dynamics of large multi-subunit protein systems. HDX-MS studies were conducted on representative proteins of two much researched protein families, namely Peroxiredoxins (Prxs) and Cullin Ring Ligases (CRLs). As part of this research we implemented tandem mass spectrometry in the data independent acquisition (MS^E) mode for the HDX-MS analysis. We also used ion mobility as a second and orthogonal dimension of separation to overcome the spectral crowdedness.

Peroxiredoxins are ubiquitous antioxidant enzymes present in many organisms. Their catalytic activity is regulated by redox dependent oligomerization and their sensitivity to overoxidation is related to the flexibility of the active site loop to undergo partial unfolding. In this research we conducted HDX-

MS experiments for determining to what extent the flexibility of the active site loop governs the sensitivity of peroxiredoxins to overoxidation. As example of a robust peroxiredoxin we studied initially the conformational properties of *Salmonella typhimurium* AhpC wild-type protein by HDX-MS. Subsequently, we conducted comparative HDX-MS analysis on the reduced form of the wild-type protein, and two single point mutants, T77V, and T77I, with the objective to decipher to what extent the stability of the dimer-dimer (A)interface affects the conformational dynamics of the active site loop. Differential HDX-MS results of the wild-type, disulfide reduced wild-type protein have exhibited a decrease in the motility of the active site loop and the C-terminal end of the protein upon disulfide reduction. The Thr77 single point mutation by valine enhanced the dimer-dimer interaction thereby stabilizing the decamer interface and increasing the motility of the active site loop. Whereas, the substitution of T77 by isoleucine increased the motility of the interfacial region which forms the dimer-dimer interface thereby promoting the dissociation of the decamer to dimers.

A technically more advanced HDX-MS experimental setup was used to study the exchange-in properties of two robust peroxiredoxins, namely the wild-type *St*AhpC and the C46S mutant of *St*AhpC, which mimicks the reduced wild-type *St*AhpC, in comparison to human Prx2, a peroxiredoxin which is considered as sensitive to overoxidation. When differential deuterium uptake of wild-type *St*AhpC, C46S mutant *St*AhpC were compared, increased conformational rigidity was observed in the C46S mutant protein compared to the wild-type Prx. The peptide with highest deuterium incorporation levels in the human Prx2 is much lower compared to the bacterial wild type and C46S mutant Prxs. These comparative HDX-MS studies have fostered our understanding of the underlying conformational dynamics that lead to robust and sensitive Prxs.

The second protein system that was studied was a representative of the Cullin Ring Ligases (CRLs), the largest family of RING-type E3 ligases that catalyze ubiquitylation of substrates. Protein

ubiquitination is a post-translational modification that regulates several important biological processes in eukaryotic cells. It involves a three enzyme enzymatic cascade consisting of an ubiquitin-activating enzyme (E1), ubiquitin-conjugating enzyme (E2) and ubiquitin ligases (E3). In this study focus was directed toward the Cullin scaffold protein, which adopts an elongated structure that allows substrate receptor binding at the N-terminal domain (NTD) via adaptor proteins. Its C-terminal domain (CTD) binds to E2-ubiquitin through the RBX ring subdomain. Covalent attachment of the ubiquitin-like protein Nedd8 to the conserved lysine residue of the CTD stimulates the transfer of ubiquitin to substrate proteins thereby promoting ubiquitination. The HDX-MS studies of CUL1-RBX1 protein and its neddylated form highlighted that neddylation induces significant flexibility in the conformational dynamics of the CUL1 and RBX1 protein. The HDX-MS results support a mechanistic model in which conformational flexibility in the C-terminal domain of CUL1 and a concomitant opening of the RBX1 protein is necessary to allow the ubiquitin-bound E2 to be placed in close proximity to the protein substrates thereby facilitating the CRL activity.

©Copyright by Sasidhar N. Nirudodhi

November 13, 2013

All Rights Reserved

Hydrogen/Deuterium Exchange Mass Spectrometry as a Technology Platform for Studying Conformational Dynamics in Large Protein Complexes

by

Sasidhar N. Nirudodhi

A DISSERTATION

submitted to

Oregon State University

in partial fulfillment of
the requirements for the
degree of

Doctor of Philosophy

Presented November 13, 2013

Commencement June 2014

Doctor of Philosophy dissertation of Sasidhar N Nirudodhi presented on November 13th 2013

APPROVED:

Major Professor, representing Chemistry

Chair of the Department of Chemistry

Dean of the Graduate School

I understand that my dissertation will become part of the permanent collection of Oregon State University libraries. My signature below authorizes release of my dissertation to any reader upon request.

Sasidhar N Nirudodhi, Author

ACKNOWLEDGEMENTS

First and foremost I would like to thank Dr. Claudia S. Maier for the support, guidance and encouragement for the last seven years at Oregon State University. I would like to extend my thanks to the committee members Dr. Victor Hsu, Dr. Vincent T. Remcho, Dr. Jan Frederik Stevens and Dr. Oksana Ostroverkhova. I would like to thank our research collaborators Dr. Ning Zheng, Dr. Haibin Mao, Laura Sheard, Dr. Leslie Poole, Dr. Derek Parsonage and Dr. Andrew Karplus.

I am grateful to all my lab-mates especially Shin-Cheng Tzeng, Liping Yang, Fereshteh Zandkarimi, Ievgen Motorykin, Lin Huang, Soyoun Ahn, Juan Chavez, Jing Wang, Jianyong Wu for all those interesting conversations that kept my research interest accelerating. Thanks to Brian Arbogast, Jeff Morre, Samanthi Wickramasekara, Michelle Romero and all the people in the mass spectrometry lab for their support and assistance. I would like to acknowledge the help and support from the office staff of the chemistry department.

I would like to thank all the people that I met and made friends at OSU who made this journey memorable. Thanks to all my friends, it is not possible to name them all but my deepest regards to all those who have been a part of my life.

Last but not the least, I would like to thank my family members who supported and stood by me throughout my graduate school. Lastly, I thank the eternal forces that made this my journey.

TABLE OF CONTENTS

TABLE OF CONTENTS (Continued)

Page

TABLE OF CONTENTS (Continued)

TABLE OF CONTENTS (Continued)

LIST OF FIGURES

Figure Page

LIST OF FIGURES (Continued)

Figures Page

LIST OF FIGURES (Continued)

Figures Page

LIST OF TABLES

Table Page

1. Chapter- Introduction

1.1 Hydrogen deuterium exchange mass spectrometry as a technology platform for determining protein mobility

Every biological system depends on the correct localization and function of proteins. Proteins are the workhorses in every biological process. The correct functioning of a protein depends on its fold structure and interaction with the environment, such as membranes and other protein systems. Protein modification and binding of other biomolecules are critical for protein activity and protein trafficking. Studying the protein structure not only relates to the functional information but also provides deeper insights into the underlying mechanistic properties. Proteins are not rigid but constantly undergo local conformational changes or a larger structural rearrangement as part of biological processes. To understand their function we need to learn about their conformational and dynamic properties in environments that relate to their biological function.

This thesis focuses on the development and application of mass spectrometry-based techniques for studying conformational properties of large protein complexes. Specifically, we will apply hydrogen/deuterium exchange as a chemical labeling method in combination with advanced biomolecular mass techniques to study large protein systems. Two protein systems were studied a) peroxiredoxins, a large group of antioxidant proteins that form large oligomeric complexes dependent on their redox state and b) cullin ligases, large protein complexes essential for protein ubiquitination.

1.2 Peroxiredoxins

Peroxiredonxins (Prxs) belong to a family of antioxidant enzymes that control the intracellular peroxide levels in the bacteria and eukaryotes [1]. Prxs are highly abundant thiol peroxidases that undergo a catalytic reaction for the removal of H_2O_2. They are also susceptible to overoxidation in the presence of excess peroxide. Recent studies have recognized the role of Prxs in oxidative stress [2] and non-stress related cellular signaling [2, 3]. Prxs can be classified into various categories based on: (i) number of cysteines (Cys) present (for e.g. 1-Cys and 2-Cys Prxs etc); (ii) formation of inter- or intra-molecular disulfide bonds (typical and atypical) or; (iii) by their oligomerization tendencies [1, 4].

The catalytic cycle of 2-Cys Prxs has been well studied (Figure 1) [4]. The first step of the catalytic mechanism involves a conserved cysteine residue (SH, FF), called peroxidatic cysteine (C_p) that reacts with various peroxide substrates to form alkyl alcohols. A partial unfolding event is required for peroxidatic cysteine (C_p) to undergo oxidation to form sulfenic acid. The next step involves a partial unfolding of the resolving cysteine (C_R) in the C-terminal of a different subunit to from an intermolecular disulfide bond (S-S) (LU). The final step is the reduction of disulfide bond that involves a reaction with a reductase (e.g. AhpF) and reducing equivalents (e.g. NAD(P)H) to regenerate the Prxs [1, 5].

Prxs have been divided into two categories: (i) sensitive and (ii) robust Prxs depending on their susceptibility to overoxidation. If the unfolding event of the resolving cysteine is unfavorable, it provides C_P an opportunity for overoxidation. C_P can react with the second molecule of the peroxide to form a sulfinic acid derivative and can further react with the third peroxide molecule to yield a sulfonic acid derivative. Thus overoxidation aborts the recycling of peroxiredoxin in the catalytic cycle. Most of the bacterial Prxs are robust and are resistant to overoxidation whereas eukaryotic Prxs are more susceptible to overoxidation [1, 4, 5]. Initially overoxidation was thought to be a dead end reaction

causing permanent inactivation but later it was found that the sulfiredoxin enzyme could revert the overoxidation step back to peroxidatic cysteine in eukaryotes [6, 7].

Salmonella typhimurium alkyl hydroperoxide reductase C (*St*AhpC) is one of the well-studied proteins for its catalytic [8, 9], oligomeric [10] and regulatory studies [3, 5]. Hence, it was selected as perfect model to represent the bacterial Prxs. We propose to study the: (i) Wild type (Wt_{S-S}) *St*AhpC, reduced from (Wt_{SH}) of Prxs to test the active site loop motility and conformational dynamics of the region after disulfide formation; and (ii) and test the impact of the single point mutation at the dimer-dimer interfacial region T77 on the decamer building interface. High resolution crystal structures of these proteins are already available, but none of these structures provide information pertaining to the solution dynamics or long range allosteric interaction caused by a single point mutation and reduction of the disulfide bond. HDX-MS has a clear advantage over other structural techniques, since no other technique readily provides us with such information.

To study the above hypothesis, HDX-MS analysis will be performed on the wild type (Wt_{S-S}) *St*AhpC, T77V, T77I single point mutants in the oxidized form (S-S, LU) and their reduced counterparts (SH, FF). T77V and T77I are single point mutations at the dimer-dimer interface that also acts as a decamer building interface. These mutations were thought to have an impact on the stability of the decamer building interface and decamers are known for higher catalytic activity of Prxs [9]. By studying the changes in the conformational dynamics of these proteins using HDX we can: (i) better understand the allosteric interactions contributed by the single point mutations and; (ii) study its impact on the stabilization of the decamer.

In second part of the study we will focus on: (i) comparing the HDX-MS conformational dynamics of the wild type (Wt_{S-S}) *St*AhpC with the crystal structure data available; (ii) deciphering the impact of single point mutation at the active site cysteine 46 (C46S) and compare the HDX-MS data with the

reduced from as a crystal structure of the reduced form of *St*AhpC (Wt_{SH}) is not available; (iii) interrogating the solution dynamics of the bacterial and eukaryotic Prxs to obtain a mere mechanistic understanding of the propensity towards overoxidation. Prx2 will be used to represent the eukaryotic Prxs whereas *St*AhpC will be used to represent the bacterial ones.

1.3 Cullins Ring Ligases

Protein ubiquitination is a post translational modification that regulates various cellular processes such as protein degradation, protein-protein interactions, enzymatic activity and protein sorting [11]. Three major enzymes E1 activating enzyme, E2 conjugating enzyme and E3 ligases, catalyze substrate ubiquitination [12]. Culling-RING ligases (CRLs) are the largest family of ubiquitin E3s present in all eukaryotes that ubiquinate protein substrates. Ubiquitination-dependent changes in proteins regulate several biological processes including cell cycle progression, gene transcription, signal transduction, DNA replication, DNA repair, and even viral and bacterial infections [13]. The active site cysteine of E1 forms a thioester bond with the C-terminus of ubiquitin. Activated ubiquitin is then transferred to the catalytic cysteine of the E2. Then, the E3 recognizes and recruits both the ubiquitin charged E2 and target substrate and catalyzes the transfer of ubiquitin to a lysine residue of the substrate.

E3 ubiquitin ligases play an important role in the process of identifying the substrates and hence their activity is highly regulated [14]. E3 ligases generally have 2 domains [15, 16]: (i) the first domain is either a HECT (Homologous to E6-AP C-Terminus) or the RING on the C-terminal end. The HECT domain usually passes the ubiquitin from E2 to substrate through an E3~ubiquitin intermediate [17] but RING facilitates the direct transfer of ubiquitin from E2 to the substrate [15]; and (ii) the second domain is an N-terminal domain that interacts with the substrate proteins through a specific adaptor-substrate

receptor partner. Several rounds of ubiquitination on the RING domain extend the ubiquitin link close to the substrate protein on the NTD that facilitates the transfer of ubiquitin to the target substrate associated with the adaptor-SR partner.

CRLs belong to the super family of multi-subunit RING class E3s assembled around a cullin scaffold protein. The CRLs cullins family of proteins (Cul1, Cul2, Cul3, Cul4A, Cul4B and Cul5) embrace an extended structure to accommodate two binding sites at opposite ends, one allowing substrate binding via adaptor-SR partners on NTD and the other being an E2 binding RING class protein such as RBX1 or RBX2 on the CTD [18]. A total of around 500 CRLs family members are generated by the selective combination of six Cullin-RING complexes with several adaptor-SR partners [13]. Structural studies of some CRLs are currently available [19-23] but the clarity on the transfer of ubiquitin from E2 to the substrate remains unexplained (Figure 2). They all showed a large gap of ~50 ^{o}A distance between the E2-ubiquitin and the substrate. Apart from that, multiple rounds of ubiquitination changes the distance and geometry between both ends and makes the ubiquitin transfer a more dynamic event. Recent studies have shown some insights into the final step of ubiquitin transfer to the substrate [24, 25]. The remaining questions can be answered by understanding how CRLs are activated by the covalent attachment of ubiquitin like proteins (UBLs) such as NEDD8 to a conserved lysine residue in the C-terminal domain of cullins. Sequence similarity of Nedd8 is very close to ubiquitin. Neddylation of cullins triggers structural and conformational changes in CRLs that induces several important E3 ubiquitin activities including binding to the E2~ubiquitin and enhancing the transfer of ubiquiitn by bringing E2~ubiquitin close to the substrate [26]. Neddylation also prevents the CAND1 (Cullin-Associated Neddylation-Dissociated 1) from binding to the CRL scaffold protein [14, 20].

Structural studies performed by Duda *et al* have revealed the effects of Nedd8 ligation on CRLs [24]. They compared crystal structure data of CRL5-CTD-RBX1 and Nedd8 modified CRL5-CTD-RBX1

complexes as they found the unmodified Cul5-CTD-RBX1 structure was in close resemblance to the corresponding region of the full length Cul5-RBX1 structure. Considering the Cul5-CTD-RBX1 as representative of the full length complex, Duda *et al* found the Cul5-CTD-RBX1 exhibited a closed confirmation where RING domains of RBX1 were bound to the Cul5-CTD. Covalent modification of Cul5-CTD-RBX1 by Nedd8 resulted in a drastic rearrangement of the RBX1 RING region and thereby Cul5-CTD adopting an open conformation (Figure 3) [24]. The unwound form of the RBX1 in the neddylated form was connected to the N-terminal β-strand bound to the Cul5-CTD resembling a bait hanging from a- fish hook. The open conformation attained by the RBX1 can accommodate the growing E2~Ub chain and its flexible conformation placed them close to the target lysine of the substrate to facilitate the ubiquitin transfer [27]. The rearrangement of RBX1 RING domain to a flexible form provides a structural basis for the ubiquitin transfer from RBX1 bound E2 to the substrate. The open conformation was also confirmed by the SAXS studies done on the Cul1-CTD-RBX1 and Nedd8 modified Cul1-CTD-RBX1 complexes as they exhibited similar conformation changes upon Nedd8 modification [24].

The gap in the understanding of the ubiquitin transfer by the Nedd8 activation of CRLs was not completely filled as the full length structure was never studied with Nedd8 covalent modification. The lack of the N-terminal domain in the published structures by Duda et al. has raised some concern since the N-terminal domain plays an important role in the formation of the E3 ligases protein ubiquitination complex. To fill this gap we proposed to study the full length structure of Nedd8 modified and unmodified CRLs using HDX-MS with the goal to use the differential deuterium uptake profiles to to determine to what extent neddylation conformational changes in the CTD causes the conformational alteration in the N-terminal and the full length E3 ligase complexes.

1.4 HDX-MS, an emerging bio-physical technique for studying protein structure and conformation

Several biophysical techniques like fluorescence spectroscopy, differential scanning calorimetry, circular dichroism and ultra-centrifugation are used to monitor the changes in protein conformations and protein-protein interactions at the global level. However the global data is not always adequate to understand the details of the protein structure completely. Initial approaches involved isotopic labeling of proteins [28] while increasing the resolution by proteolytic digestion and successive separation of peptides [29, 30] followed by the detection of isotopic exchange by 1D NMR. The instrumentation advancements in multidimensional NMR allowed selective detection of amino acids [31, 32]. Currently, X-ray crystallography and NMR are the gold standards for studying protein structures. These well-established techniques provide atomically resolved structural data of proteins and protein complexes. However, both these techniques have some limitations [33-35]. Both these techniques require large volumes of concentrated protein with high purity, however not all proteins and protein assemblies crystallize readily. Another caveat is that X-ray crystallography provides high resolution structural data for a static protein state but relatively little information about the conformational dynamic properties of the protein which is essential to its function. Protein crystal structures are derived from static crystals confined to a specific space group that inhibits obtaining information related to the dynamics of a protein and allosteric interactions that modulate protein function, ligand binding and protein-protein interactions. Modern protein NMR techniques are exquisitely powerful [36-38], however not yet applicable to large proteins (> 45 kDa) or protein complexes [34, 39]. In the world of growing demand for protein structural information, hydrogen deuterium exchange mass spectrometry (HDX-MS) has emerged as a powerful alternative method to study protein dynamics in the solution phase. HDX was initially coupled with circular dichroism and NMR. With the advent of soft ionization techniques in mass spectrometry, in particular the electrospray ionization (ESI), which enabled the transfer of biomolecular

species from solution into the gas phase ions without fragmentation, it became popular for biological studies [40-42]. Soon HDX was coupled with ESI-MS to study the structural conformations and dynamics of proteins. The HDX-MS technique was first applied for studying the protein structural dynamics in 1991 [43]. Albeit early applications indicated the power of HDX-MS for studying protein motility and folding dynamics, the technique was confined to a few specialized laboratories [44, 45].

In the current era of bio-molecular medicine, mass spectrometry has become a very powerful platform to analyze bio-molecules [46]. With the high accurate mass measuring capability of MS and the availability of protein sequence databases, mass spectrometry has become an obvious choice for protein analysis [47]. In recent years with the advancements in electronics, instrument automation and software and, HDX-MS has emerged as a major technique for conducting protein conformational studies. The steady increase in the number of publications and citations during the last 20+ years indicates that HDX-MS has become a well-accepted technique (Figure 4). Coupling hydrogen deuterium exchange with mass spectrometry provides a lot of advantages over other techniques. These include: (i) MS requires a small amount of protein for the analysis and; (ii) very large proteins and protein complexes can be analyzed without any limitation on size; (iii) solution dynamics and long range allosteric interaction can be studied. Hence, very large proteins, protein polymers, protein-ligand interactions, protein-protein complexes can be mapped and analyzed by HDX-MS to determine the structural orientation of proteins and their conformational reorientation after binding to ligands or other proteins in complex assemblies. They can also be used to understand their conformational dynamics with a kinetic perspective.

1.5 Theory of Hydrogen Deuterium Exchange

Proteins adopt a complex but thermodynamically stable structural form to perform the specific tasks in a biological system. Hydrogen deuterium exchange is based on the fact that, labile protons in a

protein exchange with the surrounding solvent hydrogen in a continuous fashion. By replacing the solvent with a different isotopic solvent, such as deuterium oxide (D_2O), will results in the exchange of the labile hydrogen in a protein with the surrounding solvent deuterium. The rate of exchange for hydrogen depends on various intrinsic and extrinsic factors. Extrinsic factors that influence the hydrogen exchange are hydrogen bonding in secondary (β-sheets, α-helices) and tertiary structural features of the protein and local inductive effects caused by the adjacent amino acid side chains -[48]. The intrinsic factors that affect the exchange are temperature, pH, and concentration of the exchange catalyst in the solvent and solvent accessibility [48-50]. Backbone amide hydrogens represent the fold structure of the protein and their exchange half-life times may vary from several milliseconds to more than a year depending on the surrounding solvent environment and the extent of hydrogen bonding under physiological conditions. Regions with the secondary structural elements, like α-helices and β-sheets, exchange slowly since they involve in hydrogen bonding, whereas the loop regions or unstructured regions with no hydrogen bonding tend to exchange fast. The back bone amide hydrogens that are solvent exposed exchange fast and the ones that are buried deep in the hydrophobic core that are not solvent exposed tend to exchange very slowly. The extent of exchange that back bone amide hydrogens indulge in gives us the information about conformational dynamics of the proteins. There are different kinds of hydrogen present in a protein and can be categorized into three types: (i) side chain hydrogen that exchange very fast; (ii) back-bone amide hydrogen; and (iii) covalently bonded hydrogen that do not exchange with the surrounding solvent (Figure 5). Based on pH and temperature dependence, the exchange reaction of the back bone amide hydrogens can be quenched at a pH of 2.5 and temperature of 0^{o}C. The quenching conditions changes the half life time of the back bone amide hydrogens from a couple of milliseconds to around ~40 mins. This gives us enough time to measure the labeled protein with minimal - back exchange. There are several excellent reviews published describing the theory, principles and methodology of HDX-MS [39, 51-55].

1.6 Mechanism of Hydrogen Deuterium Exchange

1.6.1 pH Dependence of the Hydrogen Deuterium Exchange (HDX)

All amino acid residues in a protein, except prolines possess back-bone amide hydrogens. In these proteins, there is a spontaneous exchange of hydrogen between the surrounding solvent and its backbone amide hydrogens. By replacing the solvent with D_2O, hydrogens are exchanged with deuterium and it results in the increase in mass by one unit for each hydrogen exchanged. The isotopic exchange of the backbone amide hydrogen is acid or base catalyzed and the rate constant for the HDX reaction, k_{ex}, can be expressed as the summation of two terms:

$$k_{ex} = k_H[H^+] + k_{OH}[OH^-] \qquad \text{(Eq 1)}$$

k_H and k_{OH} represent the rate constants for the acid and base catalyzed exchange reaction. At physiological conditions around pH 7, exchange is usually base or water catalyzed. The exchange rate constant for the back-bone amide hydrogen and side chain hydrogen is influenced by the physic-chemical factors such as pH (Figure 6) and temperature (Figure 7).

Primary structural effects of a peptide in a protein with variations in pH and temperature are well described in literature and reviewed comprehensively [48, 54, 56]. Summary of Figure 6 states that the back bone amide hydrogens in a polyalanine exhibits the lowest exchange rate at a pH range of 2.5 to 3, whereas rest of the side chain hydrogens exhibit relatively higher exchange rate [54].

$$k_{ex}(T) = k_{ex}(293)\, exp^{-\frac{E_a}{R}\left(\frac{1}{T}-\frac{1}{293}\right)} \qquad \text{(Eq 2)}$$

The dependence of exchange rates of hydrogen on temperature can well be described by the Eq 2. By decreasing the temperatures from 20°C to 0°C and substituting the value of T as 273K in the Eq 2, the

hydrogen exchange rates decreases by approximately tenfold [57]. The summary from the pH and temperature dependence of k_{ex} is that the exchange reaction can be quenched at a pH range of 2.5 to 3 and 0^{o}C by minimizing the k_{ex}.

The other factors that influence the isotopic exchange are inductive, stearic effects from the adjacent amino acid chains and these effects are additive and may decrease the isotopic exchange rates by ten-fold. The sequence effects are usually overtaken by the secondary and tertiary structure effects in a folded protein involving hydrogen bonding and solvent accessibility effects that may reduce the exchange rates to as low as 10^{-8} [57]. Most of the backbone amide hydrogens are involved in hydrogen bonding either intramolecularly to other parts of the protein or surrounding water molecules. Access of the solvent can be blocked to the buried regions or hydrophobic core in the interior of a protein. The lower solvent accessibility and intramolecular hydrogen bonding in those regions contributes to the low exchange rate compared to the unstructured flexible regions in a protein.

1.6.2 EX1 and EX2 Kinetics of Hydrogen Deuterium Exchange

Hydrogen deuterium exchange kinetics for folded proteins in the native state can be explained based on two major kinetic models: (i) monomolecular exchange EX1; and (ii) bimolecular exchange EX2 [58, 59]. In a properly folded protein, the isotopic exchange rate constant at each backbone amide hydrogen can be expressed as:

$$k_{ex} = k_f + k_u = (\beta + K_{unf})k_2 \qquad \text{(Eq 3)}$$

Where, k_{ex} is defined as the sum of two factors contributed by the isotopic exchange from folded (k_f) and unfolded (k_u) forms of the protein. In the folded form of the protein, isotopic exchange rate constant k_f, is expressed as:

$$k_f = \beta k_2 \qquad \text{(Eq 4)}$$

Where, β is a probability factor for the isotopic exchange in folded form of the protein and k_2 is the rate constant for the isotopic exchange for each amide hydrogen at a peptide linkage in an unstructured peptide. β is a function of several parameters such as solvent accessibility and hydrogen bonding and ranges from 0 to 1. Hydrogen exchange in the folded from of protein is predominated by the amide hydrogens at the peptide linkages located at the surface of the protein that do not involve in hydrogen bonding. In the folded form of the protein, amide hydrogens involved in intramolecular hydrogen bonding are part of the α-helices and β-sheets that do not readily undergo isotopic exchange [54].

Isotopic exchange in the unfolded form of the protein is a competing process dominated by the amide hydrogens that engage in intramolecular hydrogen bonding and that are located near the surface. This is described by k_u. It requires a significant movement of the backbone that involves local (regional) unfolding or may involve the entire protein to unfold (global unfolding) resulting in breaking of that intramolecular hydrogen bonds and exposing the regions to the surrounding solvent for exchange. In the unfolded form of the protein, the isotopic exchange rate constant depends on the rate constant for the exchange in an unstructured peptide (k_2) along with the rates of protein unfolding and refolding events represented by k_1, k_{-1}.

$$F_H \rightleftharpoons U_H \qquad \text{(Eq 5)}$$

$$k_{ex} = \frac{k_1 k_2}{k_{-1} + k_2} \qquad \text{(Eq 6)}$$

In most of the proteins present at physiological conditions (neutral pH in the absence of denaturants), inter-conversion of native state to denatured state is very rapid and so the rate of refolding is much higher compared to the exchange rates of amide hydrogens in the denatured state

(unstructured peptide) i.e., $k_{-1} >> k_2$. The exchange rate constant for second-order reaction kinetics EX2 mechanism is given by:

$$k_{ex} = \left(\frac{k_1}{k_{-1}}\right) k_2 = K_{unf} k_2 \qquad \text{(Eq 7)}$$

where K_{unf} is an equilibrium constant describing the unfolding process.

The local unfolding and refolding events can happen within a microsecond and even global unfolding may occur within 50 ms. Many such local events occur before the exchange reaction takes place. This happens to most proteins in the native state when subjected to isotopic exchange at neutral pH. This equilibrium is described as EX2 mechanism that yields a unimodal peak. In EX2, a mass shift (peak shift towards higher m/z values, i.e. to the right of a mass spectrum) is observed over an exchange reaction due to replacement of amide hydrogen by deuterium. It leads to the Deuterium occupancy at each peptide bond being consistent throughout the entire protein population.

Proteins destabilized by chemical denaturants, high pH or high temperatures will result in slowing of the inter-conversion between native state and denatured state compared to the rate of isotopic exchange of amides in peptide linkages i.e., $k_2 >> k_{-1}$. Thus the isotopic exchange reaction follows first order kinetics usually represented by EX1 mechanism and the rate constant for the exchange k_{ex} is described as:

$$k_{ex} = k_1 \qquad \text{(Eq 8)}$$

Proteins in the denatured state exhibit EX1 mechanism and result in a bimodal peak pattern when subjected to isotopic exchange. The lower mass peak belongs to a fully protected form and the higher mass peak represents a fully labeled form of the protein. Mass spectrometry can clearly observe

the shift in the intensity of peaks from the fully protected to the fully labeled form with increase in exchange reaction times.

1.7 Applications of HDX-MS

1.7.1 HDX-MS for Studying Protein Ligand Interactions

Interaction between proteins and small molecule ligands can be studied using HDX-MS. At first HDX-MS method is applied to the ligand-free (apo) and ligand-bound (holo) proteins to obtain peptide level HDX mapping. A differential HDX-MS mapping of the ligand-free (apo) and ligand-bound (holo) protein provides the regions of interest that underwent conformational changes. These changes may be confined to the regions specific to the ligand-binding domain or to other regions of the protein caused due to allosteric interactions [39]. By generating the HDX-MS fingerprint for each ligand with the receptor protein and observing the conformational changes in the differential HDX mapping, potential ligands can be screened and segregated into groups based on the similarity in the binding mode [60]. Hence, HDX-MS works as a perfect tool for screening and clustering various potential ligands for protein receptors. There are several studies focusing on the protein-ligand binding interactions of biologically important and pharmacologically relevant proteins using HDX-MS technique [61-65].

In the current era of bio-molecular medicine, proteins are the core targets of interest because of their capability of therapeutic intervention. Majority of the current pharmaceutical drugs in the market are small molecule ligands that target protein receptors and that accounts for half of all the prescription drugs. When these ligands are introduced into the biological system, they bind to the target proteins and alter their structural conformation resulting in the modulation of their function. By virtue of their biological importance, protein kinases [66-71], G protein-coupled receptors (GPCR) [72-76] and nuclear

receptors (NR) [77-83] are the most sought after proteins by the pharmaceutical industry. The first HDX-MS study of GPCR was published in 2010 [84].

Proteins are of interest, not only as receptors, but also as macromolecular drugs. For example, monoclonal antibodies and recombinant endogenous proteins or soluble decoy receptors bind to the target host proteins capable of inducing a specific biological response and can function as drugs. Among all the above-mentioned scenarios, the common factor is that binding alters the structural, conformational and dynamics of the target host proteins thereby modulating the function required for therapeutic intervention. Early interrogation of the protein binding interactions with reliable bio-analytical methods will help in accelerating the drug discovery process [85, 86]. Hence, biophysical analytical techniques such as HDX-MS that allow characterization of protein structure, conformations and dynamics are of considerable interest.

1.7.2 HDX-MS for Analyzing Biosimilars

As per the current sales and future projections, biologics such as monoclonal antibodies and recombinant versions of endogenous proteins are expected to dominate the pharmaceutical industry in the future. As patent of these drugs begin to expire, there is an opportunity for companies to manufacture generic forms of these biologics. The generic forms of such biopharmaceuticals are termed as biosimilars. Unlike small molecule drugs, biosimilars or generic biologics are more complex in nature. It is very difficult to develop and evaluate their pharmaceutical and bio-equivalence with the innovator's original drug. In recent years, the US Food and Drug Administration (FDA) has released several documents supporting the development of initial drafts of regulatory pathways that sponsors (companies developing the biosimilars) of biosimilars should follow to get drug approval. Based on the

guidelines several comparability studies were proposed [85]. Specific guidelines about the physicochemical properties were stated in ICHQ6B. One such guideline that is relevant to us is:

"comparative higher order structural analyses are recommended, including the assessment of any changes in secondary, tertiary and quaternary structures. If higher-order structural information cannot be obtained, relevant biological assays could be used to confirm or support conformational equivalency between the innovator drugs and biosimilars."

As mentioned earlier, despite the fact that X-ray crystallography and NMR provide the atomically resolved structures, their drawbacks in providing structural and conformational comparison between the two drugs limit their applicability. Hence, they are not even likely for routine analysis. The other classical biophysical techniques such as circular dichroism (CD), fluorescence, differential scanning calorimetry (DSC), isothermal calorimetry, analytical ultracentrifugation (AUC), size exclusion chromatography (SEC) and dye-binding assays can be used to attain global information that cannot be localized to specific regions of the structure. Hence, these methods are also not sufficient for such analysis. An isotopic labeling method such as HDX-MS is preferred to be the rapid, routine analysis for the kind of information obtained. In conclusion, to study the differences in the structure, conformations and dynamics between two drugs HDX-MS is the most powerful tool available to date.

1.8 References

1. **Poole, L.B., *The catalytic mechanism of peroxiredoxins.* Subcell Biochem, 2007. 44: p. 61-81.**
2. **Veal, E.A., A.M. Day, and B.A. Morgan, *Hydrogen peroxide sensing and signaling.* Mol Cell, 2007. 26(1): p. 1-14.**
3. **Wood, Z.A., L.B. Poole, and P.A. Karplus, *Peroxiredoxin evolution and the regulation of hydrogen peroxide signaling.* Science, 2003. 300(5619): p. 650-3.**
4. **Hall, A., P.A. Karplus, and L.B. Poole, *Typical 2-Cys peroxiredoxins--structures, mechanisms and functions.* FEBS J, 2009. 276(9): p. 2469-77.**
5. **Wood, Z.A., et al., *Structure, mechanism and regulation of peroxiredoxins.* Trends Biochem Sci, 2003. 28(1): p. 32-40.**
6. **Rhee, S.G., et al., *Sulfiredoxin, the cysteine sulfinic acid reductase specific to 2-Cys peroxiredoxin: its discovery, mechanism of action, and biological significance.* Kidney Int Suppl, 2007(106): p. S3-8.**
7. **Rhee, S.G., et al., *Peroxiredoxin functions as a peroxidase and a regulator and sensor of local peroxides.* J Biol Chem, 2012. 287(7): p. 4403-10.**
8. **Parsonage, D., P.A. Karplus, and L.B. Poole, *Substrate specificity and redox potential of AhpC, a bacterial peroxiredoxin.* Proc Natl Acad Sci U S A, 2008. 105(24): p. 8209-14.**
9. **Parsonage, D., et al., *Analysis of the link between enzymatic activity and oligomeric state in AhpC, a bacterial peroxiredoxin.* Biochemistry, 2005. 44(31): p. 10583-92.**
10. **Wood, Z.A., et al., *Dimers to doughnuts: redox-sensitive oligomerization of 2-cysteine peroxiredoxins.* Biochemistry, 2002. 41(17): p. 5493-504.**
11. **Hershko, A. and A. Ciechanover, *The ubiquitin system.* Annu Rev Biochem, 1998. 67: p. 425-79.**
12. **Pickart, C.M., *Mechanisms underlying ubiquitination.* Annu Rev Biochem, 2001. 70: p. 503-33.**

13. **Zimmerman, E.S., B.A. Schulman, and N. Zheng, *Structural assembly of cullin-RING ubiquitin ligase complexes.* Curr Opin Struct Biol, 2010. 20(6): p. 714-21.**

14. **Siergiejuk, E., et al., *Cullin neddylation and substrate-adaptors counteract SCF inhibition by the CAND1-like protein Lag2 in Saccharomyces cerevisiae.* EMBO J, 2009. 28(24): p. 3845-56.**

15. **Deshaies, R.J. and C.A. Joazeiro, *RING domain E3 ubiquitin ligases.* Annu Rev Biochem, 2009. 78: p. 399-434.**

16. **Kee, Y. and J.M. Huibregtse, *Regulation of catalytic activities of HECT ubiquitin ligases.* Biochem Biophys Res Commun, 2007. 354(2): p. 329-33.**

17. **Scheffner, M., U. Nuber, and J.M. Huibregtse, *Protein ubiquitination involving an E1-E2-E3 enzyme ubiquitin thioester cascade.* Nature, 1995. 373(6509): p. 81-3.**

18. **Petroski, M.D. and R.J. Deshaies, *Function and regulation of cullin-RING ubiquitin ligases.* Nat Rev Mol Cell Biol, 2005. 6(1): p. 9-20.**

19. **Angers, S., et al., *The KLHL12-Cullin-3 ubiquitin ligase negatively regulates the Wnt-beta-catenin pathway by targeting Dishevelled for degradation.* Nat Cell Biol, 2006. 8(4): p. 348-57.**

20. **Goldenberg, S.J., et al., *Structure of the Cand1-Cul1-Roc1 complex reveals regulatory mechanisms for the assembly of the multisubunit cullin-dependent ubiquitin ligases.* Cell, 2004. 119(4): p. 517-28.**

21. **Zheng, N., et al., *Structure of the Cul1-Rbx1-Skp1-F boxSkp2 SCF ubiquitin ligase complex.* Nature, 2002. 416(6882): p. 703-9.**

22. **Schulman, B.A., et al., *Insights into SCF ubiquitin ligases from the structure of the Skp1-Skp2 complex.* Nature, 2000. 408(6810): p. 381-6.**

23. **Zheng, N., et al., *Structure of a c-Cbl-UbcH7 complex: RING domain function in ubiquitin-protein ligases.* Cell, 2000. 102(4): p. 533-9.**

24. **Duda, D.M., et al., *Structural insights into NEDD8 activation of cullin-RING ligases: conformational control of conjugation.* Cell, 2008. 134(6): p. 995-1006.**

25. **Saha, A. and R.J. Deshaies, *Multimodal activation of the ubiquitin ligase SCF by Nedd8 conjugation.* Mol Cell, 2008. 32(1): p. 21-31.**

26. **Saifee, N.H. and N. Zheng, *A ubiquitin-like protein unleashes ubiquitin ligases.* Cell, 2008. 135(2): p. 209-11.**

27. **Duda, D.M., et al., *Structural regulation of cullin-RING ubiquitin ligase complexes.* Curr Opin Struct Biol, 2011. 21(2): p. 257-64.**

28. **Englander, S.W., *A Hydrogen Exchange Method Using Tritium and Sephadex: Its Application to Ribonuclease.* Biochemistry, 1963. 2: p. 798-807.**

29. **Rosa, J.J. and F.M. Richards, *An experimental procedure for increasing the structural resolution of chemical hydrogen-exchange measurements on proteins: application to ribonuclease S peptide.* J Mol Biol, 1979. 133(3): p. 399-416.**

30. **Englander, S.W., et al., *Individual breathing reactions measured in hemoglobin by hydrogen exchange methods.* Biophys J, 1980. 32(1): p. 577-89.**

31. **Stassinopoulou, C.I., G. Wagner, and K. Wuthrich, *Two-dimensional 1H NMR of two chemically modified analogs of the basic pancreatic trypsin inhibitor. Sequence-specific resonance assignments and sequence location of conformation changes relative to the native protein.* Eur J Biochem, 1984. 145(2): p. 423-30.**

32. **Wagner, G., C.I. Stassinopoulou, and K. Wuthrich, *Amide-proton exchange studies by two-dimensional correlated 1H NMR in two chemically modified analogs of the basic pancreatic trypsin inhibitor.* Eur J Biochem, 1984. 145(2): p. 431-6.**

33. **Blundell, T.L. and S. Patel, *High-throughput X-ray crystallography for drug discovery.* Curr Opin Pharmacol, 2004. 4(5): p. 490-6.**

34. **Homans, S.W., *NMR spectroscopy tools for structure-aided drug design.* Angew Chem Int Ed Engl, 2004. 43(3): p. 290-300.**

35. **Kohn, J.E., et al., *Evidence of functional protein dynamics from X-ray crystallographic ensembles.* PLoS Comput Biol, 2010. 6(8).**

36. **Wang, Y. and N. Tjandra, *Structural insights of tBid, the caspase-8 activated Bid, and its BH3 domain.* J Biol Chem, 2013.**

37. **Francis, K., V. Stojkovic, and A. Kohen, *Preservation of Protein Dynamics in Dihydrofolate Reductase Evolution.* J Biol Chem, 2013.**

38. **Kuo, L.H., et al., *Effect of Charged Amino Acid Side Chain Length at Non-Hydrogen Bonded Strand Positions on beta-Hairpin Stability.* Biochemistry, 2013.**

39. **Chalmers, M.J., et al., *Differential hydrogen/deuterium exchange mass spectrometry analysis of protein-ligand interactions.* Expert Rev Proteomics, 2011. 8(1): p. 43-59.**

40. **Fenn, J.B., et al., *Electrospray ionization for mass spectrometry of large biomolecules.* Science, 1989. 246(4926): p. 64-71.**

41. **Cech, N.B. and C.G. Enke, *Practical implications of some recent studies in electrospray ionization fundamentals.* Mass Spectrom Rev, 2001. 20(6): p. 362-87.**

42. **Kebarle, P. and U.H. Verkerk, *Electrospray: from ions in solution to ions in the gas phase, what we know now.* Mass Spectrom Rev, 2009. 28(6): p. 898-917.**

43. **Katta, V. and B.T. Chait, *Conformational changes in proteins probed by hydrogen-exchange electrospray-ionization mass spectrometry.* Rapid Commun Mass Spectrom, 1991. 5(4): p. 214-7.**

44. **Freitas, M.A. and A.G. Marshall, *Gas phase RNA and DNA ions 2. Conformational dependence of the gas-phase H/D exchange of nucleotide-5'-monophosphates.* J Am Soc Mass Spectrom, 2001. 12(7): p. 780-5.**

45. **Englander, S.W., et al., *Mechanisms and uses of hydrogen exchange.* Curr Opin Struct Biol, 1996. 6(1): p. 18-23.**

46. **Aebersold, R. and M. Mann, *Mass spectrometry-based proteomics.* Nature, 2003. 422(6928): p. 198-207.**

47. **Yates, J.R., C.I. Ruse, and A. Nakorchevsky, *Proteomics by mass spectrometry: approaches, advances, and applications.* Annu Rev Biomed Eng, 2009. 11: p. 49-79.**

48. **Bai, Y., et al., *Primary structure effects on peptide group hydrogen exchange.* Proteins, 1993. 17(1): p. 75-86.**

49. **Smith, D.L., Y. Deng, and Z. Zhang, *Probing the non-covalent structure of proteins by amide hydrogen exchange and mass spectrometry.* J Mass Spectrom, 1997. 32(2): p. 135-46.**

50. **Zhang, Z. and D.L. Smith, *Determination of amide hydrogen exchange by mass spectrometry: a new tool for protein structure elucidation.* Protein Sci, 1993. 2(4): p. 522-31.**

51. **Engen, J.R., *Analysis of protein conformation and dynamics by hydrogen/deuterium exchange MS.* Anal Chem, 2009. 81(19): p. 7870-5.**

52. **Englander, S.W., *Hydrogen exchange and mass spectrometry: A historical perspective.* J Am Soc Mass Spectrom, 2006. 17(11): p. 1481-9.**

53. **Yan, X. and C.S. Maier, *Hydrogen/deuterium exchange mass spectrometry.* Methods Mol Biol, 2009. 492: p. 255-71.**

54. **Percy, A.J., et al., *Probing protein interactions with hydrogen/deuterium exchange and mass spectrometry-a review.* Anal Chim Acta, 2012. 721: p. 7-21.**

55. **Woods, V.L., Jr. and Y. Hamuro, *High resolution, high-throughput amide deuterium exchange-mass spectrometry (DXMS) determination of protein binding site structure and dynamics: utility in pharmaceutical design.* J Cell Biochem Suppl, 2001. Suppl 37: p. 89-98.**

56. **Connelly, G.P., et al., *Isotope effects in peptide group hydrogen exchange.* Proteins, 1993. 17(1): p. 87-92.**

57. **Englander, S.W. and N.R. Kallenbach, *Hydrogen exchange and structural dynamics of proteins and nucleic acids.* Q Rev Biophys, 1983. 16(4): p. 521-655.**

58. **Krishna, M.M., et al., *Hydrogen exchange methods to study protein folding.* Methods, 2004. 34(1): p. 51-64.**

59. **Bai, Y., *Equilibrium amide hydrogen exchange and protein folding kinetics.* J Biomol NMR, 1999. 15(1): p. 65-70.**

60. **Dai, S.Y., et al., *Prediction of the tissue-specificity of selective estrogen receptor modulators by using a single biochemical method.* Proc Natl Acad Sci U S A, 2008. 105(20): p. 7171-6.**

61. **Garcia, R.A., D. Pantazatos, and F.J. Villarreal, *Hydrogen/deuterium exchange mass spectrometry for investigating protein-ligand interactions.* Assay Drug Dev Technol, 2004. 2(1): p. 81-91.**

62. **Chalmers, M.J., et al., *Probing protein ligand interactions by automated hydrogen/deuterium exchange mass spectrometry.* Anal Chem, 2006. 78(4): p. 1005-14.**

63. **Zhu, M.M., et al., *Quantification of protein-ligand interactions by mass spectrometry, titration, and H/D exchange: PLIMSTEX.* J Am Chem Soc, 2003. 125(18): p. 5252-3.**

64. **Hopper, E.D., et al., *Throughput and efficiency of a mass spectrometry-based screening assay for protein-ligand binding detection.* J Am Soc Mass Spectrom, 2008. 19(9): p. 1303-11.**

65. **Powell, K.D., et al., *A general mass spectrometry-based assay for the quantitation of protein-ligand binding interactions in solution.* J Am Chem Soc, 2002. 124(35): p. 10256-7.**

66. **Chen, S., et al., *The Abl SH2-kinase linker naturally adopts a conformation competent for SH3 domain binding.* Protein Sci, 2007. 16(4): p. 572-81.**

67. **Chen, S., et al.,** ***Tyrosine phosphorylation in the SH3 domain disrupts negative regulatory interactions within the c-Abl kinase core.*** **J Mol Biol, 2008. 383(2): p. 414-23.**

68. **Chen, S., et al.,** ***Abl N-terminal cap stabilization of SH3 domain dynamics.*** **Biochemistry, 2008. 47(21): p. 5795-803.**

69. **Iacob, R.E., et al.,** ***Conformational disturbance in Abl kinase upon mutation and deregulation.*** **Proc Natl Acad Sci U S A, 2009. 106(5): p. 1386-91.**

70. **Zhang, J., et al.,** ***Targeting Bcr-Abl by combining allosteric with ATP-binding-site inhibitors.*** **Nature, 2010. 463(7280): p. 501-6.**

71. **Zhang, H.M., et al.,** ***Drug binding and resistance mechanism of KIT tyrosine kinase revealed by hydrogen/deuterium exchange FTICR mass spectrometry.*** **Protein Sci, 2010. 19(4): p. 703-15.**

72. **George, S.R., B.F. O'Dowd, and S.P. Lee,** ***G-protein-coupled receptor oligomerization and its potential for drug discovery.*** **Nat Rev Drug Discov, 2002. 1(10): p. 808-20.**

73. **Palczewski, K., et al.,** ***Crystal structure of rhodopsin: A G protein-coupled receptor.*** **Science, 2000. 289(5480): p. 739-45.**

74. **Conn, P.J., A. Christopoulos, and C.W. Lindsley,** ***Allosteric modulators of GPCRs: a novel approach for the treatment of CNS disorders.*** **Nat Rev Drug Discov, 2009. 8(1): p. 41-54.**

75. **Cherezov, V., et al.,** ***High-resolution crystal structure of an engineered human beta2-adrenergic G protein-coupled receptor.*** **Science, 2007. 318(5854): p. 1258-65.**

76. **Rasmussen, S.G., et al.,** ***Crystal structure of the human beta2 adrenergic G-protein-coupled receptor.*** **Nature, 2007. 450(7168): p. 383-7.**

77. **Wright, E., et al.,** ***Helix 11 dynamics is critical for constitutive androstane receptor activity.*** **Structure, 2011. 19(1): p. 37-44.**

78. **Yan, X., et al.,** ***Dynamics and ligand-induced solvent accessibility changes in human retinoid X receptor homodimer determined by hydrogen deuterium exchange and mass spectrometry.*** **Biochemistry, 2004. 43(4): p. 909-17.**

79. **Xia, G., et al.,** ***Structure, energetics, and dynamics of binding coactivator peptide to the human retinoid X receptor alpha ligand binding domain complex with 9-cis-retinoic acid.*** **Biochemistry, 2011. 50(1): p. 93-105.**

80. **Bruning, J.B., et al.,** ***Partial agonists activate PPARgamma using a helix 12 independent mechanism.*** **Structure, 2007. 15(10): p. 1258-71.**

81. **Chandra, V., et al.,** ***Structure of the intact PPAR-gamma-RXR- nuclear receptor complex on DNA.*** **Nature, 2008. 456(7220): p. 350-6.**

82. **Hamuro, Y., et al.,** ***Hydrogen/deuterium-exchange (H/D-Ex) of PPARgamma LBD in the presence of various modulators.*** **Protein Sci, 2006. 15(8): p. 1883-92.**

83. **Zhang, J., et al.,** ***Hydrogen/deuterium exchange reveals distinct agonist/partial agonist receptor dynamics within vitamin D receptor/retinoid X receptor heterodimer.*** **Structure, 2010. 18(10): p. 1332-41.**

84. **Zhang, X., et al.,** ***Dynamics of the beta2-adrenergic G-protein coupled receptor revealed by hydrogen-deuterium exchange.*** **Anal Chem, 2010. 82(3): p. 1100-8.**

85. **Berkowitz, S.A., et al.,** ***Analytical tools for characterizing biopharmaceuticals and the implications for biosimilars.*** **Nat Rev Drug Discov, 2012. 11(7): p. 527-40.**

86. **Pacholarz, K.J., et al.,** ***Mass spectrometry based tools to investigate protein-ligand interactions for drug discovery.*** **Chem Soc Rev, 2012. 41(11): p. 4335-55.**

Figure Legends

Figure 1 Catalytic cycle of Prxs. (1) Peroxidation (2) Resolution (3) Recycling and (4) Oxidative inactivation.

Figure 2 Model of the CUL1-RBX1 E3 ligase complex. The hypothetical structure was created by our collaborator Dr. Ning Zheng, HHMI and University of Washington.

Figure 3 Model of the CUL1-RBX1 E3 ligase complex after Nedd8 modification based on the partial structure of the complex published by Dude et al [24]. The model was created by our collaborator Dr. Ning Zheng, HHMI and University of Washington

Figure 4 The growth of the graph shows number of (a) publications and (b) citations obtained from the Web of Knowledge (Thompson Reuters) by searching with the keyword "hydrogen deuterium exchange mass spectrometry". The search was conducted for the period 1990-2013.

Figure 5 Types of hydrogens in a polypeptide. Green colored hydrogens are covalently bound non-exchanging hydrogens, blue colored hydrogens are fast exchanging side chain hydrogens and red colored hydrogens are backbone amide hydrogens.

Figure 6 Rate constants for the isotopic exchange of backbone amide hydrogen in a polyalanine, side chain hydrogen using a dipeptide models for Arg, Asn, Gln, Trp were calculated using the equation (1) where the values of k_H and k_{OH} at a temperature 278^{o}K are given in Bai et al 1993 [48]. The rate constants for α-COOH, α-NH_2, Ser and Thr were obtained from the "Creighton, T.E. Proteins: Structures and molecular proteomics; Freeman, W.H. and Co.: New York, 1993; p282".

Figure 7 The dependence of exchange rates of hydrogen on temperature is described in the plot. Decreasing the temperature by 20 ^{o}C reduces the exchange rate by approximately 10 fold. Figure was copied from Englander & Kallenbach, 1983 [57].

Figure 1

1 **Catalytic cycle of Prxs**

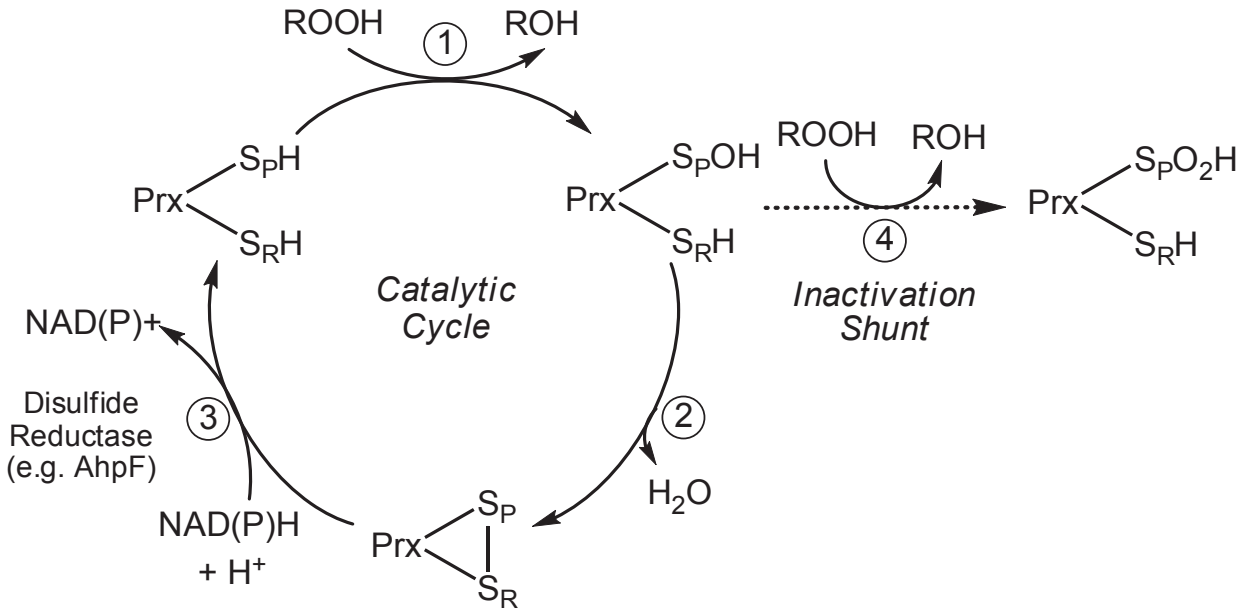

Figure 2

2 CUL1-RBX1 E3 ligase complex

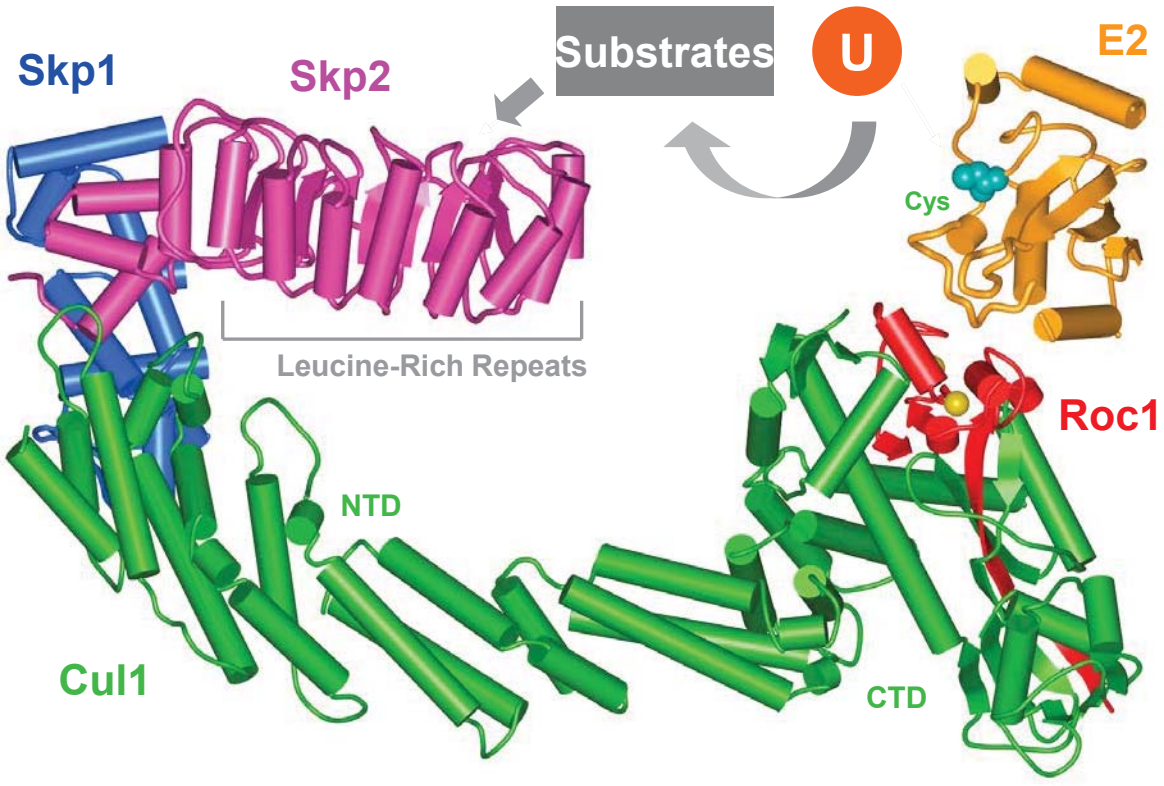

Figure 3

3 CUL1-RBX1 E3 ligase complex after Nedd8 modification

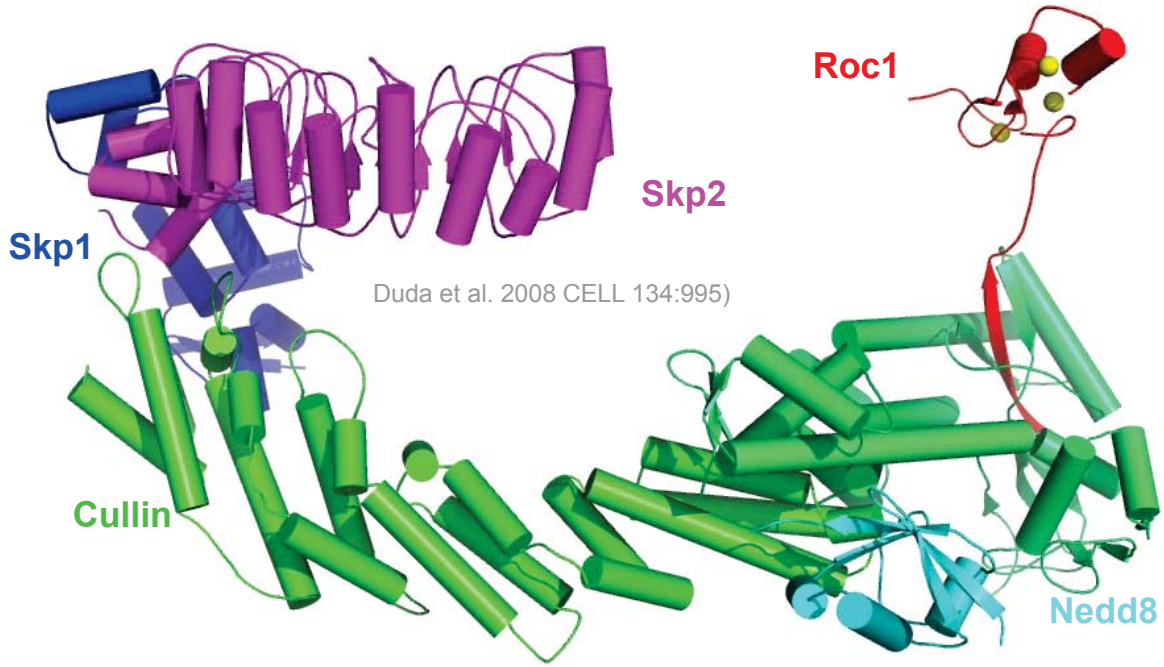

Figure 4

4 **Growth of the graph shows number of publications and citations**

(a)

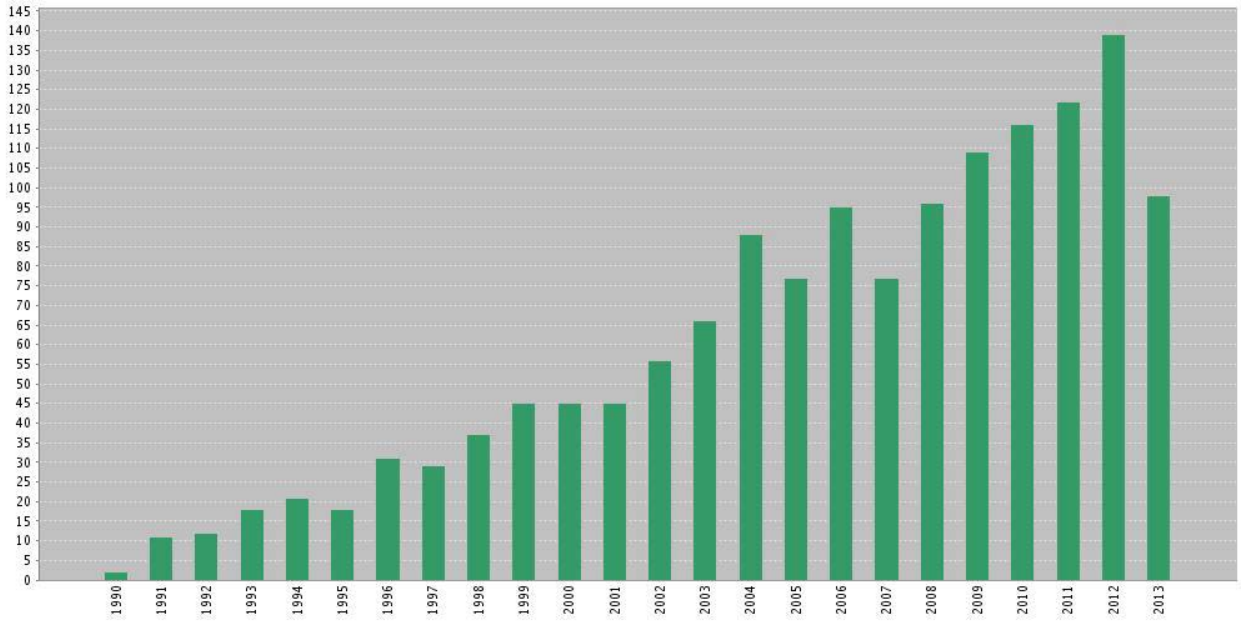

(b)

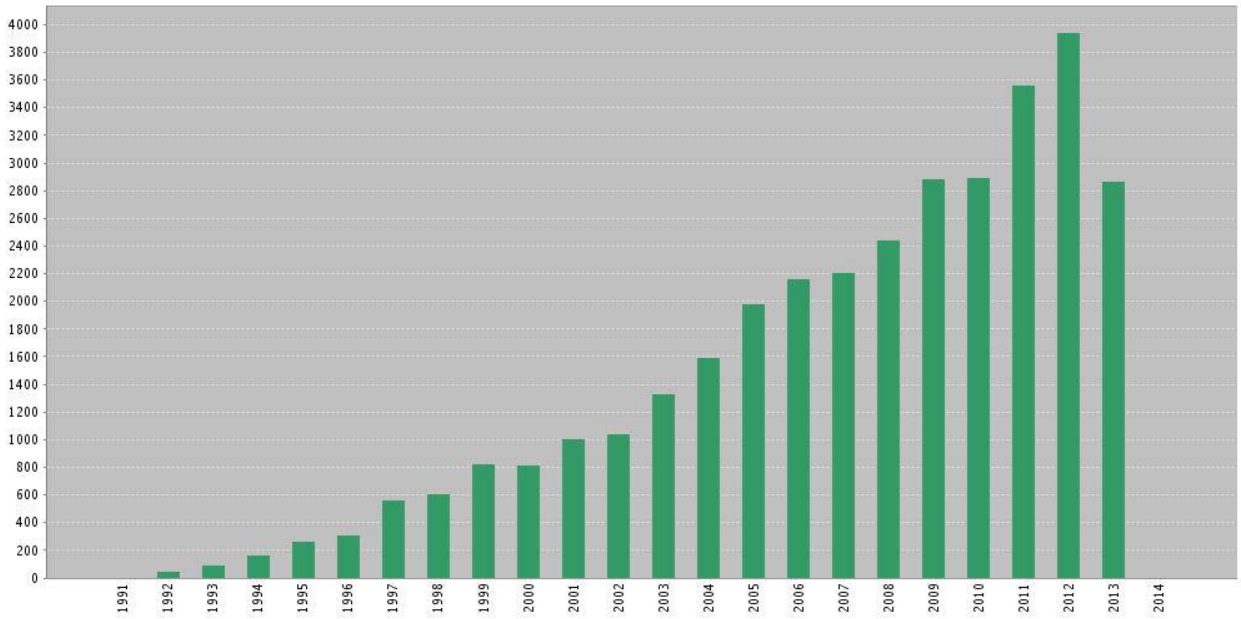
4000
3800
3600
3400
3200
3000
2800
2600
2400
2200
2000
1800
1600
1400
1200
1000
800
600
400
200
0
1991
1992
1993
1994
1995
1996
1997
1998
1999
2000
2001
2002
2003
2004
2005
2006
2007
2008
2009
2010
2011
2012
2013
2014

Figure 5

5 Types of hydrogens in a poly peptide

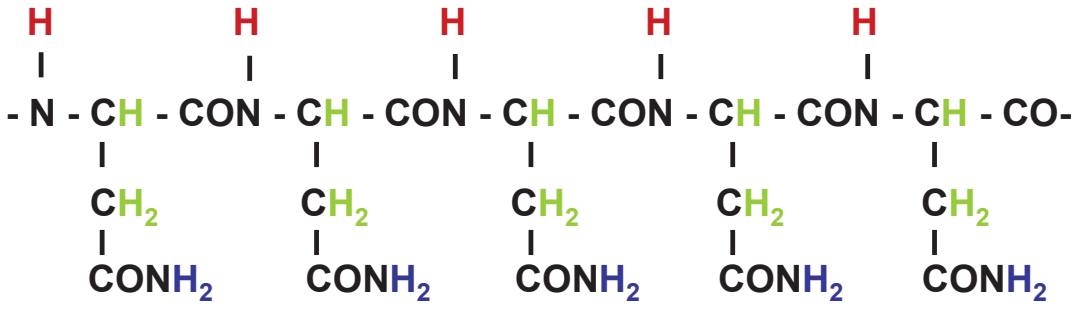

Figure 6

6 **Rate constants for the isotopic exchange of backbone amide hydrogen in a polyalanine with pH**

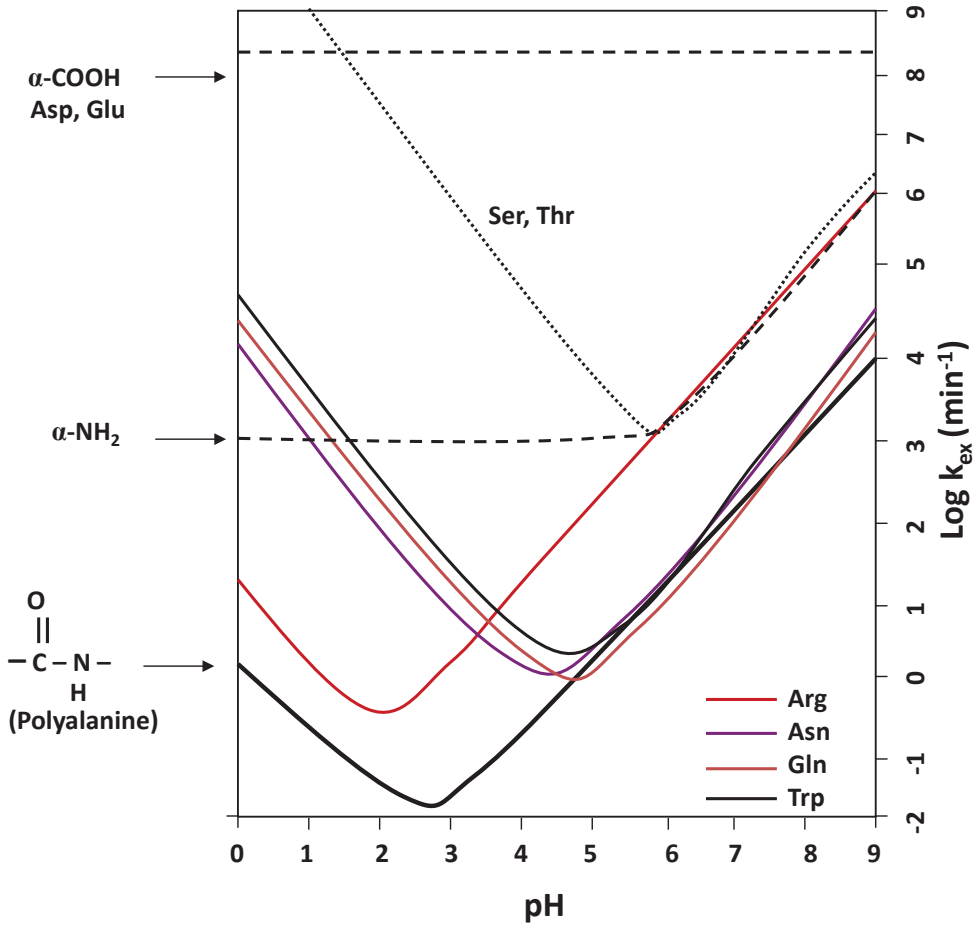

Figure 7

7 **The dependence of exchange rates of hydrogen on temperature**

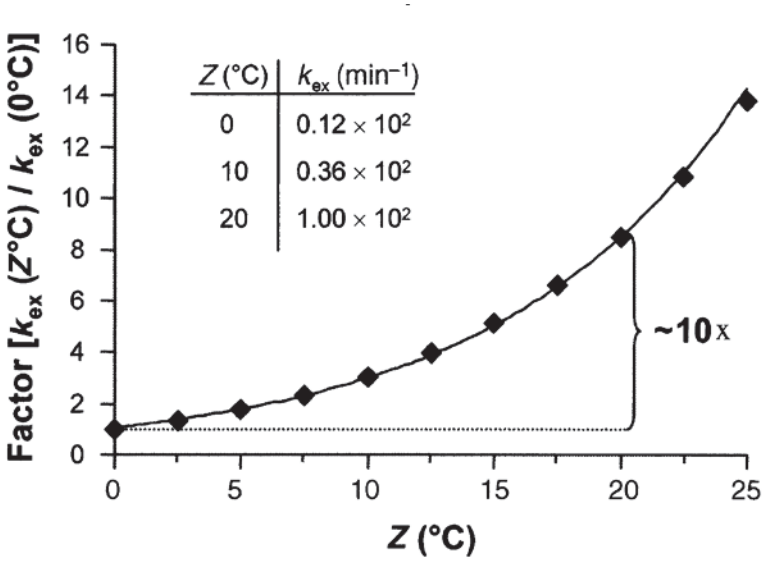

2 CHAPTER – Techniques and Methods

2.1 Biomolecular Mass spectrometry Techniques

A mass spectrometer is an analytical instrument used for the quantitative and qualitative analysis of analyte molecules. It is able to convert these molecules into gas phase ions and measures them based on their mass-to-charge ratio (m/z). All mass spectrometers are comprised of these three major components: (i) An ionization source that converts the sample analytes into gas phase ions; (ii) mass analyzer that sorts and separates the ions in space and time based on their m/z values; and (iii) a detector that measures the quantity of ions for each m/z value. Three decades ago mass spectrometry was confined to small molecular analysis but advances in the technology and development in instrumentation have paved the way for its usage to analyze now also very large molecules [1]. There are several ionization techniques available, however the advent of electrospray ionization (ESI) by Fenn et al., made mass spectrometric analysis of biomolecules possible [2]. ESI had a great impact on the biological and biomolecular medicine field since it revolutionized the characterization of biomolecules. There are several mass analyzers available, however the most prevalent are quadrupole (Q), time-of-flight (TOF), ion trap (IT), Fourier transform ion cyclotron resonance (FT-ICR) [3, 4] and orbitrap (OT) analyzers [5-7]. New generation mass spectrometers consisted of two or more mass analyzers in their instrument design since each one of these mass analyzers possesses unique strengths as well as weaknesses.

2.1.1 Electrospray Ionization

ESI is a soft ionization technique that uses the electric energy to transfer the analyte solution to the gas phase without fragmentation in the ionization source (Figure 1) [2]. The other popular soft ionization technique is matrix assisted laser desorption ionization (MALDI) [8]. We focused on ESI for this research. ESI is a desorption ionization method in which a high voltage of around 1-6 kV is maintained between the emitter electrode and the end of separation line. When the analyte solution is passed through this emitter a fine spray of highly charged solvent-analyte droplets is formed. These droplets form a Taylor cone at the tip of the emitter with the aid of a nebulizer gas (such as nitrogen). Heated stream of desolvation gas (such as nitrogen) evaporates the solvent from charged droplets to droplets of a smaller size. As the radius of the droplets decreases, its surface charge density increases resulting in the coulombic explosion of droplets, further generating smaller droplets [9]. This process of solvent evaporation and charge induced droplet disintegration continues until gas phase ions are generated. The generated ions can be multiply charged. Next these ions enter the mass analyzer [10, 11]. The LC separation can be directly connected to the ESI source and the eluting analytes can further be mass analyzed continuously. LC coupled with ESI-MS yields a very powerful tool for biomolecular analysis.

2.1.2 Mass Analyzers

As mentioned above, several mass analyzers are available today; most modern mass spectrometers have multiple mass analyzers in them to exploit their different strengths enhancing the capability of the mass spectrometry. Based on the types of analytes and need of analysis, specific combinations of mass analyzers are selected. For most part of the research described in this thesis quadrupole time-of-flight (Q-TOF) type hybrid instruments were employed.

The instruments used for this research were: (i) Micromass/Waters LCT TOF (Only non-hybrid instrument with a TOF analyzer); (ii) Micromass/Waters Q-TOF Ultima Global; and (iii) Waters Synapt G1 HDMS mass spectrometers. All three mass spectrometers were equipped with an ESI source and a Z spray design for better transmission of analyte ions into the mass analyzer. In the LCT TOF instrument, ions generated at the source are focused and transferred using two hexapole RF lenses to the orthogonal acceleration TOF analyzer. Both the Waters Q-TOF Ultima Global and the Waters Synapt G1 are Q-TOF based hybrid quadrupole time-of-flight mass spectrometers. They have two modes of operation. In the TOF-MS mode, the quadrupole is operated with only the RF voltage as an ion guide (transfer lens) and in the MS/MS mode, the quadrupole operates with both the RF and DC voltages and is used as a mass selection device (mass filter).

Ions generated at the source of the ESI are transferred through the travelling wave ion guide (TWIG) to the quadrupole. Based on mode of operation the quadrupole operates as a transfer lens or a mass filter. The ions then enter the collision cell (T-Wave), if in the collision mode the ions undergo collision induced dissociation (CID) fragmentation in this cell else the ions only get transferred. The ions finally enter the orthogonal TOF reflectron that acts as a last mass resolving device before getting detected by the microchannel plate detector (MCP).

The major advancement in the Synapt G1 HDMS mass spectrometer (Figure 2) over the previous generations is the replacement of the collision cell by a Tri-wave^{TM} device. As the name implies, the Tri-wave device has 3 components, namely (i) a trap; (ii) an ion mobility separation (IMS) cell; and (iii) transfer regions. Fragmentation can be carried out in either the trap cell, the transfer cell or in both of them. The IMS cell provides a second dimension of separation based on drift time and collision cross section (CCS).

2.2 Data Dependent Acquisition (DDA) Vs Data Independent Acquisition Techniques (MS^E)

The data independent acquisition (MS^E) mode is configured to alternate between low and high energy functions in the collision cell for each scan. The low energy function does a survey scan of all the precursor peptide ions with almost no fragmentation whereas the high energy function fragments all the precursor peptide ions in the gas collision cell. This provides an accurate mass measurement of all the precursor ions and their respective product ions [12, 13]. The precursor and product ions are correlated and time aligned based on the chromatographic peak retention time window produced by UPLC separation. The traditional data dependent acquisition (DDA) commonly selects three most intense precursor peptide ions from the MS survey scan for fragmentation. Comparing DDA Vs MS^E, DDA selects a specific charge state of the precursor ion for fragmentation whereas MS^E scans all charge states and all isotopes for each precursor ion and fragments all of them (Figure 3) [12]. Therefore, the duty cycle of LC-MS^E is much higher than the traditional DDA method [14].

For peptide identification we use tandem mass spectrometry. We use a short LC gradient in our HDX-MS protocol to minimize back exchange. Using DDA in a short gradient data acquisition yields very low sequence coverage. To overcome this limitation, we therefore adoptedthe MS^E mode of acquisition for the studies described in Chapters 4 and 5 once the Synpat G1 platform became available in the laboratory in mid 2010.

2.3 Mobile Proton Model

Dissociation or fragmentation of the protonated peptide ions upon low energy excitation conditions can be best described by the mobile proton model (Figure 4). Peptides have multiple protonation sites (N-terminal amino group, amide nitrogens, amide oxygens and several side chain groups) that can form various isomers upon protonation. Excitation of the protonated peptide ion

during the migration of the proton to different protonation sites will determine the site of cleavage and so the ionizing proton has a direct impact on the peptide fragmentation [15]. Most of the protonated peptides follow charge directed cleavage.

Peptide ions can be divided into two major classes based on the energies of isomers produced upon protonation. Protonation on the more basic protonated side chain amino group is kinetically more favorable compared to the amide oxygens and nitrogens that leads to the sequestering of the proton and excitation results in the charge-remote fragmentation. Peptides with side chains arginine, lysine and histidine fall under the first group and these peptides need large amount of energy to mobilize the sequestered proton to the other less favored protonation sites (amide oxygens and nitrogens). The second group is represented by the important amide oxygens and nitrogens that have small energy range for protonation. Upon excitation, internal energy of the peptide ions increases and this results in the increase in the population of energetically less favorable protonated sites in the peptide ions leading to the dissociation at the backbone amide bond [16]. When compared protonation at the amide nitrogen is thermodynamically less favorable compared to the amide oxygen or N-terminal amino group or basic side chain groups. But from the decomposition point of view protonation at the amino nitrogens is more favorable. This model has been verified by theoretical models [17].

2.4 HDX-MS Methods

Exchange-in HDX-MS experiments were performed on the two protein systems to study their structural dynamics and conformations [18]. The basic exchange-in HDX-MS protocol was followed with some modifications and improvements and is described in detail below (Figure 5).

2.4.1 Method 1

2.4.1.1 Global HDX-MS Analysis

To attain global protein conformational data, hydrogen deuterium exchange was performed on intact protein. Protein stock solution was equilibriated for 30 min at room temperature. The equilibriated protein was subjected to labeling reaction by dilution in deuterated buffer for several time points. Labeling reaction was arrested by adding acidic pre-cooled quench buffer (pH 2.5). To attain global protein structural information (Figure 6), the labeling reaction is arrested by adding acidic quench buffer (pH 2.5) and was flash frozen in liquid nitrogen until further LC-MS analysis.

2.4.1.2 Peptide level HDX-MS analysis

Isotopic labeling can be localized to specific regions of the protein by peptic proteolysis. In earlier studies (described in Chapter 3) we used for digesting the protein immobilized pepsin beads suspended in pre-cooled acidic quench buffer. The labeled protein solution was the added to the slurry . After short proteolysis on ice the the immobilized pepsin was separated from the labeled protein solution by centrifugation. The peptic peptides in the supernatant solution were pipetted out using GELoader tips and flash frozen in liquid nitrogen until further analysis. All the parameters and instrument conditions were maintained the same. The same LC-MS analysis protocol was followed for both protein and peptides level LC-MS analysis. The only exception is that mass spectra were acquired over a mass range of 400-2000 for the global protein analysis whereas for the peptide level analysis mass spectral data was acquired over m/z 400-1500.

A nanoAcquity UPLC system (Waters, Milford, MA) coupled with a LC-T ESI-TOF mass spectrometer (Waters, Milford, MA) was used for LC–ESI MS analysis. Trap pre-column, analytical column and the LC solvents were immersed in the ice bath and maintained at a temperature of around 0^{o}C to minimize the back exchange during LC-MS analysis. These frozen samples were thawed at room

temperature and placed in the autosampler for sample injection. After the sample injection, peptic peptides were trapped on a BEH C_{18} pre-column and washed to remove salts and buffer. Peptides were then eluted on to a BEH C_{18} analytical column for peptide separation using a short solvent gradient. The separated peptic peptides were sprayed directly into an ESI source of LCT for further mass analysis. The entire LC-MS data acquisition took 15 min for each sample. Three replicates were analyzed for each time point of every sample (including the undeuterated sample). The HDX data for the entire set of samples was acquired in the LC-MS mode.

For peptide identification, an undeuterated control sample was subjected to LC-MS/MS analysis using a nanoAcquity UPLC coupled to Waters/Micromass QTof Ultimate Global mass spectrometer equipped with a lockmass sprayer. For peptide identification based on DDA acquisitions a 65 min long gradient was used to separate the peptic peptides. Then, the peptides were eluted into a mass spectrometer for tandem mass spectral analysis. The raw data acquired for the control sample was processed using Mascot server (Matrix Science). A user defined database was searched for exact mass and fragment ion match. This match was used to assign peptic peptides to the protein sequence. Subsequently the corresponding peptide m/z in the short run were then assigned based on the hierarchy of peptides, matching their m/z and retention times in the 65-min chromatogram.

2.4.2 Semi-automated Data analysis

For easier comparison, a set of peptic peptides common among all the mutants with a good peptide spectra were chosen to cover the entire sequence. The relative mass difference between the undeuterated and the deuterated centroid mass gave us the number of deuteriums that were exchanged for each peptide. The peptide spectra was manually selected from the series of deuterated time points and undeuterated chromatograms and transferred into an excel sheet. Using an excel based

program called HX-Express, the centroid mass for all the spectra and the relative deuterium uptake were calculated [19]. This was repeated for the selected set of peptides for all the three replicate samples. Thus the peptide level deuterium uptake data was calculated for all three mutants. Details of this mode of data analysis are in section 2.6.2.

2.4.3 Major changes to the method

Starting mid-2010 major changes were made to the HDX-MS experimental setup used to study the C46S mutant *St*AhpC, Prx2 and CRLs protein systems. Modifications to the HDX-MS method included: (i) using online acid proteolytic digestion; (ii) usage of different instrumentation setup; and (iii) data analysis using advanced software. The changes to the instrumentation setup include: (i) the installation of the HDX Chiller module integrated with the Waters nano Acquity UPLC. The trap column, separation columns and peek tubing were enclosed in the HDX chiller module. It used a robust setup to maintain a temperature of 0^{o}C during the entire experiment. This system also had an online peptic proteolytic digestion as an integral part of the HDX chiller module. It had a separate provision for pepsin column to maintain a higher temperature for better digestion; (ii) the usage of Waters Synapt G1 HDMS mass spectrometer for mass spectrometric analysis. This new instrumentation setup made the entire HDX-LC-MS data acquisition process more robust and highly reproducible for maintaining and monitoring the operation conditions (Figure 7). Tandem mass spectrometric data was acquired using MS^{E} mode (described in section 2.4). Different data analysis software used as described below.

As described in the section 2.4.1.2. in our initial experimental setup, a 65 min long gradient LC run with a tandem mass spectrometric analysis was performed for peptide identification whereas. HDX-MS data was acquired using a short 10 min LC gradient and mass spectral data was acquired in the MS survey scan acquisition mode. This necessitated that the hierarchy of the peptide ions from a short

gradient chromatogram needed to be matched with the long gradient MS/MS run for enabling the m/z values to to peptide assignment. In mid-2010, as the Synapt G1 platform became available this cumbersome two step process was replaced by adapting the faster MS^E data independent fragmentation method in the new experimental setup. All HDX-MS data (acquired after July 2010 and described in chapters 4 and 5) were acquired using the MS^E fragmentation method in a short LC runs.

2.5 Data Analysis Software

2.5.1 ProteinLynx Global SERVER (PLGS)

PLGS was used to process the .RAW data files for the peptide identification. .RAW data was acquired for the C46S mutant *St*AhpC, Prx2 and CRLs protein systems in the MS^E mode. These .RAW data files for the three replicates of the control samples were processed using PLGS. PLGS uses two algorithms to process the raw data; (i) Peptide 3D which is a deconvolution algorithm; (ii) Apex 3D that assists in the identification process. The Apex 3D algorithm uses the low energy and elevated energy nature of MS^E data to determine various properties such as mass to charge ratio, retention times and the intensity of all the ions derived from the chromatographic and mass spectrometric peaks. The chromatographic peak attributes that describe the common physical and chemical properties of the ions such as peak shape, peak start, stop time and peak width at haft height associated with the precursor and product ions are also determined by the Apex 3D algorithm. It locates the peak apex in the data, calibrates and lock-mass corrects it to create a peak list of precursor and product ions. Apex 3D considers the product ions as a possible match for the precursor ion if it falls within the one-tenth of the chromatographic peak width of the precursor ions. PLGS creates an ion accounting file in the .CSV format which lists all the identified peptides with its respective characteristics such as m/z, retention times etc. The ion accounting files provides us the information regarding the protein sequence coverage

achieved and this gives us a decent heads-up ahead of the complete data analysis. During the time course of this thesis several HDX-MS data analysis software have become available and that provide deuterium uptake information cutting down the time intensive manual process. As part to this thesis research several software packages were evaluated. In the following section each of these software packages are briefly described and their capabilities and limitation are discussed.

2.5.2 Semi-Automated Analysis using HX-Express

2.5.2.1 Pre HX-Express processing

Peptides with high intensities and no overlap were selected manually from the peptide list obtained from PLGS ensuring maximum sequence coverage of the protein. For each peptide, its m/z at that specific retention time window was searched among all the chromatograms. The peptide spectra listed for all labeled time points were smoothed using Savitzky Golay filter. The spectrum list or the spectrum was used for centroid and peak width calculations using HX-Express. Difference in the centroid mass of the control and labeled peaks gives the relative deuterium uptake for each labeled time point. In short, this is a laborious manual process to scavenge the mass spectra for each peptide over all labeled time points and their replicates.

2.5.2.2 HX-Express

HX-Express is an excel based program [19]. Mass spectral data obtained from pre HX-Express processing can be imported from the MassLynx software to an excel sheet using HX-Express. Imported peak m/z values and their intensities were arranged in adjacent columns. Each column was labeled with its respective exchange time points. HX-Express calculates the centroid mass and peak width values of

all the undeuterated and deuterated spectra. It provides summary of the relative deuterium uptake at each labeling time. It also provides the summary plots of exchange time point versus relative deuterium uptake and exchange time point versus peak width. The relative deuterium uptake values were calculated for all the peptides. These values were normalized to aid comparison among different peptides. The relative deuterium uptake for each peptide was normalized to a percentage by dividing the relative deuterium uptake with the number of exchangeable backbone amide hydrogens present in a respective peptide times hundred (equation 1). Hence, the resulting percentages can be compared among all the peptides irrespective of the size of the peptide (i.e. the number of amino acids present).

$$D\% = \frac{D}{N} * 100 \qquad \text{(Equation 1)}$$

2.5.3 HDX Browser-1.2.5

Waters' HDX browser was the first semi-automated data analysis software to automate the pre-HX Express processing (section 2.6.2.1). As described above, three replicates of the .RAW data of control samples (undeuterated runs) were processed by PLGS for peptide identification, sequence assignment and protein sequence coverage. The outputs from the PLGS were ion accounting files in .CSV format. These files include the information about: peptide sequence, mass over charge ratio, charge state, intensity, retention time, sum of the matched product ion intensity, peptide score etc. The ion accounting files were loaded into the HDX browser. Peptides were filtered by setting the required thresholds for different parameters such as intensity, no. of products ions matched for a given peptide and sequence length of peptides. Peptides that pass the threshold are retained to be part of the analysis. Control and deuterated raw data files are added to the HDX browser. All of these files are labeled with their exchange time points. For all the peptides in the list, HDX browser searches the respective spectra among all the .RAW data files based on the retention time window, m/z values and other information available from the ion accounting files added. It processes and displays the control

and deuterated spectra for all labeled time points added for each peptide. Peptides spectra with low intensities and bad isotopic pattern were deleted from the list manually. The retained deuterated spectra list for each peptide was cross checked manually. This assures that all the peptides considered for HDX-MS study were of high quality. HDX browser has an import option wherein the overlaid spectra list for each peptide was imported as a .CSV file. Each .CSV file has the m/z versus intensities listed in adjacent columns for every labeled time points. These files were processed using HX-express to obtain the relative deuterium uptake values for each peptide as described in section 2.6.2.2. HDX-Browser helped in cutting down the manual scavenging of mass spectra; however, it did not entirely eliminate the manual HX-Express processing and data interpretation.

2.5.4 DynamX Software

DynamX is the first tool that automates and integrates the two steps of data analysis and data interpretation. It was first released in 2011 by Waters. It supports .RAW data files from most of the Waters instruments for analysis. Multiple PLGS search results of the control undeuterated samples were imported to the DynamX software. It combines all ion accounting files from the search results of PLGS to generate an aggregate list of peptides available for interrogation for the experiment performed. Aggregate peptide list can be modified to fit our needs of analysis. We can filter the peptides belonging to a specific protein by selecting it or select multiple proteins using Ctrl. The peptide list can be filtered by setting thresholds for various parameters. Peptide thresholds parameters include: (i) minimum intensity - total intensity for all isotopes for all charge states of a peptide; (ii) minimum sequence length - number of amino acids in a peptide; (iii) minimum products for amino acid - minimum number of product ions identified per amino acid residue; (iv) minimum consecutive products - minimum number of consecutive product ions identified; (v) minimum sum intensity for products - minimum total intensity

of all identified product ions; (vi) minimum score and maximum MH+ error (ppm) - maximum mass error in parts per million; and (vii) minimum products - minimum number of product ions identified. To disable all the thresholds and avoid filtering the peptides, the threshold for minimum score and maximum MH+ error should be set to "-1" and the remaining thresholds should be set to 0.

Peptides can also be filtered based on replication threshold. It has three filters: (i) File threshold - the minimum number of search results required to identify the peptide; (ii) retention time RSD - maximum allowed relative standard deviation for a peptide's retention time; (iii) intensity RSD - maximum allowed relative standard deviation for a peptide's total intensity (sum intensity of all isotopes in all charge states). Replication threshold measures data variability. Software rejects peptides that fail to satisfy a threshold and the reason for the rejection can be viewed by selecting the peptide. We can retain the peptide despite its rejection and also reject the peptide in spite of its retention. After the filtering, software displays the list of peptides that passed the final thresholds and provides an estimated percentage of the protein sequence coverage.

To assess the protein conformational changes, all .RAW data files were added to the DynamX. User can define the exposure time, state of the protein and lock mass charge. Other fields such as chromatographic Peak Width, MS TOF resolution, lock mass window and low energy threshold can be left default as automatic or can be changed based on the experimental conditions [20]. DynamX scans for the detected ions and searches the ions across the peptide list. Peptides are finally matched and assigned. It calculates and displays the deuterium uptake for each peptide across all exposure times automatically. It aggregates data as a function of replication and experimental state. It has an option to display the standard deviation from the replicates. It visualizes data for easier interpretation and navigation. It allows interaction with data to modify results if necessary [21]. Deuterium uptake is

presented in a XY scatter plot with relative uptake versus exposure times and it has an option to display it in either logarithmic or linear scale. We can export the deuterium uptake information into a .CSV file.

The processed DynamX file can also be saved and opened using DynamX browser as needed. A stacked spectra view will display all the spectra for a peptide in a specific protein state. Multiple windows of stacked spectra can be opened. A spectrum once selected from the stacked spectra will be displayed in the main window and it can be altered there. We can assign or unassign the ions in a given spectra by double clicking it. Deuterium uptake of all the peptides in a protein in two different states can be compared using the butterfly plot option available. The coverage map option can display a graphical representation of the overlapping peptides that cover the entire protein sequence. There is also a heat map display to represent the deuterium uptake data. In the case of overlapping peptides for any given residue, the exposure data rendered is decided by the shortest peptide. If multiple peptides are of the shortest length, DynamX uses the peptide with the residue closest to the peptide C-terminus, to render the exposure data.

Despite all the automation DynamX 1.0 provided, it had many bugs that limited usage for any significant data analysis. DynamX 2.0 released in December 2012 fixed all bugs making it the best data analysis tool in the market. We used DynamX 2.0 to analyze most of our data. One of the major advancements in DynamX 2.0 is its capability to process the .RAW data files acquired in ion mobility separation (IMS) mode.

2.5.5 HDExaminer-1.0

When struggling with DynamX 1.0, we resorted to HDExaminer. It is the only other tool that reads the Waters .RAW data files and automates the data analysis process. It is released by Sierra Analytics. Peptide list with m/z values and corresponding retention times were added to the HDExaminer (ref). When .RAW data files are added to HDExaminer, it searches for the ion peaks at the

same retention time in the raw data files and processes the data to display deuteriated peaks for each peptide for the entire series of time points [22]. We manually reviewed the deuteriated peaks for all peptides and selected the ones with good intensity to compile a list of peptides to be included for analysis. HDExaminer also displays the deuterium level verses time plots for each peptide. It also provides the coverage map and the heat map from the peptide deuterium uptake data available that can be easily copied to a word file. The exchange data can be transferred into a .CSV file for further analysis [23]. HDExaminer universally supports .RAW data files from all major instrument manufacturers giving HDExaminer an added advantage over other data analysis software. Though HDExaminer is completely automated, it takes a long time to process .RAW data files and its memory requirement is high. Due to these limitations it could not process the entire set of .RAW data files in one process. It required data to be fragmented and processed and the results to be manually combined. It also lacks the peptide filtering options making the peptide selection process manual. When DynamX 2.0 was released we preferred it over HDExaminer 1.0.

2.6 Emerging techniques

HDX-MS has become a powerful tool in studying the structural dynamics of proteins in solution phase. However, it has limited our understanding to the peptide level as the deuterium uptake information cannot be assigned to the single residue level. The only way to get a better resolution using HDX-MS experiments is to compare overlapping peptide spectra. Usually it is rare to find overlapping peptides specific to distinct regions of interest. Complementing the HDX data at medium spatial resolution using the tandem mass spectrometry approach would allow us to overcome this limitation. The most commonly used fragmentation technique “Collision induced dissociation (CID)” is reported to induce “hydrogen scrambling” [24, 25] resulting in the loss of deuterium uptake information. This would

make the tandem HDX-MS data unreliable [24, 26]. Thus, alternative complimentary fragmentation techniques, such as electron capture dissociation (ETD) or electron transfer dissociation (ECD) must be employed to minimize hydrogen scrambling under optimum conditions. So far these methods have been rarely employed in studying small to medium size proteins [27].

2.6.1 Collision induced dissociation versus Electron Capture Dissociation and Electron Transfer Dissociation

CID is the most commonly used gas phase fragmentation technique in tandem mass spectrometry. It involves the collision of the peptides (or protein) ions with neutral gas atoms (like Argon, helium, molecular nitrogen). Analyte ions acquire energy upon collision with the target gaseous atoms. This energy is distributed with an equal probability among all the internal modes of the ions. The internal energy acquired is redistributed as vibrational energy. Due to this excessive vibrational excitation of deuterated peptide ions in the gas phase, the protons and deuterons interchange among all exchangeable sites. The internal energy slowly increases in small steps until the weakest bond in the ion is cleaved, thus producing b- and y- type fragment ions. CID is an ergodic process [28] and it usually yields selective fragmentation [29]. There are many studies that discussed the extent of intramolecular gas-phase migration of exchangeable hydrogens (i.e., hydrogen scrambling) observed in peptide and protein ions upon CID [25, 26], thus questioning this approach for the gas-phase fragmentation in HDX-MSMS analysis [25, 30].

ECD is an alternative tandem mass spectrometric technique first introduced by McLafferty et al., in 1998 to study proteins and peptides. ECD requires static electric and magnetic fields and is carried out mostly in FTICR type instruments. This technique has been widely used for the top-down approach to

fragment the intact protein in the gas phase. ECD involves irradiation of protein or polypeptide ions with low-energy electrons in the gaseous phase producing an aminoketyl radical typically cleaving N-C_α backbone resulting in the c and z type fragment ions. ETD is also an alternative and complimentary gas phase fragmentation technique recently introduced by Donald F. Hunt and coworkers [31]. Transfer of an electron from a chemical anion to a positively charged peptide ion leads to the cleavage of N-C_α producing c and z ions similar to ECD [32]. ETD and ECD [33] are considered as non-ergodic processes, implying that the bond cleavage occurs before the energy is randomly redistributed and the N-C_α is cleaved with a limited vibrational excitation before the hydrogen scrambling can take place [27, 32]. ETD can be carried out in all the instruments that can trap ions using radio frequency (RF) oscillating electric field such as orbitrap-type mass spectrometers [27].

Top down HDX-MS approach with the new fragmentation techniques such as ECD and ETD provide an average deuterium uptake resolution of less than two amino acids residues without hydrogen scrambling. They also provide an opportunity to select a specific protein conformer in the gas phase before fragmentation. Supercharging agents were found to be of great help in the top-down approach using ECD or ETD. They do not cause any major changes to the protein structure. By adding supercharging agents such as 1% m-NBA will help to denature the protein in the electrospray droplet thereby increasing the number of protein charge states produced [34]. This in turn helps in attaining better spatial resolution while measuring deuterium uptake using ECD or ETD. Supercharging agents do not cause back exchange as the time spent as ESI droplet is relatively very low compared to the half-life of hydrogen/deuterium exchange. These techniques were found to be very efficient in analyzing proteins conformations, but this has been confined to the small to medium size proteins. Top down approach has not yet reached the stage where large and very large protein complexes can be analyzed on a routine basis. To overcome this limitation, ETD can be used over ECD as LC can be easily coupled to ETD instruments.

2.7 References

1. Aebersold, R. and M. Mann, *Mass spectrometry-based proteomics.* Nature, 2003. **422**(6928): p. 198-207.
2. Fenn, J.B., et al., *Electrospray ionization for mass spectrometry of large biomolecules.* Science, 1989. **246**(4926): p. 64-71.
3. Schmid, D.G., et al., *FTICR-mass spectrometry for high-resolution analysis in combinatorial chemistry.* Biotechnol Bioeng, 2000. **71**(2): p. 149-61.
4. Bogdanov, B. and R.D. Smith, *Proteomics by FTICR mass spectrometry: top down and bottom up.* Mass Spectrom Rev, 2005. **24**(2): p. 168-200.
5. Yates, J.R., C.I. Ruse, and A. Nakorchevsky, *Proteomics by mass spectrometry: approaches, advances, and applications.* Annu Rev Biomed Eng, 2009. **11**: p. 49-79.
6. Hu, Q., et al., *The Orbitrap: a new mass spectrometer.* J Mass Spectrom, 2005. **40**(4): p. 430-43.
7. Zubarev, R.A. and A. Makarov, *Orbitrap mass spectrometry.* Anal Chem, 2013. **85**(11): p. 5288-96.
8. Hillenkamp, F., et al., *Matrix-assisted laser desorption/ionization mass spectrometry of biopolymers.* Anal Chem, 1991. **63**(24): p. 1193A-1203A.
9. Kebarle, P. and U.H. Verkerk, *Electrospray: from ions in solution to ions in the gas phase, what we know now.* Mass Spectrom Rev, 2009. **28**(6): p. 898-917.
10. Nguyen, S. and J.B. Fenn, *Gas-phase ions of solute species from charged droplets of solutions.* Proc Natl Acad Sci U S A, 2007. **104**(4): p. 1111-7.
11. Kebarle, P. and U.H. Verkerk, *Electrospray: From Ions in Solution to Ions in the Gas Phase, What We Know Now.* Mass Spectrometry Reviews, 2009. **28**(6): p. 898-917.

12. Geromanos, S.J., et al., *The detection, correlation, and comparison of peptide precursor and product ions from data independent LC-MS with data dependant LC-MS/MS.* Proteomics, 2009. **9**(6): p. 1683-95.

13. Bern, M., et al., *Deconvolution of mixture spectra from ion-trap data-independent-acquisition tandem mass spectrometry.* Anal Chem, 2010. **82**(3): p. 833-41.

14. Plumb, R.S., et al., *UPLC/MS(E); a new approach for generating molecular fragment information for biomarker structure elucidation.* Rapid Commun Mass Spectrom, 2006. **20**(13): p. 1989-94.

15. Paizs, B. and S. Suhai, *Fragmentation pathways of protonated peptides.* Mass Spectrom Rev, 2005. **24**(4): p. 508-48.

16. Wysocki, V.H., et al., *Mobile and localized protons: a framework for understanding peptide dissociation.* J Mass Spectrom, 2000. **35**(12): p. 1399-406.

17. Boyd, R. and A. Somogyi, *The mobile proton hypothesis in fragmentation of protonated peptides: a perspective.* J Am Soc Mass Spectrom, 2010. **21**(8): p. 1275-8.

18. Nirudodhi, S., et al., *Conformational studies of the robust 2-Cys peroxiredoxin Salmonella typhimurium AhpC by solution phase hydrogen/deuterium (H/D) exchange monitored by electrospray ionization mass spectrometry.* Int J Mass Spectrom, 2011. **302**(1-3): p. 93-100.

19. Weis, D.D., J.R. Engen, and I.J. Kass, *Semi-automated data processing of hydrogen exchange mass spectra using HX-Express.* J Am Soc Mass Spectrom, 2006. **17**(12): p. 1700-3.

20. Kim, M., et al., *Antibody mechanics on a membrane-bound HIV segment essential for GP41-targeted viral neutralization.* Nat Struct Mol Biol, 2011. **18**(11): p. 1235-43.

21. Karageorgos, I., et al., *Active-Site Inhibitors Modulate the Dynamic Properties of Human Monoacylglycerol Lipase: A Hydrogen Exchange Mass Spectrometry Study.* Biochemistry, 2013.

22. Englander, J.J., et al., *Protein structure change studied by hydrogen-deuterium exchange, functional labeling, and mass spectrometry.* Proc Natl Acad Sci U S A, 2003. **100**(12): p. 7057-62.

23. Horn, J.R., et al., *The role of protein dynamics in increasing binding affinity for an engineered protein-protein interaction established by H/D exchange mass spectrometry.* Biochemistry, 2006. **45**(28): p. 8488-98.

24. Hoerner, J.K., et al., *Is there hydrogen scrambling in the gas phase? Energetic and structural determinants of proton mobility within protein ions.* J Am Chem Soc, 2004. **126**(24): p. 7709-17.

25. Ferguson, P.L., et al., *Hydrogen/deuterium scrambling during quadrupole time-of-flight MS/MS analysis of a zinc-binding protein domain.* Analytical Chemistry, 2007. **79**(1): p. 153-60.

26. Rand, K.D. and T.J.D. Jorgensen, *Development of a peptide probe for the occurrence of hydrogen (H-1/H-2) scrambling upon gas-phase fragmentation.* Analytical Chemistry, 2007. **79**(22): p. 8686-8693.

27. Zehl, M., et al., *Electron transfer dissociation facilitates the measurement of deuterium incorporation into selectively labeled peptides with single residue resolution.* J Am Chem Soc, 2008. **130**(51): p. 17453-9.

28. Rand, K.D., et al., *Protein hydrogen exchange measured at single-residue resolution by electron transfer dissociation mass spectrometry.* Analytical Chemistry, 2009. **81**(14): p. 5577-84.

29. Ueberheide, B.M., et al., *Rapid sensitive analysis of cysteine rich peptide venom components.* Proc Natl Acad Sci U S A, 2009. **106**(17): p. 6910-5.

30. Demmers, J.A., et al., *Factors affecting gas-phase deuterium scrambling in peptide ions and their implications for protein structure determination.* J Am Chem Soc, 2002. **124**(37): p. 11191-8.

31. Syka, J.E., et al., *Peptide and protein sequence analysis by electron transfer dissociation mass spectrometry.* Proc Natl Acad Sci U S A, 2004. **101**(26): p. 9528-33.

32. Rand, K.D., et al., *Gas-phase hydrogen/deuterium exchange in a traveling wave ion guide for the examination of protein conformations.* Analytical Chemistry, 2009. **81**(24): p. 10019-28.

33. Pan, J., et al., *Hydrogen/deuterium exchange mass spectrometry with top-down electron capture dissociation for characterizing structural transitions of a 17 kDa protein.* J Am Chem Soc, 2009. **131**(35): p. 12801-8.

34. Sterling, H.J. and E.R. Williams, *Real-Time Hydrogen/Deuterium Exchange Kinetics via Supercharged Electrospray Ionization Tandem Mass Spectrometry.* Anal Chem, 2010.

Figure Legends

Figure 1 Schematic of Electrospray Ionization in a positive ion mode. Adopted from Juan Chavez PhD thesis titled "Mass Spectrometry-based Identification and Characterization of Protein and Peptide Adducts of Lipoxidation-Derived Aldehydes", page 37, 2009.

Figure 2 Schematic of Synapt G1 HDMS Q-TOF type mass spectrometer was copied from Waters presentation titled "SYNAPT-Introduction to HDMS" slide 3, 2011.

Figure 3 Cartoon presentation for illustrating the essential characteristics of the MS^E versus DDA tandem mass spectrometric process. Figure was compiled from slides 4, 5 of a Waters presentation available on the web . http://www.waters.com/webassets/cms/library/docs/local_seminar_presentations/CoreFacilitiesTechSummit/Blackburn_WatersPublic.pdf on October 20th 2013.

Figure 4 The mobile proton model. Adopted from website below on October 20th 2013.

(http://www.lamondlab.com/MSResource/LCMS/MassSpectrometry/mobileProtonModel.php)

Figure 5 A general overview of the global and peptide level HDX-MS workflow.

Figure 6 Display of the protein labeling reaction at the global level.

Figure 7 Experimental work flow of the HDX-MS with online digestion setup and Waters HDX chiller module setup.

Figure 1

8 **Schematic of Electrospray Ionization**

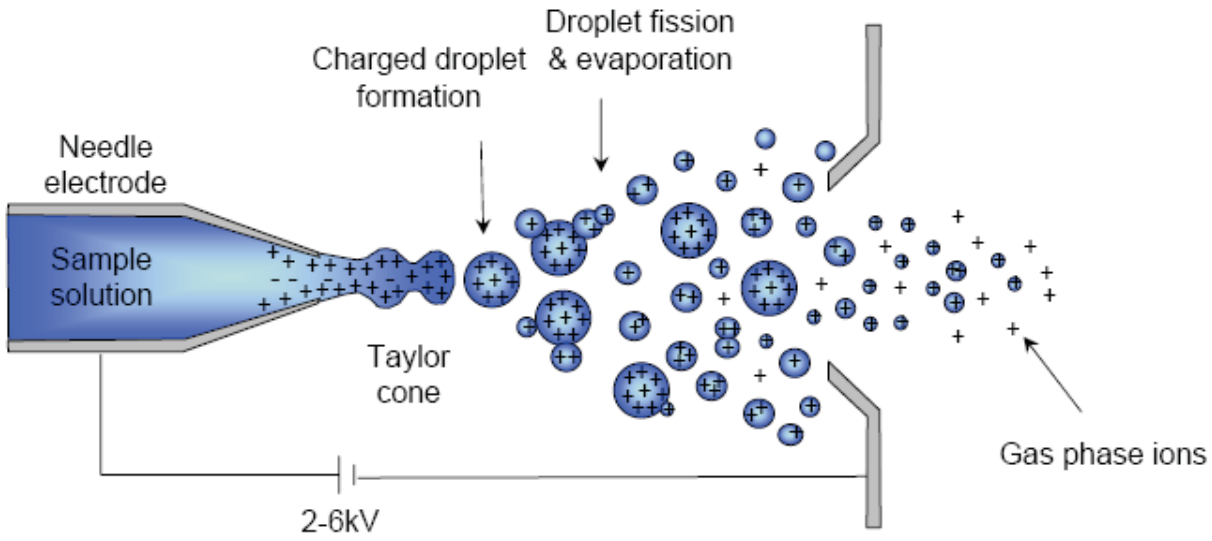

Figure 2

9 **Schematic of Synapt G1 HDMS Q-TOF type mass spectrometer**

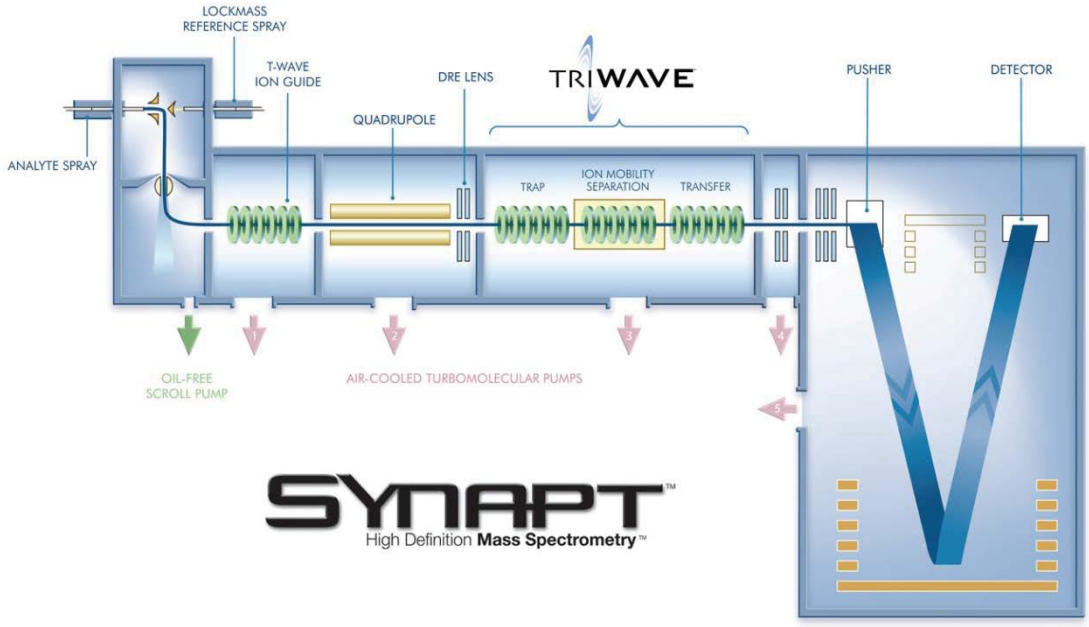

Figure 3

10 Comparison of MSE versus DDA mode of acquisition

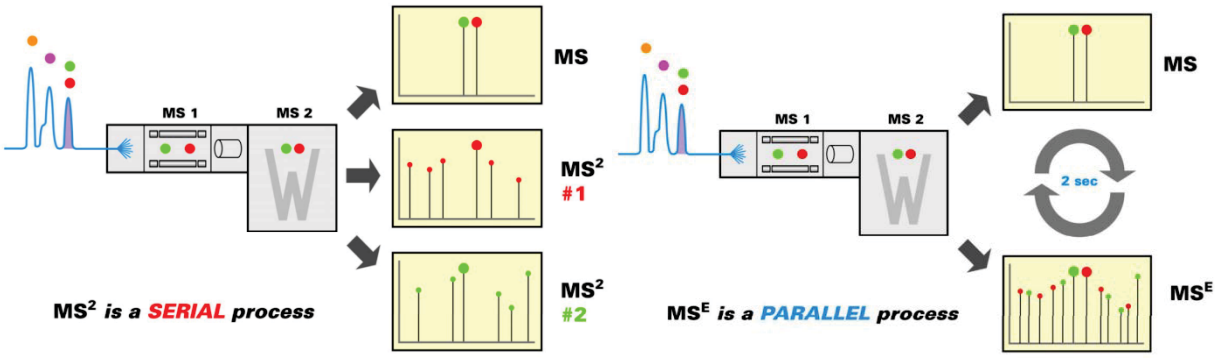

Figure 4

11 **Mobile proton model**

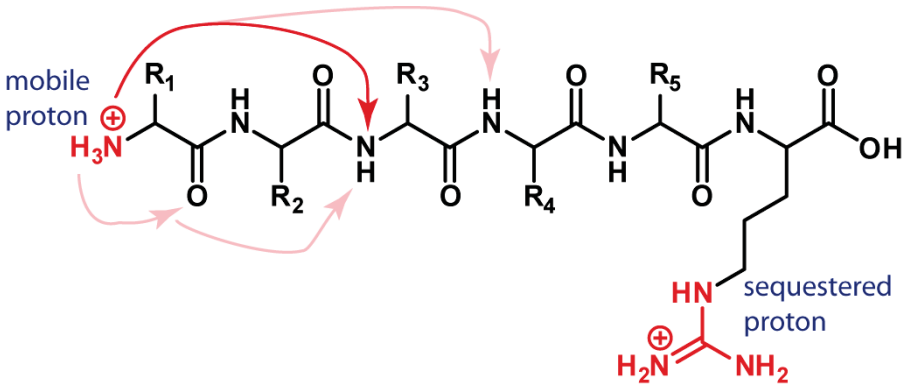

Figure 5

12 Overview of the global and peptide level HDX-MS workflow

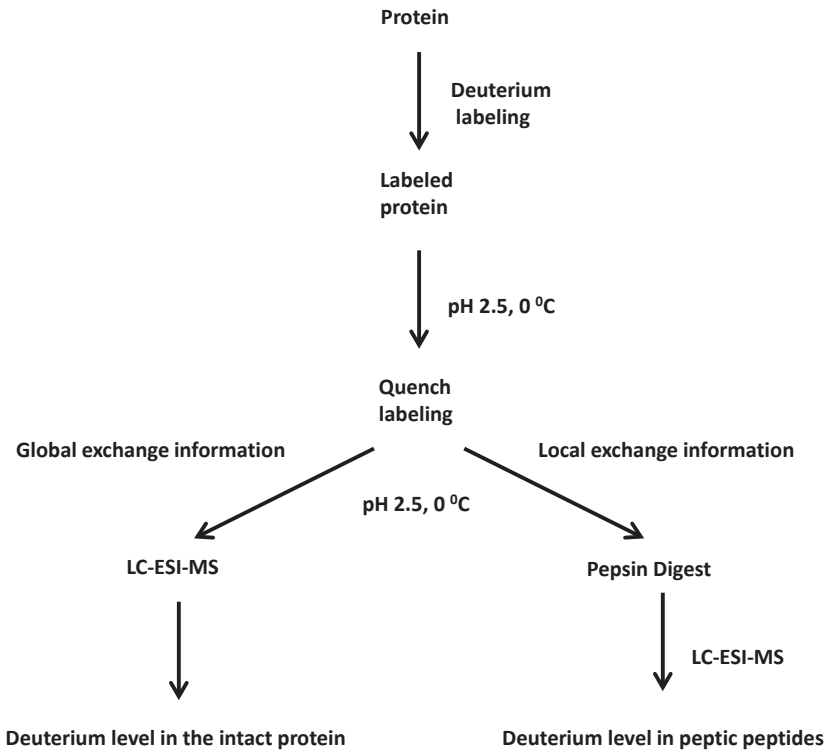

Figure 6

13 **Protein labeling reaction at the global level**

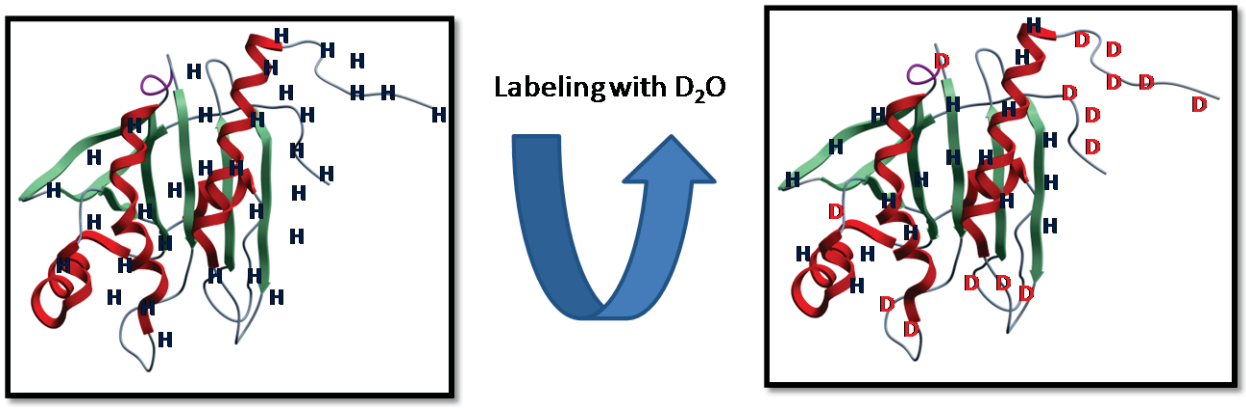

Figure 7

14 **Experimental work flow adopted for the HDX-MS studies as the peptide level**

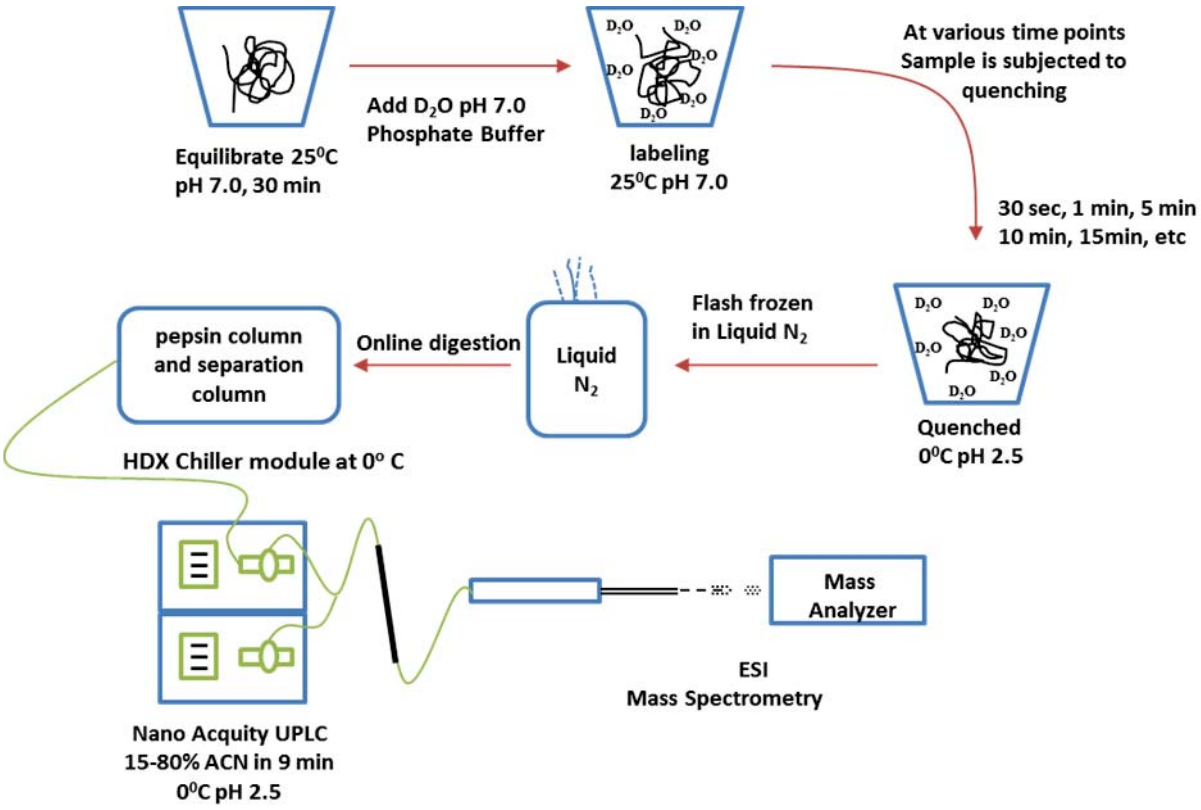

3 Chapter

Conformational studies of the robust 2-Cys peroxiredoxin *Salmonella typhimurium* AhpC by solution phase hydrogen/deuterium (H/D) exchange monitored by electrospray ionization mass spectrometry

Sasidhar Nirudodhi[1], Derek Parsonage[2], P. Andrew Karplus[3], Leslie B. Poole[2], and Claudia S. Maier[1]

[1] Department of Chemistry, Oregon State University, Corvallis, Oregon 97331, USA

[2] Department of Biochemistry, Wake Forest University School of Medicine, Medical Center Boulevard, Winston-Salem, NC 27157, USA

[3] Department of Biochemistry and Biophysics, Oregon State University, Corvallis, Oregon 97331, USA

Corresponding author:

Email: claudia.maier@oregonstate.edu

Phone: 541-737-9533

Fax: 541-737-2062

International Journal of Mass Spectrometry 302 (2011) 93–100

Abbreviations

AhpC, Alkyl hydroperoxide reductase C-22 (peroxidase component); AhpF, alkyl hydroperoxide reductase F component (flavoprotein reductase); C_P, peroxidatic cysteine (Cys-46 of *Salmonella typhimurium* AhpC); C_R, resolving cysteine (Cys-165 of *Salmonella typhimurium* AhpC); *St*AhpC, *Salmonella typhimurium* AhpC; wt, wild type.

3.1 ABSTRACT

This is the first comprehensive HDX-MS study of a "robust" 2-Cys peroxiredoxin (Prx), namely *Salmonella typhimurium* AhpC (*St*AhpC). Prx proteins control intracellular peroxide levels and are abundant antioxidant proteins in eukaryotes, archaea and bacteria blue. Crystal structural analyses and structure/activity studies of several bacterial and mammalian 2-Cys Prxs have revealed that the activity of 2-Cys Prxs is regulated by redox-dependent oligmerization and a sensitivity of the active site cysteine residue to overoxidation. The propensity to overoxidation is linked to the conformational flexibility of the peroxidatic active site loop. The HDX-MS results emphasize the modulation of the conformational motility of the active site loop by disulfide formation. To obtain information on the conformational impact of decamer formation on the active site loop motility, mutants with Thr77 substituted by Ile, a decamer-disrupting mutation or by Val, a decamer-stabilizing mutation, were studied. For the isoleucine mutant, enhanced mobility was observed for regions encompassing the α4 helix located in the dimer-dimer interface and regions surrounding the peroxidatic loop. In contrast, the T77V mutation resulted in an increase in conformational stability in most regions of the protein except for the active site loop and the region encompassing the resolving cysteine.

KEYWORDS

mass spectrometry; hydrogen exchange; deuterium; conformation, folding, peroxiredoxins

3.2 Introduction

Peroxiredoxins (Prxs, EC 1.11.1.15) are ubiquitous thiol peroxidases found in archaeal, bacterial and eukaryotic cells. Prxs are highly abundant antioxidant enzymes. In bacteria, removal of H_2O_2 is predominately achieved by the enzyme alkyl hydroperoxide reductase C22 (AhpC) [*1-3*]. Because of its peroxide-reducing activities, AhpC helps to protect pathogenic bacteria from the host immune response, and, therefore, AhpC is a possible target for the development of new antibiotics for combating infectious diseases [*3*]. AhpC belongs to the typical 2-Cys class of Prxs. This means that they contain two redox active Cys residues involved in catalysis and they form an intersubunit disulfide in the oxidized state. Whereas, 1-Cys Prxs only contain one Cys residue which yields a cysteine sulfenic acid (Cys-SOH) upon oxidation [*3*]. More recently, the dual role of eukaryotic 2-Cys Prxs as antioxidant proteins and key participants in oxidative stress signaling has been recognized [*4*].

Details of the chemistry and structural changes that accompany catalysis for various Prxs have been recently reviewed [*4-6*]. All 2-Cys Prxs have a conserved cysteine residue, the peroxidatic cysteine residue (C_P or Cys-S_PH) to reduce various peroxide substrates (ROOH) to the respective alkyl alcohols (ROH). During this first catalytic step the Cp thiol group will be oxidized to the sulfenic acid (Cys-S_POH) (Figure 1A). All known peroxiredoxins have in close proximity to the active site cysteine C_P a conserved arginine residue which likely contributes to the low pK_a (between 5 to 6) observed for the peroxidatic thiol by stabilizing its thiolate form. A second free thiol, the resolving S_RH, is necessary to complete the catalytic step [*4, 5, 7*]. In typical 2-Cys Prxs, the resolving cysteine residue resides on the second subunit of the dimer and an intersubunit disulfide bond is formed. The catalytic cycle is completed when the disulfide bond is reduced, which requires a reductase (e.g. AhpF) and reducing equivalents, e.g. NAD(P)H [*8*].

In order to allow for formation of the intersubunit disulfide bond, the active site loop and the C-terminal region encompassing the C_R residue must locally unfold [*4*]. In "sensitive" Prxs, whereby sensitivity refers to the tendency of the protein to become overoxidized, these unfolding events are unfavorable, causing a kinetic arrest which in turn makes the Cys-S_P vulnerable to overoxidation by a second molecule of peroxide with formation of a sulfinic acid derivative (Cys-S_PO_2H) [*5*]. In contrast, "robust" Prxs, such as *Salmonella typhimurium* AhpC (*St*AhpC) and some other bacterial Prxs, seem to be resistant to overoxidation, even at relatively high (mM) concentration of H_2O_2. In addition, some of the 2-Cys Prxs undergo redox-dependent oligomerization. For example, *St*AhpC undergoes a decamer to dimer transition upon oxidation (Figure 1B) [*1, 5, 9*].

Here, we describe conformational studies of *St*AhpC and two mutants in which Thr-77, located in the decamer-building A-type interface, was replaced by valine, a decamer-stabilizing mutation, and isoleucine, a decamer-disrupting mutation [*6*]. Hydrogen/deuterium (H/D) exchange monitored by mass spectrometry (HDX-MS) was used to study the impact of the intersubunit disulfide linkage on the conformational dynamics of *St*AhpC,) and to investigate how dimer-dimer interactions affect the conformational properties of the peroxidatic active-site loop in *St*AhpC.

3.3 Experimental

3.3.1 Materials

Deuterium oxide (99.999 atom % D) was purchased from Aldrich Chemical Co. Immobilized pepsin and tris(2-carboxy-ethylphosphine) hydrochloride (TCEP·HCl) were from Thermo/Pierce (Rockford, IL). Biochemical grade potassium phosphate monobasic (KH_2PO_4) and potassium phosphate dibasic anhydrous (K_2HPO_4) were obtained from Sigma-Aldrich.

The wild-type protein, and both mutants, T77V and T77I, of *St*AhpC were prepared and purified in Dr. Poole's laboratory (Wake Forest University) according to published protocols [*10*] and stored at -80^{o}C. Reduced proteins were obtained by adding 0.5 μL 0.01 M TCEP (in 25 mM phosphate buffer, pH 7) to 0.5 μL protein stock solution (10 mg/mL in 25 mM potassium phosphate buffer containing 1mM EDTA, pH 7). Reduction was performed for 30 min at room temperature.

Deuterated phosphate buffer was prepared by lyophilizing potassium phosphate (0.01 M, pH 7) and reconstituting the residue in deuterium oxide. Immobilized pepsin was resuspended in 0.1 M potassium phosphate buffer (pH 2.5) containing 0.01 M TCEP·HCl [*11*]. The volumetric ratio of pepsin beads to phosphate buffer was 1:2. TCEP·HCl was added during digestion to reduce the disulfide bond in the oxidized proteins which enabled the observation of the peptides encompassing the catalytically active Cys-46 and Cys-165 residue by LC-MS/MS analysis. The immobilized pepsin slurry was stored in ice bath before use.

3.3.2 HDX-MS analysis at the protein level

Protein stock solutions (10 mg/mL) were equilibrated at room temperature for 30 min prior to use. The protein was labeled by diluting 0.5 μl stock solution in 10 μL of 0.01 M deuterated phosphate buffer (pH 7) at various periods of time (30 s, 1, 5, 10, 15, 30, 60 min). The exchange-in reaction was arrested with ice-cold quenching buffer (0.1 M potassium phosphate containing 0.01 M TCEP·HCl, pH 2.5). Quenched samples were flash-frozen in liquid nitrogen until the analysis was performed.

A nanoAcquity UPLC system (Waters, Milford, MA) coupled with a LCT ESI-TOF mass spectrometer (Waters, Milford, MA) was used for LC-MS analysis. Frozen samples were thawed at room temperature, placed in the autosampler and injected. A 6-min time period was needed for thawing the sample and for making the injection. After injection, the samples were trapped on an Acquity UPLC BEH

C_{18} (5 µm) trap immersed in an ice bath (around 0^{o}C) and desalted with 15 µL of 97% of solvent A (acetonitrile/H_2O/formic acid, 5/94.9/0.1) and 3% of solvent B (acetonitrile/H_2O/formic acid, 94.9/5/0.1) for 1 min. By using a switching valve, the trapped proteins were diverted onto an Acquity UPLC BEH C_{18} column (1.7 µm particle size, 100 µm x 100 mm) immersed in a ice bath maintained at approximately 0 ^{o}C. Proteins were eluted with a gradient from 15% B to 70% B in 3 min and 70% B to 80% B over the next 3 min. The flow rate was 0.47 µL/min. The LC-T time-of-flight (TOF) mass spectrometer was equipped with an electrospray source operated at 3 kV. Mass spectra were acquired over an m/z-range of 400-2000. Cesium iodide was used to calibrate the instrument. Deuterium incorporation at each exchange time point was determined by subtracting the mass of the undeuterated protein from the mass of the protein at each exchange point. The same sets of experiments were performed for the oxidized and reduced forms of wild type protein, *St*AhpC T77V and *St*AhpC T77I.

3.3.3 Peptic proteolysis and mass spectral analysis of deuterium-labeled peptides

The exchange reaction was performed as described above for similar time points. The resulting deuterated samples were quenched and digested with ice-cold digestion buffer and pepsin, 0.1 M potassium phosphate buffer pH 2.5, 0.01M TCEP·HCl) for 1 min. It was thoroughly mixed and then centrifuged to separate the immobilized pepsin from the solution to stop further digestion. GELoader tips were used to pipette the supernatant into the UPLC vials to avoid the immobilized pepsin from entering the vial. Sample vials were flash frozen in liquid nitrogen to avoid the back exchange until the analysis was performed [*12, 13*]. The peptide solutions were injected into the nanoAcquity UPLC for further analysis as described above. All the parameters and conditions were maintained constant for the UPLC separation of peptides. The resulting peptides were directed into the LC-T ESI mass spectrometer under the similar conditions to those described above except that the mass spectra were acquired over

the m/z range of 400-1500. Deuterium levels in peptides were calculated using the Excel-based program HX Express [*14*]. No correction for back-exchange was performed [*15*]. Relative deuterium levels (in %) were calculated by dividing the number of deuterons incorporated by the number of backbone amide hydrogens present in each peptide. Three independent experiments were performed for each peptide-level experiment. The same sets of experiments were performed for the oxidized and reduced forms of wild-type (wt) *St*AhpC, and the T77V and T77I mutants.

3.3.4 Sequence analysis and assignment of peptic peptides

To obtain sequence assignments for the peptic peptides, an undeuterated peptide sample was analyzed by LC-MS/MS using a Waters/Micromass QTof Ultimate Global mass spectrometer equipped with a lockmass sprayer and coupled to a nanoAcquity UPLC. The chromatographic setup was the same as described above except that for peptide elution the following gradient program was used: 1) 5% B to 35% B in 60 min, 2) 35% B to 85% B by 65 min, and 3) maintain 85% until 72 min. Mass spectra were obtained over a m/z-range of 400-2000. Peptic peptides were identified based on mass measurement and fragment ion information. For the assignment of tandem mass spectral data, Mascot software (Matrix Science) was used. Complete sequence coverage was routinely obtained for the wild-type *St*AhpC protein and both mutants after disulfide reduction.

3.4 Results and Discussion

3.4.1 Global HDX-MS analysis of wild-type *St*AhpC and Thr77 mutant proteins

To study the impact of the intersubunit disulfide bond on the conformational compactness of the typical 2-Cys Prx, *St*AhpC, we performed a deuterium exchange-in analysis of *St*AhpC in the absence and

presence of the disulfide reducing agent, TCEP. The time course study of the intact protein, having an intersubunit disulfide involving Cys-46 at one subunit and Cys-165 on the other subunit, showed a mass increase from 41,242.6 +/- 0.3 Da to 41,317.6 +/- 0.4 Da, which corresponds to an uptake of approximately 75 deuteriums per disulfide-linked dimer (for the 60-min time point). With other words, this represents a deuterium incorporation level of ~21 % (based on 178 backbone amide hydrogens per monomer). In contrast, reduction of the intersubunit disulfide bonds resulted in an increase of overall deuterium incorporation levels. For the reduced protein, a deuterium exchange level to~ 32 % (of 178 backbone NHs) at the 60-min was determined (Figure 1C). Deuterium incorporation profiles for the two Thr77 mutants were also obtained. In accord to the wild-type *St*AhpC protein, the global HDX-MS analyses showed that deuterium incorporation levels for the oxidized mutants were consistently lower than the deuterium levels observed for the reduced mutant proteins (Figure 1C). Removal of the intersubunit disulfide linkage resulted in an approximately 30 % increase in deuterium uptake for the T77V as well as for the T77I mutant compared to the respective disulfide-containing proteins (Figure 1C).

3.4.2 Exchange-in characteristics of *St*AhpC at medium spatial resolution derived by combining peptic proteolysis and HDX-MS analysis

The H/D exchange-in profiles revealed overall trends in conformational stability for the disulfide-containing proteins and the thiol-containing forms. In order to obtain information on the conformational dynamics with medium spatial resolution, we added to the exchange-in labeling experiments peptic proteolysis under conditions that maintain the deuterium labeling information. Over 70 peptic peptides were identified of which sixteen peptides were chosen that cover the entire protein sequence for all three proteins investigated. In order to allow the comparison of deuterium uptake at the peptide level,

the relative percentage of exchange-in was calculated for each peptide by dividing the number of deuterium incorporated in a particular peptide by the number of backbone amide hydrogens present in the peptide.

Figure 2 summarizes the time-dependent H/D exchange-in data for 16 peptides arranged according to their sequence for the intact *St*AhpC protein. The bar graph presentation allows to roughly group the peptides into three exchange categories (compiled in Supplemental Material Table S1): low-exchanging peptides, that show little deuterium incorporation over the exchange-in period tested; 2) medium-exchanging peptides, i.e. peptides that exhibit a consistent deuterium uptake over the 60-min time frame; and 3) high-exchanging peptides, that rapidly reach their high exchange-in plateaus. Peptides that belong to the "low-exchanging" category are encompassing the following partial sequences, 68-87, 96-110, 111-122, 123-132 and 148-156. Peptides of the "medium-exchanging" group are part of the N-terminal region of *St*AhpC and include the peptides 1-20, 21-35, 36-43 and the peptides 61-67 and 88-95. Peptides that were grouped into the "high-exchanging" category included peptides 43-50, 51-60, 133-147, 156-176, 177-182 and 181-186.

"High-exchanging" regions in StAhpC. It is evident from Figure 2A and Table S1 that the active site loop region, which is covered by peptide 43-50, and the C-terminal region represented by the peptides 156-176, 177-182, and 181-186 of the wild-type *St*AhpC, have higher deuterium incorporation levels compared to the rest of the protein. These "high-exchanging" peptides showed ~35% deuterium incorporation within the first 30 s and little subsequent increase in deuterium uptake for the remaining time points. High deuterium incorporation levels imply that these regions are less protected (or more flexible) compared to the rest of the protein. The high exchange-in rate and associated high flexibility of the C-terminal region is in concurrence with the absence of this region starting at residue 166 in the crystal structure of *St*AphC (pdb 1YEP).

Local unfolding of the peroxidatic active site loop of StAhpC. The active site region, peptide 43-50, exhibited the highest exchange-in rate in the oxidized *St*AhpC protein (Figure 2B). Deuterium uptake reached ~40 % within the first 30 s followed by a slow increase at the 5 and 10-min time points reaching thereafter the exchange-in plateau. The active site loop is locally unfolded in the oxidized *St*AhpC in order to accommodate the conformational constraints imposed by the disulfide linkage between Cys-46 and Cys-165 [*1, 2, 4*]. The observed HDX-MS data gives testimony of this intrinsic unfolding paradigm for *St*AphC proteins on which their catalytic function is based.

"Medium-exchanging" regions in StAhpC. For the regions encompassing the peptides 1-20, 36-43, 88-95 a steady increase in the exchange was observed over time. The peptide region of 88-95 exhibited an initial deuterium incorporation of 20% after 30 s and deuterium incorporation levels gradually increased to 35% after 60 min.

Exchange-protected, "low-exchanging" regions in StAhpC. A few regions of *St*AhpC represented by the peptides 68-87, 111-122, 148-156 were well protected from the exchange and showed very low deuterium incorporation levels (around 10%) and no further increase in deuterium uptake with increase in time. The large peptide 68-87, which represents the dimer-to-dimer interfacial region and encompasses the α4 helix and half of 3_{10} helix, showed only a minimal uptake of < 2 deuteriums (~10 % out of a total of 19 possible backbone amide hydrogen) over the time course tested (Figure 2). The low exchange-in rate observed for this partial sequence indicates a substantial protection against exchange-in due to strong hydrogen-bonding and solvent exclusion occurring at the dimer-to-dimer, A-interface of *St*AhpC protein oligomers. The slow exchanging properties of the partial sequences 96-110, representing the α5-helix, and 110-122, covering the β1' and β2' strands and part of the β6 strand, agree well with their secondary structural properties and the proximity to the A-interface. Another exchange-in

protected region in *St*AhpC is represented by the peptide 148-156. This peptide encompassed residues of the α6 helix and protection against exchange-in is gained by interactions with helices α2, α3 and α6 of the other subunit of the *St*AhpC homodimer.

3.4.3 Effect of disulfide bond reduction on the conformational mobility of the active site loop.

The disulfide bond involving Cys-46 and Cys-165 in *St*AhpC was reduced with TCEP and then the deuterium exchange-in experiments at various time points were carried out the same way as for the intact protein. Figure 3 reports the differences in deuterium incorporation observed as a result of reducing the disulfide bond in *St*AhpC. Most peptic peptide regions of the reduced *St*AhpC protein exhibited higher deuterium incorporation levels compared to the disulfide-containing protein. However, certain regions showed higher deuterium uptake in oxidized protein than in the reduced form. This was particularly obvious for the regions covered by the peptides 36-43 and 43-50, encompassing the active site loop helix region, and the peptides 156-176, 177-182 and 181-186, representing the C-terminal region which includes the "resolving" cysteine at position 165. The lower deuterium uptakes observed for these peptides derived from the reduced protein allowed us to conclude that the active site loop region in the reduced protein and part of the C-terminal tail region is more protected against exchange-in in absence of the disulfide bond. The adoption of a"fully folded (FF)" state in absence of the disulfide bond has been repeatedly described in structural studies of typical 2-Cys Prxs [*3, 4*]. The "fully folded" conformation was first seen in the X-ray structure of the *St*AhpC C46S mutant, which cannot form a disulfide bond [*2*]. Formation of the disulfide bond demands local unfolding of the active site region around Cys-46 and parts of the C-terminal region encompassing the resolving Cys-165 residue. The increased conformational flexibility in the "locally unfolded" state is well reflected in the higher

deuterium uptake observed for the peptides 36-43, 43-50 and 156-186 derived from the reduced *St*AhpC protein.

H/D exchange profiles were also obtained for both mutants, T77I and T77V, in their oxidized and reduced forms (Figure 4 and Supplemental Materials Figures S2 and S3 (oxidized forms) and S5 and S6 (reduced forms)). As observed for the wild-type protein, reduction of the intersubunit disulfide bond resulted in increased conformational mobility in most parts of both mutant proteins except for the partial sequence encompassing the peroxidatic Cys-46 residue and the C-terminal region beyond Cys-165 which is absent in either crystal structure (1YFO, Ile mutant, and 1YF1, Val mutant). Thus, both mutants obey the conceptual model in which the active site loop mobility represents a locally unfolded region necessary for disulfide formation and this region becomes more compact upon disulfide reduction [*4*].

3.4.4 Conformational consequences of mutating Thr77, a critical residue in the decamer building, dimer-dimer interface of *St*AhpC

The structure/activity relationship of 2-Cys Prxs is governed by their redox-dependent partitioning between dimeric and decameric states. Previous mutation studies involving Thr-77, located at the dimer-to-dimer decamer-building interface, showed that decamer-disrupting mutations, e.g. the replacement of Thr-77 with the larger Ile residue, destabilizes the decamer-building interface leading to decamer dissociation and reduced catalytic efficiency. In contrast, mutation of Thr-77 with Val had a stabilizing effect on the dimer-dimer interface and decamer formation and increased catalytic activity [*1, 3, 6*]. We therefore set out to look closer at the changes in conformational dynamics caused by the mutations of Thr-77 by H/D exchange.

HDX-MS analysis of StAhpC T77I. To observe the altered dynamics at various sites in the protein upon mutation of T77, HDX-MS experiments were carried out for the T77I mutant. Peptides were identified for the T77I mutant that provided complete sequence coverage. When the peptides were mapped onto the sequence, approximately 54% of the residues in the T77I mutant showed higher deuterium incorporation suggesting that the T77I mutation overall negatively impacted the conformational integrity of the wild-type protein (Figure 5). Differential analysis of the deuterium uptake reveals that the peptides covering the partial sequence 61-87 encompassing parts of α3, β4, α4 and parts of the 3_{10} helix were less protected against exchange-in and consequently destabilized in the T77I mutant (compared to the wild-type protein). In addition, increased deuterium uptake relative to the wild-type protein was observed in the sequence 96-122 which partly forms the interfacial region and covers the α5 helix (peptide 96-110), the short β1' and β2' strands (peptide 111-122) and subsequently leads into the β7 strands. Increased exchange-in levels were also observed for the peroxidative active site loop covered by peptides 21-35, 36-43 and 43-50. Regions that showed less protection against exchange-in in the Ile mutant compared to the wild-type protein are indicated in red in Figure 5B. In contrast, regions that were found to be more protected against exchange-in in the T77I mutant were located in the region 51-60 and the C-terminal partial sequence 156-186 covered by the peptides 156-176, 177-182, 181-186. These regions are indicated in blue in Figure 5B.

The replacement of Thr-77 with Ile disturbs and destabilizes not only the decamer-building interface but also allosterically destabilized the loop that encompasses the peroxidatic active site. The observed allosteric changes in the conformational dynamics caused by mutating Thr77 to Ile in AhpC supports our working hypothesis that destabilization of the active site loop associated with increased flexibility will remove conformational restraints allowing facile disulfide formation and confer protection against overoxidation [*6*]. Earlier reported sedimentation velocity studies showed that the T77I mutant is predominantly present as dimer in solution [*1*]. The results of the H/D exchange-in studies support

well a structural model in which destabilization of the decamer-building interface by the T77I mutation shifts the oligmerization equilibrium towards the dimeric form.

HDX-MS analysis of StAhpC T77V. When the deuterium incorporation data of the T77V mutant was compared to the data obtained for wild-type *St*AhpC (Figure 6), it became apparent that about 75% of the protein backbone of T77V protein exhibited more protection against deuterium exchange-in than the wild-type AhpC protein. Less than 10% of the protein backbone exhibited higher deuterium incorporation in the T77V mutant. For the remaining regions (about 15% of the residues) similar levels of deuterium incorporation were observed for both the wild-type protein and the T77V mutant. Differential analysis of the H/D exchange-in profiles of T77V and wild-type protein revealed that the N-terminal parts of the protein backbone (1-43), regions in proximity to the A-interface (51-67 and 88-110) and a large section encompassing the residues 111 to 176 gained conformational stability upon replacement of Thr-77 by valine. These regions are indicated in blue in Figure 6B. For the interfacial peptides, 68-87 (α4 helix) and 111-122 (β1'-β2' loop and part of β6), no or little change in exchange-in dynamics was observed. In contrast, the active site loop peptide (43-50) and the C-terminal region (177-182) displayed higher deuterium incorporation in the T77V mutant compared to the wild-type AhpC protein. Regions with reduced levels of protection against exchange-in are indicated in red in the Figure 6B. The exchange-in behavior observed for the T77V mutant allowed concluding that the introduction of the valine residue at the dimer-dimer interface resulted in gain of conformational stabilization in the majority of the protein except for active site loop encompassing Cys-46 and the C-terminal partial sequence.

3.5 Conclusion

We report the first HDX-MS analyses for a "robust" 2-Cys Prxs, namely of the bacterial peroxiredoxin from *Salmonella typhimurium*, *St*AhpC. The current studies provide proof of principle that HDX-MS is a suitable approach for studying the modulation of the conformational properties of Prxs by redox state and oligomerization. A combination of H/D exchange labeling experiments, peptic proteolysis under conditions that retain the deuterium labeling information and LC-ESI-MS was used to study how the conformational flexibility of the active site loop is governed by the redox state and associated competence of forming decameric assemblies. The reported H/D exchange studies emphasize the adaption of a locally unfolded active site loop in the disulfide-linked dimeric protein. Whereas, increased conformational rigidity in the active site loop region was observed upon reduction of the intersubunit disulfide bond. Thus, our HDX-MS results provide support to a structure/activity concept in which the conformational flexibility of the active site loop determines the sensitivity of the peroxidative cysteine to overoxidation [*2-4*].

In addition, two single amino acid substitution mutants, *St*AhpC T77V and T77I in their oxidized and reduced forms were studied. Previous ultracentrifugation studies indicated that the T77V is a decamer promoting mutation, whereas T77V is a decamer-disruptive mutation [*1*]. The HDX-MS studies revealed that the Thr77 mutation located at the A-interface impacts not only the dimer-dimer interactions but also the active site loop motility. Compared to the wild-type protein, enhanced motility was observed for the T77V mutation. There is no other technique that will allow delineate the impact of a single mutation on the allosteric interactions within a protein assembly of this size. Future work will focus on defining differences in the conformational properties of "robust" Prxs proteins, such as the bacterial AhpCs, compared to "sensitive" Prxs, such as the mammalian peroxiredoxins, e.g. the human PrxII protein [*16*].

3.6 Acknowledgement

This study was supported by a grant from the National Institutes of Health to L.B.P. with a subcontract to P.A.K. and C.S.M. (R01 GM050389). The OSU mass spectrometry facility and services core is supported in part by NIH/NIEHS grant P30 ES000210.

3.7 Supplementary Data:

Table S1 summarizes observed exchange behaviors of peptic peptides derived from *St*AhpC and two single amino acid mutants, T77V and T77I, in their oxidized (ox) and reduced (red) forms. Figures S1 to S6 show deuterium incorporation charts and H/D exchange maps for oxidized and reduced forms of *St*AhpC, T77I and T77V. This material is available free of charge via the Internet.

3.8 References:

[1] Wood, Z. A., Poole, L. B., Hantgan, R. R. and Karplus, P. A., Dimers to doughnuts: redox-sensitive oligomerization of 2-cysteine peroxiredoxins, Biochemistry. 41 (2002) 5493-5504.

[2] Wood, Z. A., Poole, L. B. and Karplus, P. A., Peroxiredoxin evolution and the regulation of hydrogen peroxide signaling, Science. 300 (2003) 650-653.

[3] Wood, Z. A., Schroder, E., Robin Harris, J. and Poole, L. B., Structure, mechanism and regulation of peroxiredoxins, Trends Biochem Sci. 28 (2003) 32-40.

[4] Hall, A., Karplus, P. A. and Poole, L. B., Typical 2-Cys peroxiredoxins--structures, mechanisms and functions, Febs J. 276 (2009) 2469-2477.

[5] Parsonage, D., Karplus, P. A. and Poole, L. B., Substrate specificity and redox potential of AhpC, a bacterial peroxiredoxin, Proc Natl Acad Sci U S A. 105 (2008) 8209-8214.

[6] Parsonage, D., Youngblood, D. S., Sarma, G. N., Wood, Z. A., Karplus, P. A. and Poole, L. B., Analysis of the link between enzymatic activity and oligomeric state in AhpC, a bacterial peroxiredoxin, Biochemistry. 44 (2005) 10583-10592.

[7] Poole, L. B., The catalytic mechanism of peroxiredoxins, Subcell Biochem. 44 (2007) 61-81.

[8] Jonsson, T. J., Ellis, H. R. and Poole, L. B., Cysteine reactivity and thiol-disulfide interchange pathways in AhpF and AhpC of the bacterial alkyl hydroperoxide reductase system, Biochemistry. 46 (2007) 5709-5721.

[9] Barranco-Medina, S., Lazaro, J. J. and Dietz, K. J., The oligomeric conformation of peroxiredoxins links redox state to function, FEBS Lett. 583 (2009) 1809-1816.

[10] Poole, L. B. and Ellis, H. R., Flavin-dependent alkyl hydroperoxide reductase from Salmonella typhimurium. 1. Purification and enzymatic activities of overexpressed AhpF and AhpC proteins, Biochemistry. 35 (1996) 56-64.

[11] Yan, X., Zhang, H., Watson, J., Schimerlik, M. I. and Deinzer, M. L., Hydrogen/deuterium exchange and mass spectrometric analysis of a protein containing multiple disulfide bonds: Solution structure of recombinant macrophage colony stimulating factor-beta (rhM-CSFbeta), Protein Sci. 11 (2002) 2113-2124.

[12] Hamuro, Y., Coales, S. J., Morrow, J. A., Molnar, K. S., Tuske, S. J., Southern, M. R. and Griffin, P. R., Hydrogen/deuterium-exchange (H/D-Ex) of PPARgamma LBD in the presence of various modulators, Protein Sci. 15 (2006) 1883-1892.

[13] Houde, D., Arndt, J., Domeier, W., Berkowitz, S. and Engen, J. R., Characterization of IgG1 conformation and conformational dynamics by hydrogen/deuterium exchange mass spectrometry, Anal Chem. 81 (2009) 2644-2651.

[14] Weis, D. D., Engen, J. R. and Kass, I. J., Semi-automated data processing of hydrogen exchange mass spectra using HX-Express, J Am Soc Mass Spectrom. 17 (2006) 1700-1703.

[15] Zhang, Z. and Smith, D. L., Determination of amide hydrogen exchange by mass spectrometry: a new tool for protein structure elucidation, Protein Sci. 2 (1993) 522-531.

[16] Barranco-Medina, S., Kakorin, S., Lazaro, J. J. and Dietz, K. J., Thermodynamics of the dimer-decamer transition of reduced human and plant 2-cys peroxiredoxin, Biochemistry. 47 (2008) 7196-7204.

Figure Legends:

Figure 1.

Structure/activity characteristics of StAhpC and HDX-MS analysis. (A) Catalytic cycle of the typical 2-Cys peroxiredoxin, *St*AhpC. Cp, peroxidatic cysteine residue (Cys-46); C_R, resolving cysteine residue (Cys-165). (B) Redox-dependent oligomerization of *St*AhpC. (3) Global deuterium incorporation profiles of wild-type *St*AphC, and the two single amino acid mutants, T77V and T77I, in their oxidized and reduced forms. Enhanced conformational mobility in *St*AhpC, T77V and T77I upon reduction of the intersubunit disulfide bridge.

Figure 2.

Summary of deuterium incorporation data observed for peptic peptides derived from *St*AhpC. (A) H/D exchange profile; (B) H/D exchange map, and (C) deuterium exchange-in data overlaid on the X-ray structure of *St*AhpC (1YEP). For (C), the color coding for the deuterium incorporation levels is simplified to 5 categories ranging from blue to red. Blue regions indicate regions with lowest deuterium incorporation and the highest level of protection against exchange-in. Red regions indicate regions exhibiting the highest levels of deuterium incorporation and hence mark regions with the highest exchange rates and lowest level of protection against deuterium exchange-in.

Figure 3.

Comparative HDX-MS study of the oxidized and reduced forms of *St*AhpC. (A) Differential HDX-MS profile, WT_{red}-WT_{ox}, comparing relative changes in deuterium incorporation levels between the reduced and oxidized protein. Positive bars indicate regions that showed higher deuterium incorporation levels in the reduced form. (B) Deuterium exchange-in data is overlaid on the X-ray structure of *St*AhpC (1YEP). Red regions show higher deuterium incorporation levels in the reduced form relative to the oxidized form. Blue regions represent regions that show lower deuterium uptake, i.e. are more protected against exchange-in, in the reduced form relative to the oxidized protein.

Figure 4.

Deuterium incorporation data at the peptide level is overlaid on the respective crystal structures of *St*AhpC and the two mutant T77V and T77I in presence (ox) and absence (red) of the intersubunit disulfide bridge. The same color coding scheme as in Figure 2C is used. Deuterium incorporation levels increase from blue to red. Blue regions show the lowest levels of deuterium incorporation. Red regions exhibit the highest deuterium incorporation levels. The following X-ray structures were used: 1YEP, wt *St*AhpC; 1YF1, *St*AhpC T77V; 1YFO, *St*AhpC T77I.

Figure 5.

Comparative HDX-MS study of StAhpC and the T77I mutant, a decamer disruption mutant. (A) Differential HDX-MS profile chart, WT Ox - T77I Ox. In this plot, positive bars indicate regions exhibiting higher deuterium levels in the wild-type protein compared to the isoleucine mutant. Negative bars indicate regions that showed higher deuterium incorporation in the mutant protein relative to the wild-

type protein. Regions that show more deuterium increase and thus less protection in the T77I mutant are depicted in red in Figure 5B. Bars indicate average differences in deuterium uptake from three independent measurements. (B) Deuterium exchange-in data is overlaid on the X-ray structure of *St*AhpC (1YEP). Red regions mark regions that show higher deuterium uptake and hence less protection against exchange-in indicating increased conformational mobility in the T77I mutant compared to the wild-type *St*AhpC protein. The Thr residue in position 77 is depicted in CPK style.

Figure 6.

Comparative HDX-MS study of *St*AhpC and the T77V mutant, a decamer promoting mutant. HDX-MS data demonstrates increased conformational rigidity for the T77V mutant relative to the wild-type protein. (A) Differential HDX-MS profile chart, WT Ox - T77V Ox. In this plot, positive bars indicate regions that exhibit higher deuterium incorporation levels in the wild-type protein relative to the valine mutant. Whereas, negative bars indicate regions that showed increased deuterium incorporation in the mutant protein and hence indicate regions that are less protected against exchange-in in the T77V mutant. These regions are indicated in red in Figure 6B. Bars indicate average differences in deuterium uptake from three independent measurements. (B) Deuterium exchange-in data is overlaid on the X-ray structure of *St*AhpC (1YEP). Red regions mark regions that show elevated deuterium uptake and less protection against exchange-in as a consequence of the T77V mutation relative to the wild-type *St*AhpC protein. The Thr residue in position 77 is depicted in CPK style.

Figure 1

15 **Catalytic cycle of the typical 2-Cys peroxiredoxin**

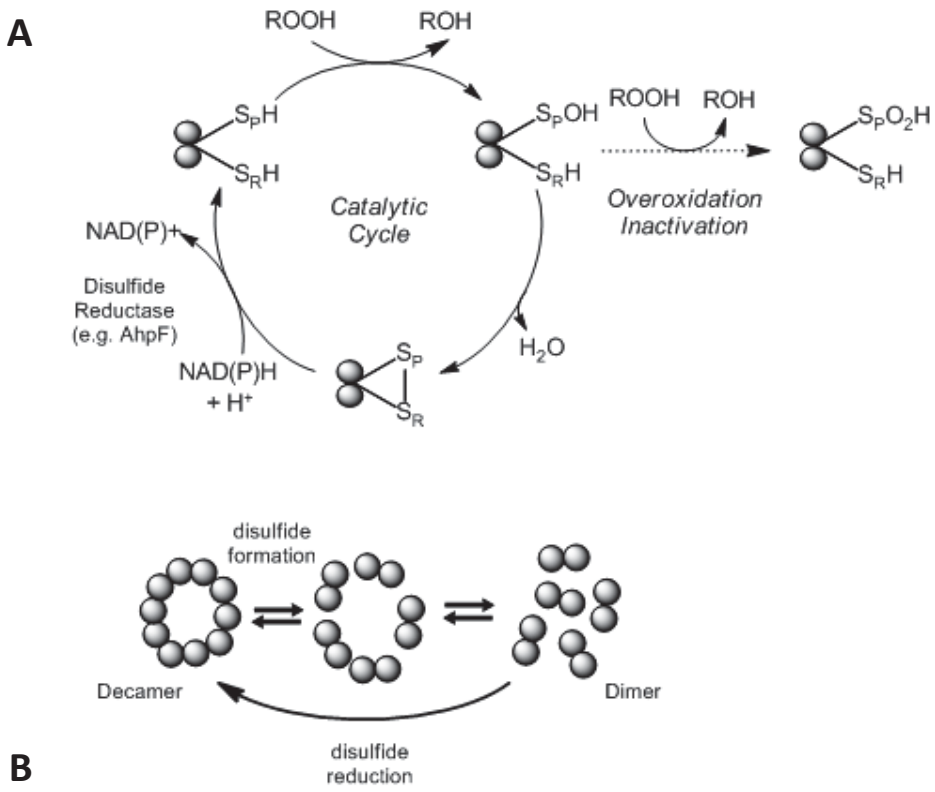

C

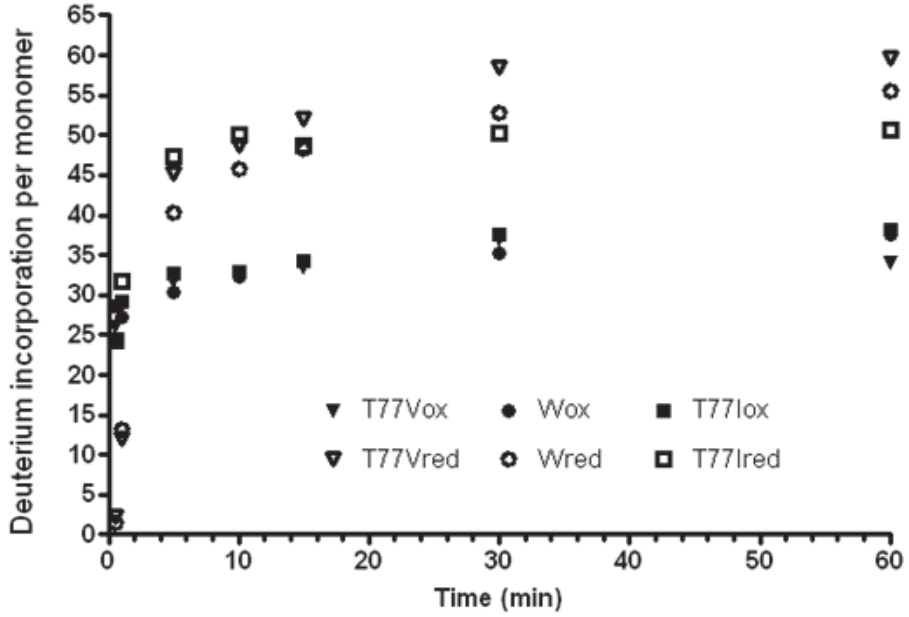

16 Global deuterium incorporation profiles of wild-type StAphC and mutants

Figure 2

17 **HDX-MS profiles**

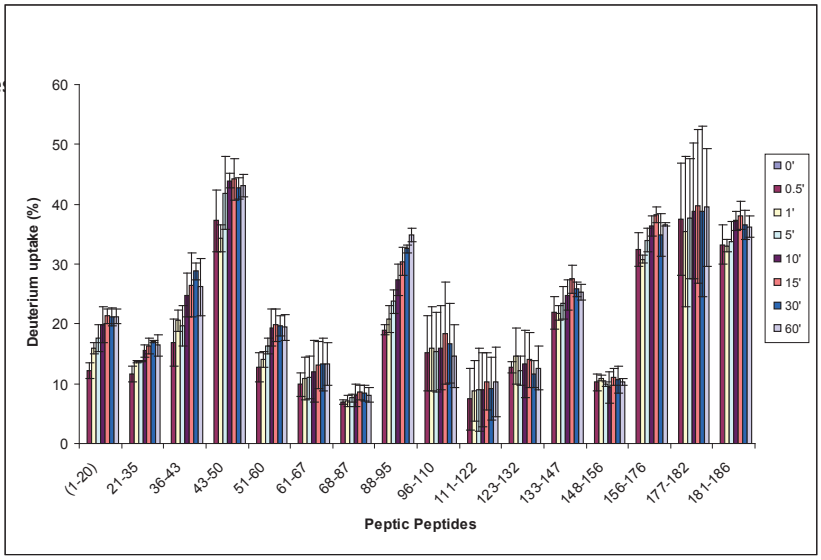

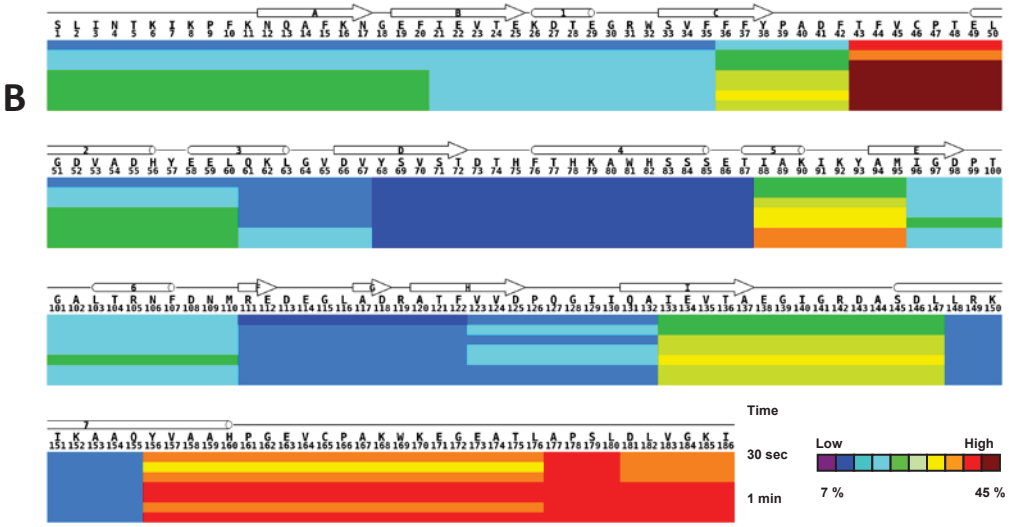

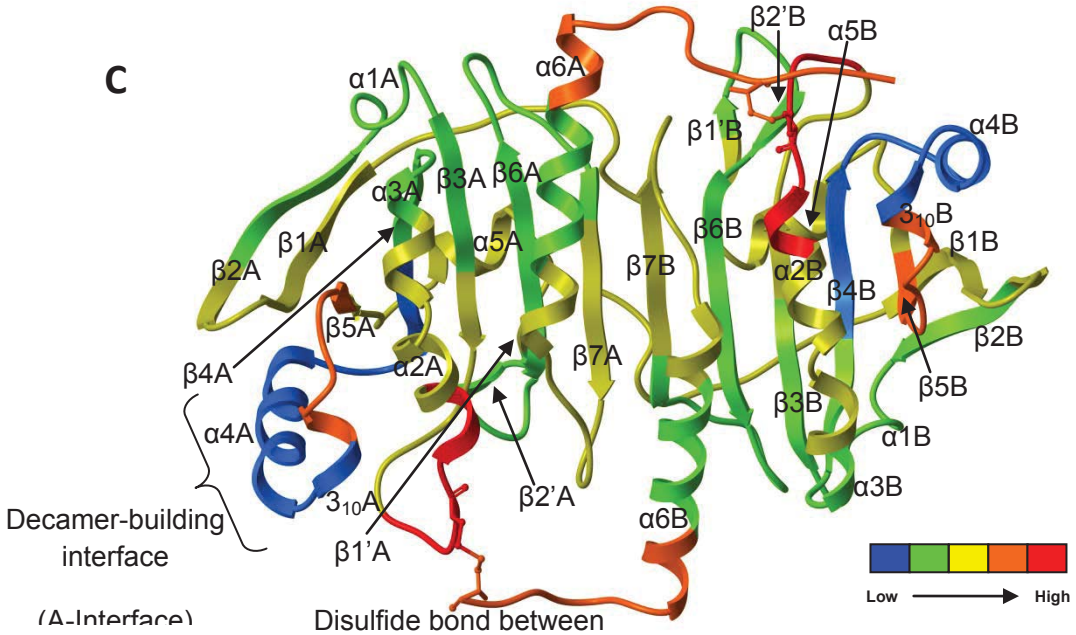

Figure 3

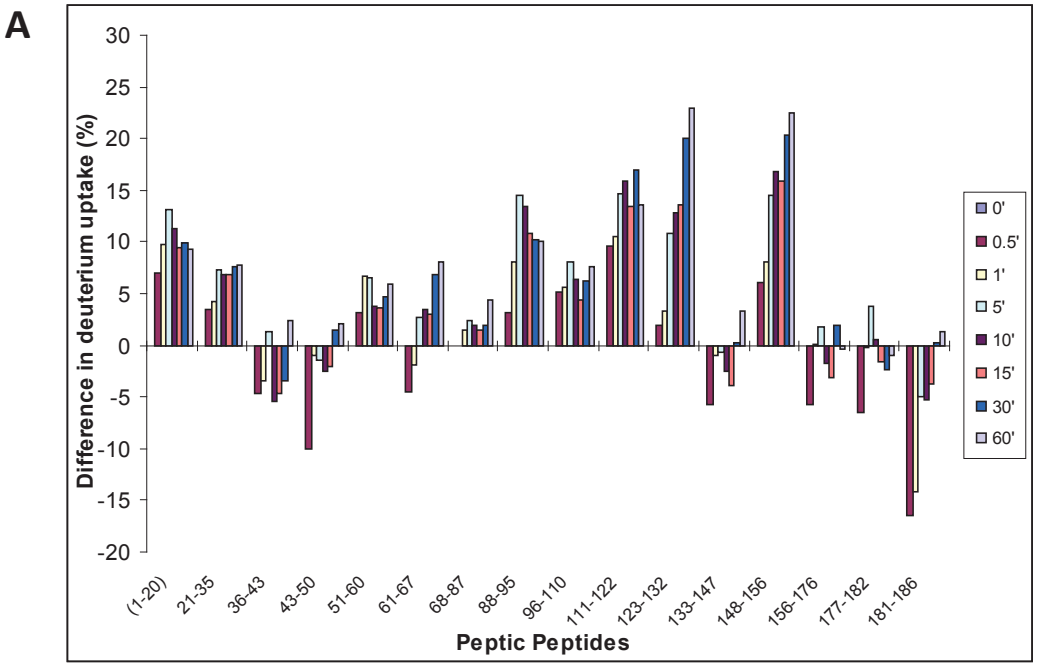

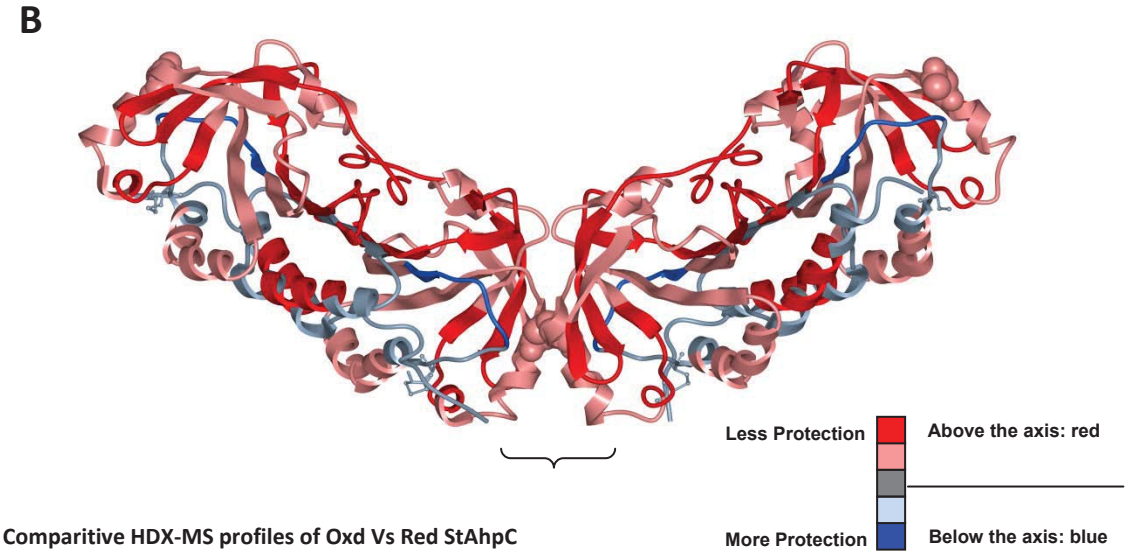

18 Comparitive HDX-MS profiles of Oxd Vs Red StAhpC

A-type Interface

Figure 4

19 **Summary of deuterium uptake overlaid on respective X-ray crystal structures**

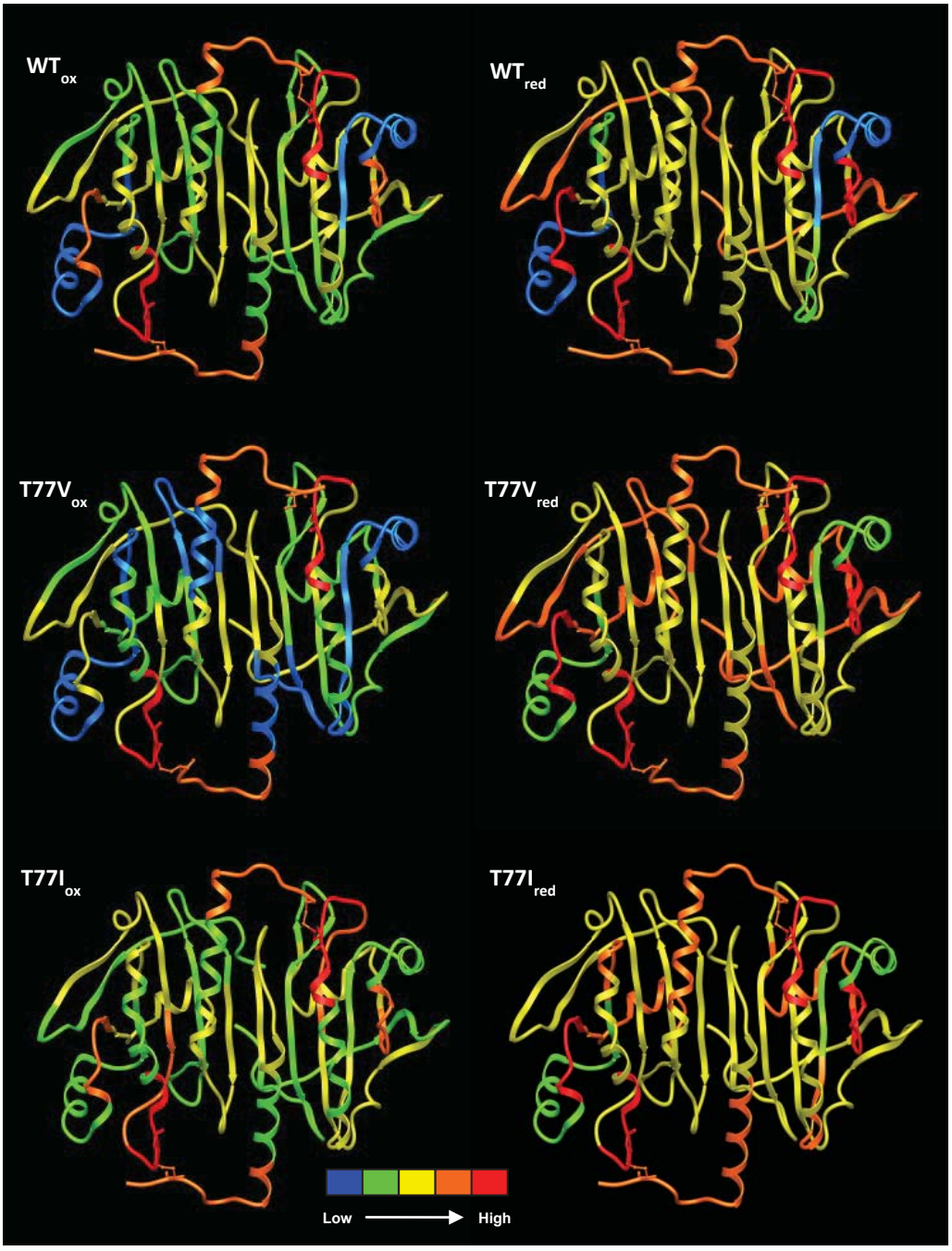

Figure 5

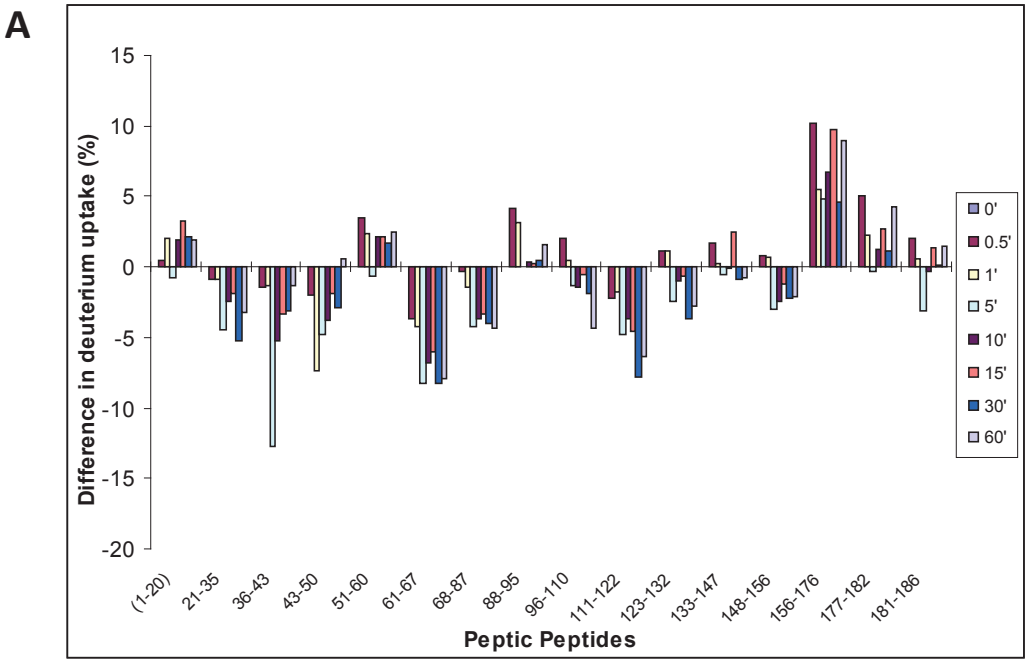

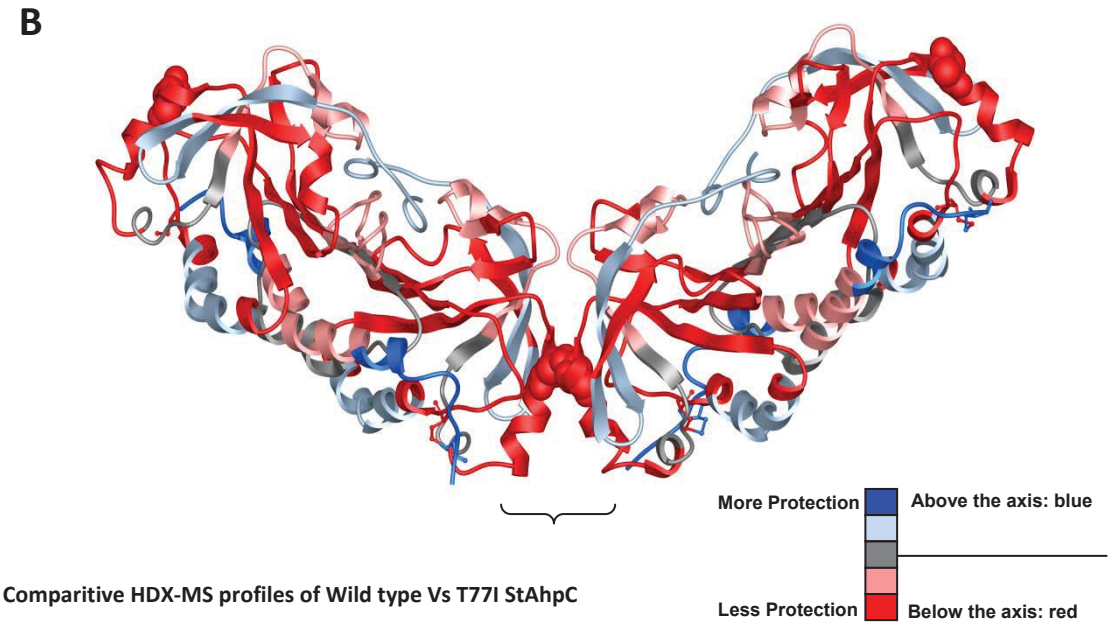

20 Comparitive HDX-MS profiles of Wild type Vs T77I StAhpC

Figure 6

21 Comparitive HDX-MS profiles of wild-type Vs T77I StAhpC

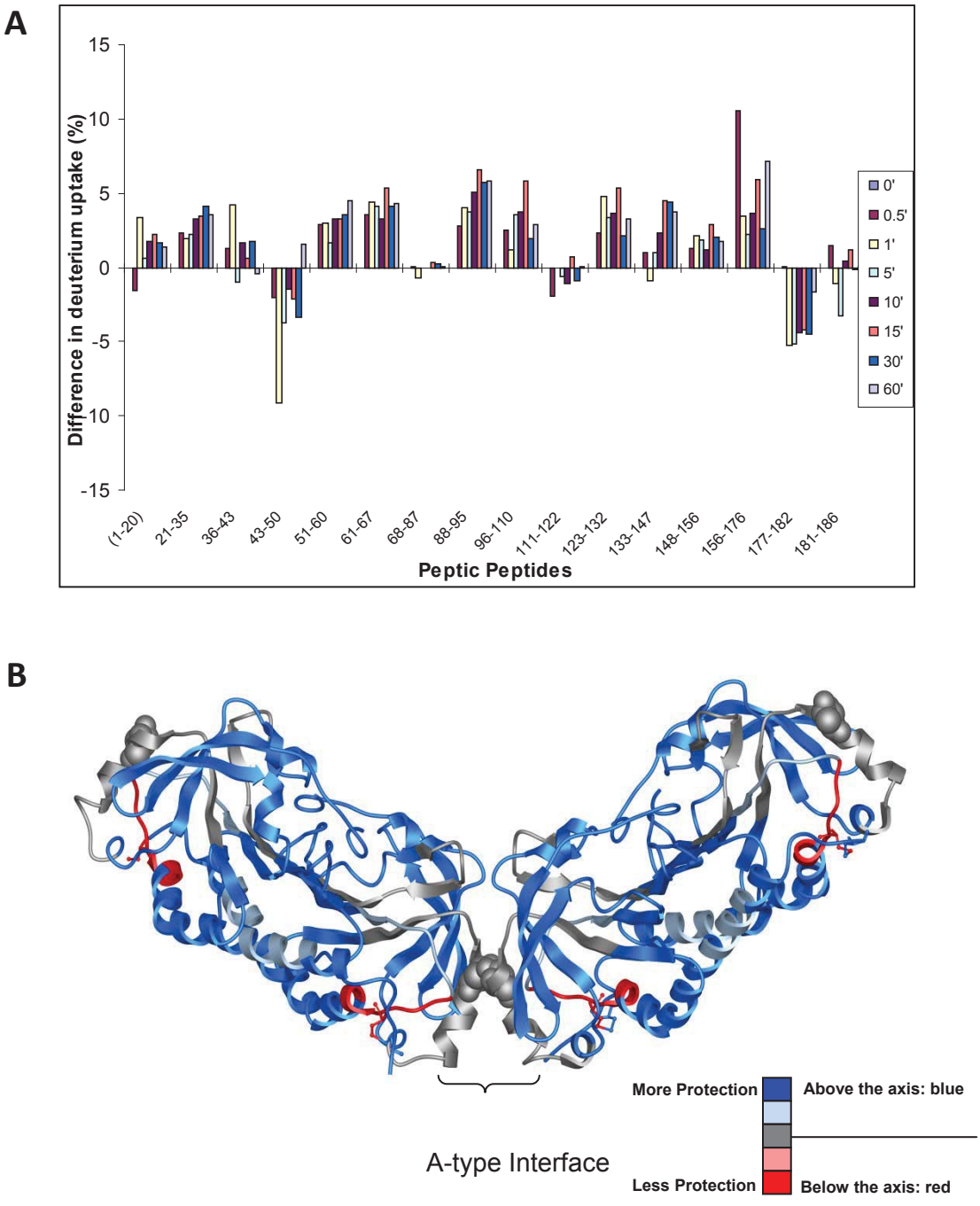

SUPPLEMENTARY DATA

Conformational studies of the robust 2-Cys peroxiredoxin *Salmonella typhimurium* AhpC by solution phase hydrogen/deuterium (H/D) exchange monitored by electrospray ionization mass spectrometry

Sasidhar Nirudodhi[1], Derek Parsonage,[2] Andrew Karplus,[3] Leslie B. Poole,[2] and Claudia S. Maier[1]

[1] Department of Chemistry, Oregon State University, Corvallis, Oregon 97331, USA

[2] Department of Biochemistry, Wake Forest University School of Medicine, Medical Center Boulevard, Winston-Salem, NC 27157, USA

[3] Department of Biochemistry and Biophysics, Oregon State University, Corvallis, Oregon 97331, USA

Table S1. Observed exchange behaviors of peptic peptides derived from *St*AhpC and two single amino acid mutants, T77V and T77I, in their oxidized (ox) and reduced (red) forms.

Figure S1 to S3. Deuterium incorporation chart and H/D exchange map for oxidized *St*AhpC, T77I and T77V.

Figure S1 to S3. Deuterium incorporation chart and H/D exchange map for reduced *St*AhpC, T77I and T77V.

Legends of Figures

Figure S1. (A) Deuterium incorporation chart for oxidized *St*AhpC. Error bars represent the standard deviations derived from three independent analyses. (B) H/D exchange map for oxidized *St*AhpC. Blue blocks represent regions exhibiting low deuterium incorporation levels and these regions correspond to exchange-protected regions. Red blocks mark regions that show high deuterium incorporations corresponding to regions with high conformational mobility.

Figure S1. (A) Deuterium incorporation chart for oxidized *St*AhpC. Error bars represent the standard deviations derived from three independent analyses. (B) H/D exchange map for oxidized *St*AhpC. Blue blocks represent regions exhibiting low deuterium incorporation levels and these regions correspond to exchange-protected regions. Red blocks mark regions that show high deuterium incorporations corresponding to regions with high conformational mobility.

Figure S2. (A) Deuterium incorporation chart for oxidized *St*AhpC T77I. Error bars represent the standard deviations derived from three independent analyses. (B) H/D exchange map for oxidized *St*AhpC T77I. Blue blocks represent regions exhibiting low deuterium incorporation levels and these regions correspond to exchange-protected regions. Red blocks mark regions that show high deuterium incorporations corresponding to regions with high conformational mobility.

Figure S3. (A) Deuterium incorporation chart for oxidized *St*AhpC T77V. Error bars represent the standard deviations derived from three independent analyses. (B) H/D exchange map for oxidized *St*AhpC T77V. Blue blocks represent regions exhibiting low deuterium incorporation levels and these regions correspond to exchange-protected regions. Red blocks mark regions that show high deuterium incorporations corresponding to regions with high conformational mobility.

Figure S4. (A) Deuterium incorporation chart for reduced *St*AhpC. Error bars represent the standard deviations derived from three independent analyses. (B) H/D exchange map for reduced *St*AhpC. Blue blocks represent regions exhibiting low deuterium incorporation levels and these regions correspond to exchange-protected regions. Red blocks mark regions that show high deuterium incorporations corresponding to regions with high conformational mobility.

Figure S5. (A) Deuterium incorporation chart for reduced *St*AhpC T77I. Error bars represent the standard deviations derived from three independent analyses. (B) H/D exchange map for reduced *St*AhpC T77I. Blue blocks represent regions exhibiting low deuterium incorporation levels and these regions correspond to exchange-protected regions. Red blocks mark regions that show high deuterium incorporations corresponding to regions with high conformational mobility.

Figure S6. (A) Deuterium incorporation chart for reduced *St*AhpC T77V. Error bars represent the standard deviations derived from three independent analyses. (B) H/D exchange map for reduced *St*AhpC T77V. Blue blocks represent regions exhibiting low deuterium incorporation levels and these regions correspond to exchange-protected regions. Red blocks mark regions that show high deuterium incorporations corresponding to regions with high conformational mobility.

Table S1. Observed exchange behaviors of peptic peptides derived from *St*AhpC and two single amino acid mutants, T77V and T77I, in their oxidized (ox) and reduced (red) forms.

1 **Observed exchange behaviors of peptic peptides derived from StAhpC and two single amino acid mutants, T77V and T77I, in their oxidized (ox) and reduced (red) forms**

	Exchange Category		
Protein	Low	Medium 	High 
WT_{ox}	68-87, 96-110, 111-122, 123-132, 148-156	1-20, 21-35, 36-43, 61-67, 88-95	43-50, 51-60, 133-147, 156-176, 177-182, 181-186
WT_{red}	96-110, 68-87	36-43, 43-50, 51-60, 61-67, 88-95, 123-132, 133-147, 148-156, 181-186	1-20, 21-35, 111-122, 156-176, 177-182
$T77V_{ox}$	68-87, 96-110, 111-122, 123-132, 148-156	1-20, 21-35, 36-43, 61-67, 88-95	43-50, 51-60, 133-147, 156-176, 177-182, 181-186
$T77V_{red}$	68-87	21-35, 36-43, 123-132, 148-156	1-20, 43-50, 61-67, 88-95, 96-110, 111-122, 133-147, 156-176, 177-182, 181-186, 51-60

$T77I_{ox}$	1-20, 21-35, 68-87, 123-132, 148-156	88-95, 111-122	36-43, 43-50, 51-60, 61-67, 96-110, 133-147, 156-176, 177-182, 181-186
$T77I_{red}$	68-87	36-43, 123-132	1-20, 21-35, 43-50, 51-60, 61-67, 88-95, 96-110, 111-122, 133-147, 148-156, 156-176, 177-182, 181-186

Figure S1. HDX-MS analysis of oxidized *St*AhpC

22 **HDX-MS analysis of oxidized StAhpC**

A

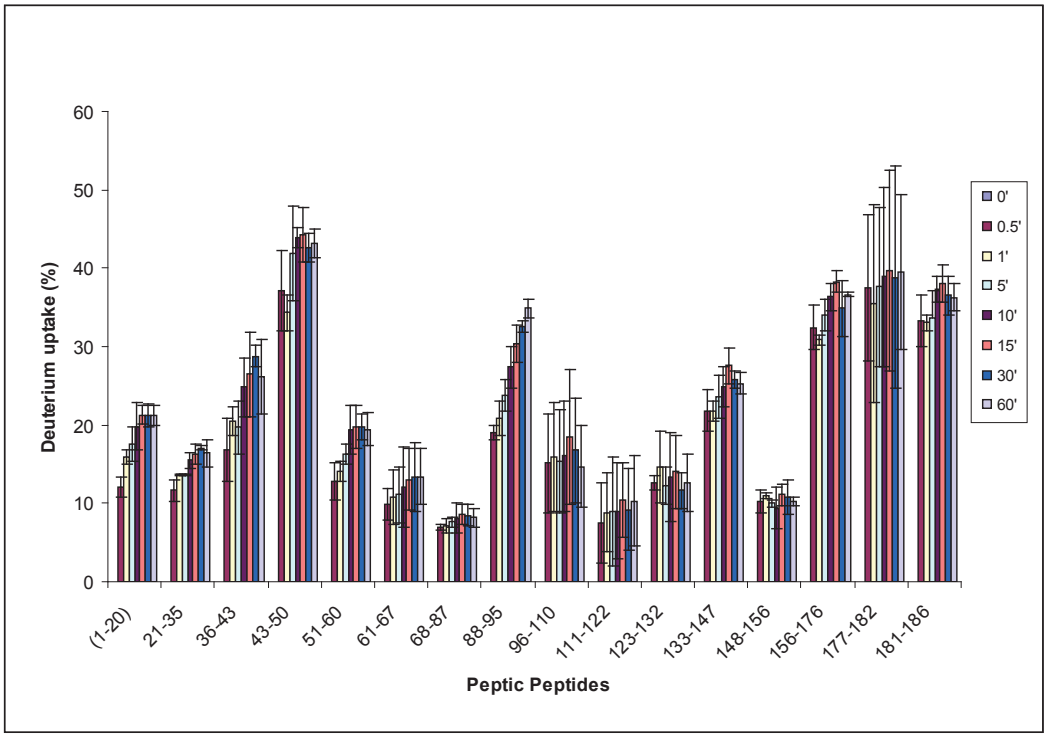

B

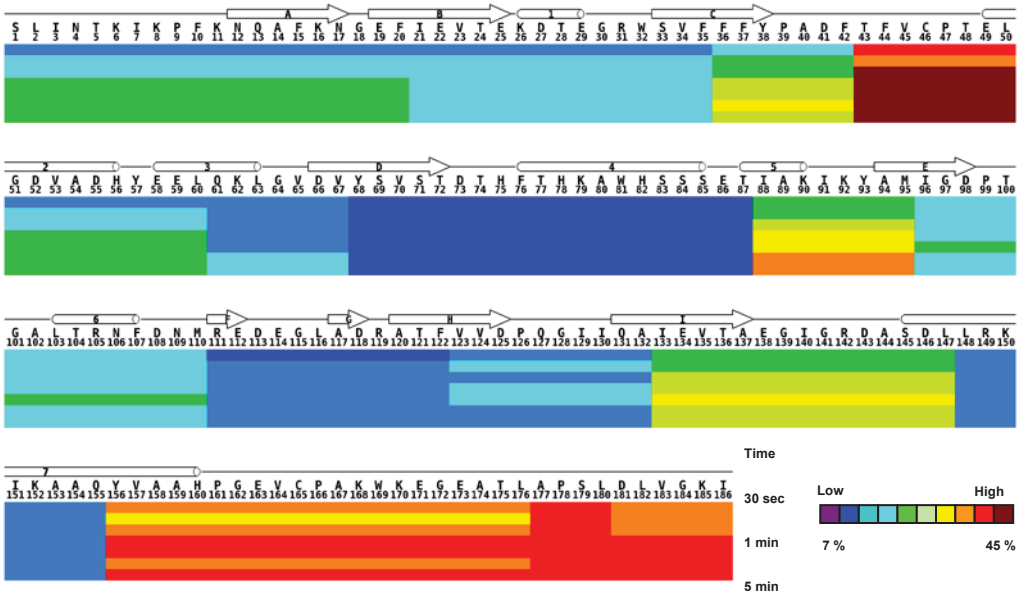

Figure S2. HDX-MS analysis of oxidized *St*AhpC T77I

23 **HDX-MS analysis of oxidized StAhpC T77I**

A

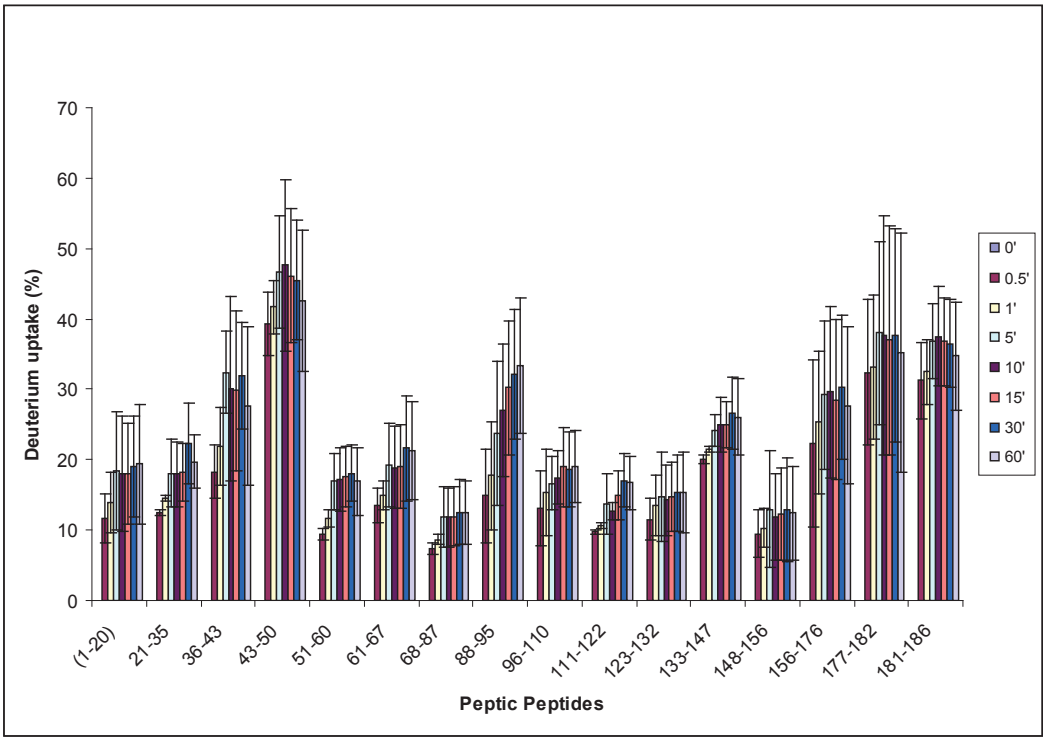

B

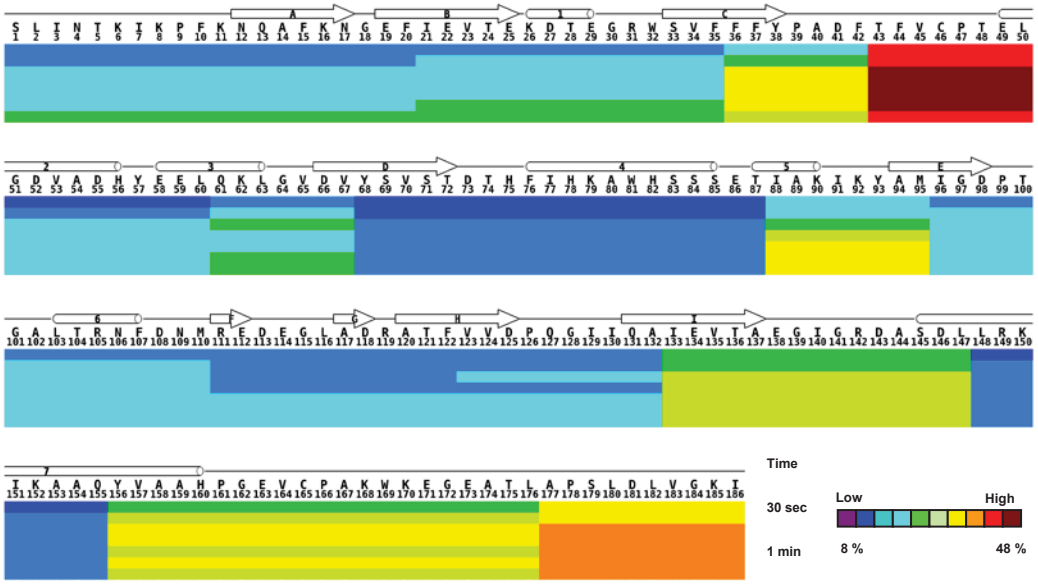

Figure S3. HDX-MS analysis of oxidized *St*AhpC T77V

24 **HDX-MS analysis of oxidized StAhpC T77V**

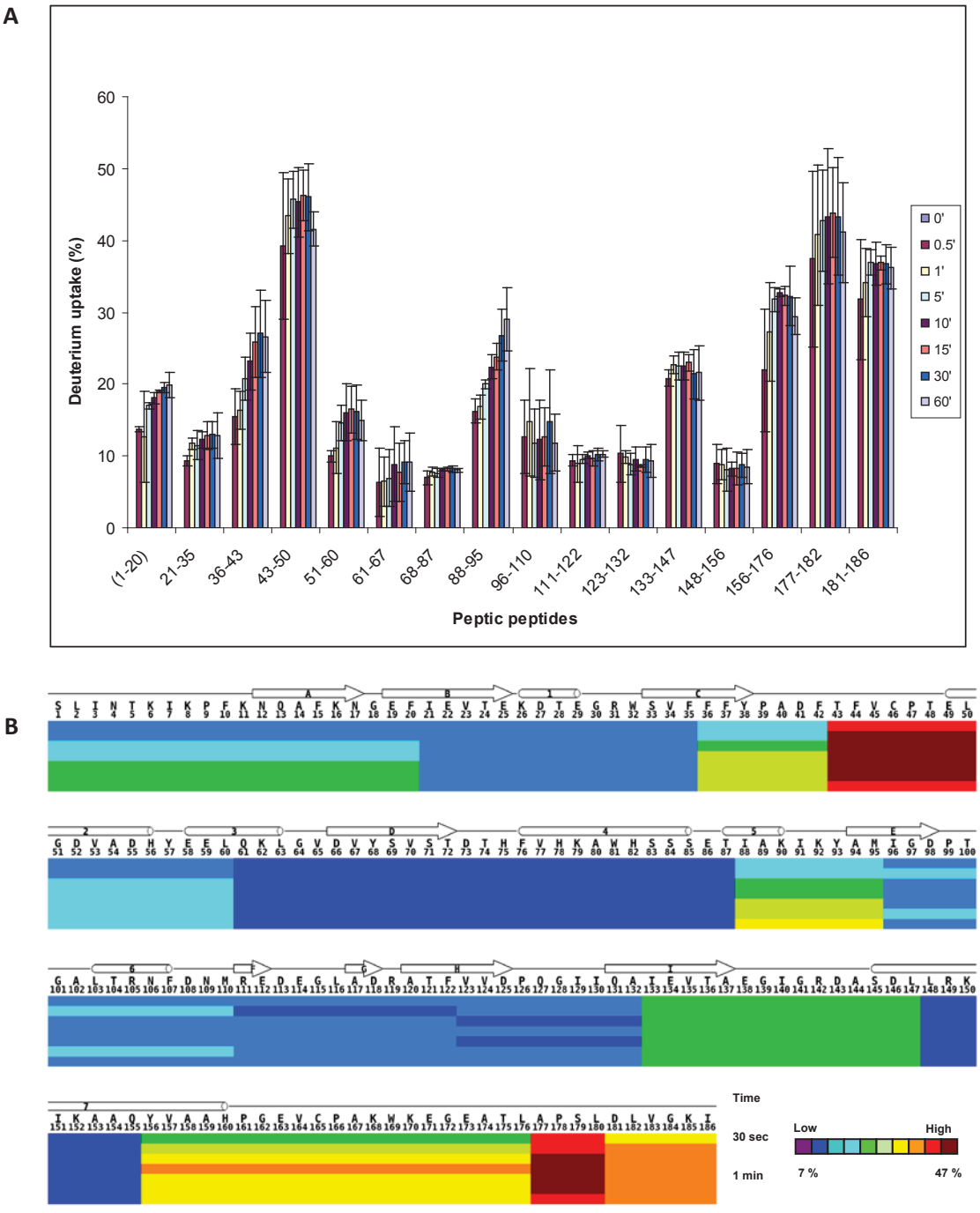

Figure S4. HDX-MS analysis of reduced *St*AhpC

25 **HDX-MS analysis of reduced StAhpC**

A

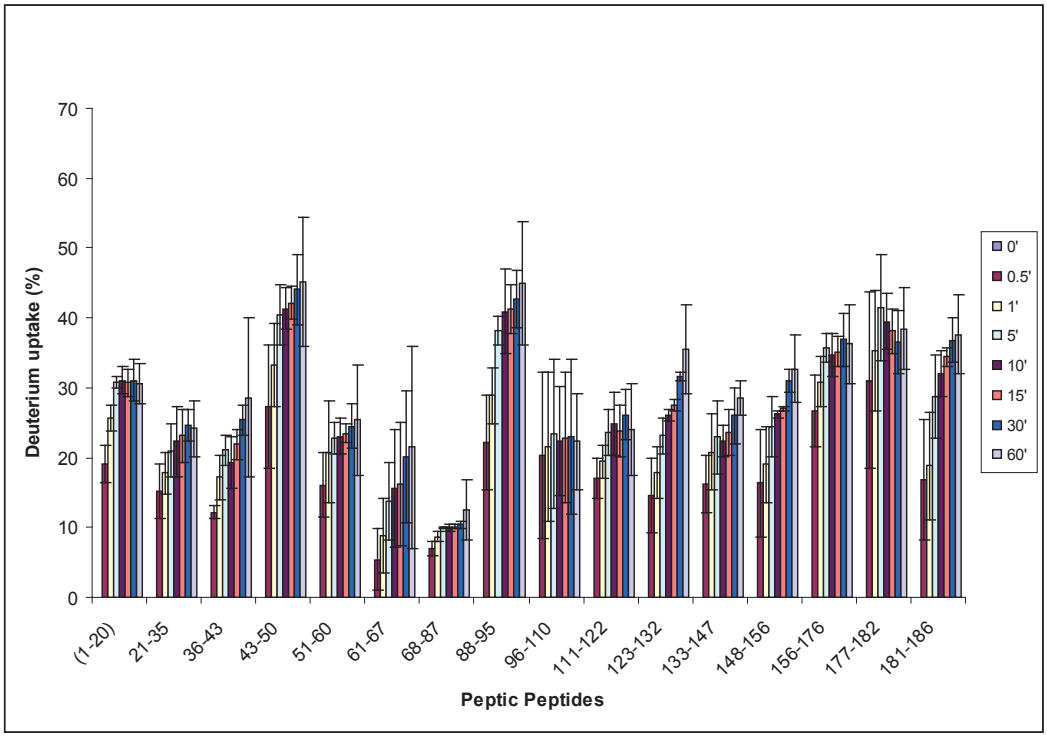

B

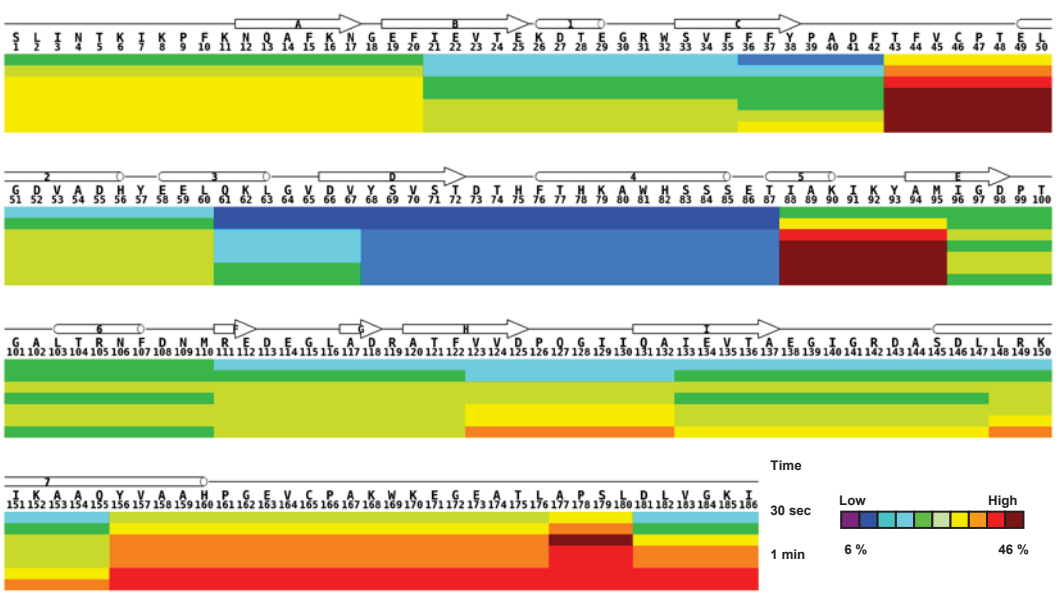

Figure S5. HDX-MS analysis of reduced *St*AhpC T77I

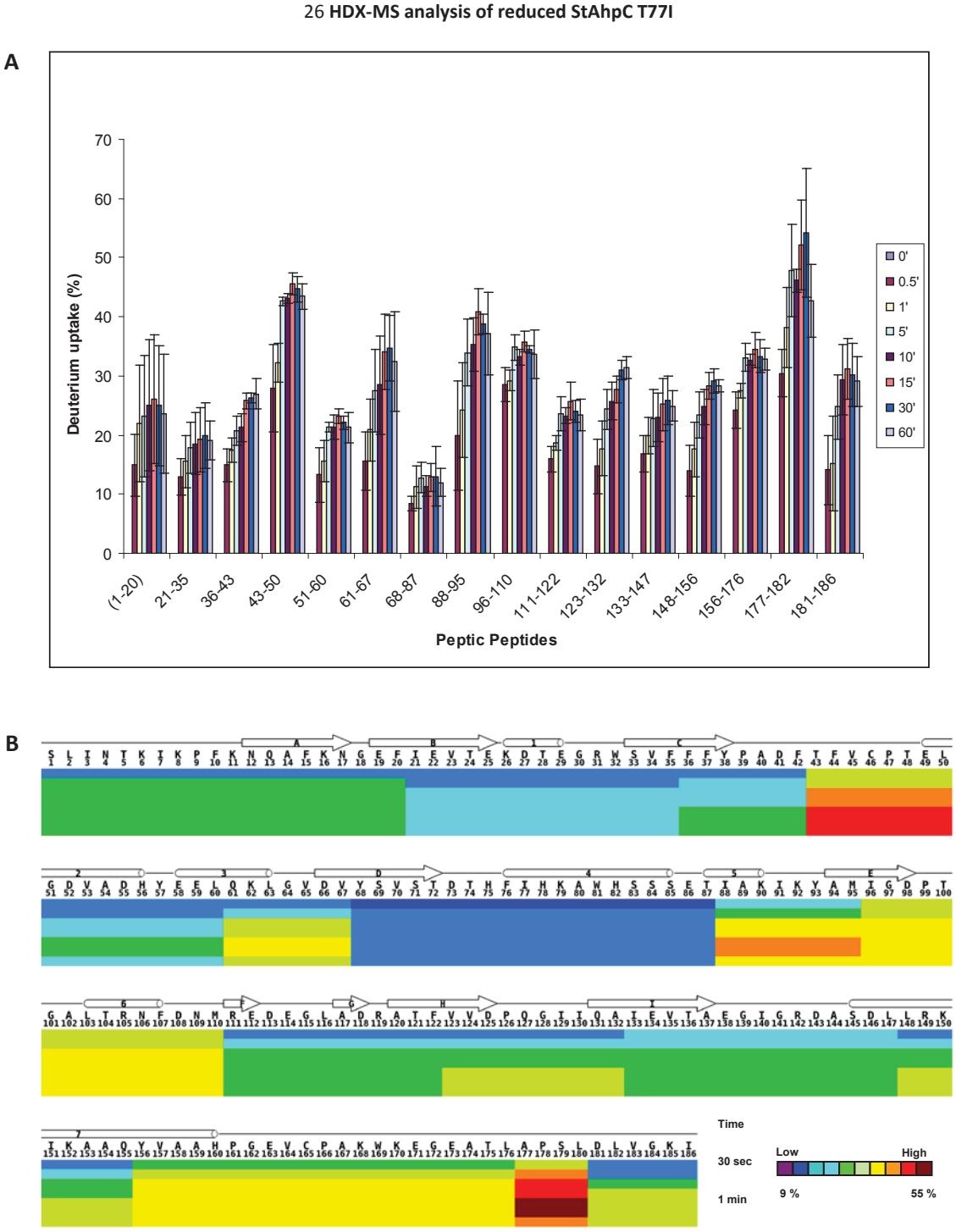

HDX-MS analysis of reduced *St*AhpC T77V

27 **HDX-MS analysis of reduced StAhpC T77V**

A

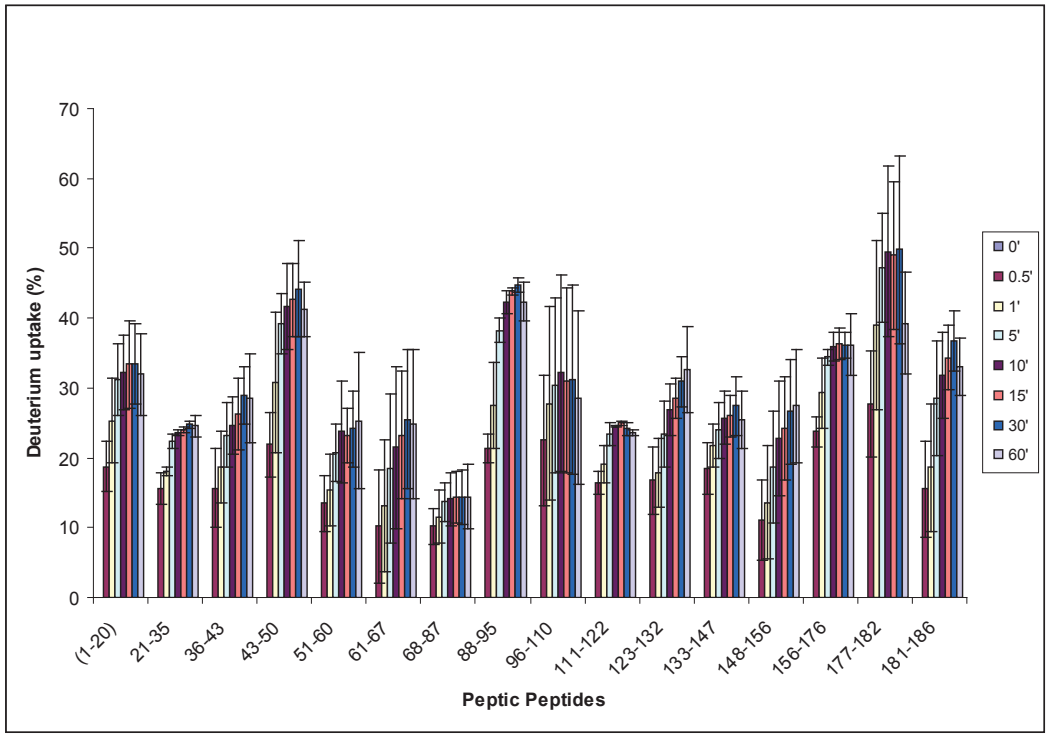

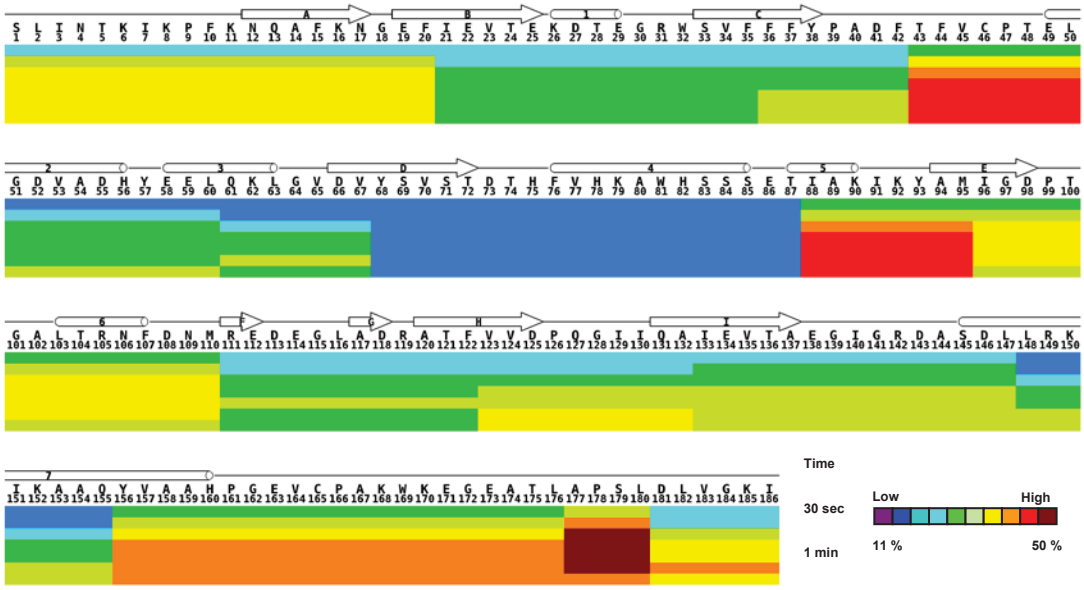

4 Chapter

Comparative Studies of Solution Dynamics of the Robust *Salmonella typhimurium* AhpC and Sensitive Human Peroxiredoxin2 using Hydrogen Deuterium Exchange Mass Spectrometry

Sasidhar Nirudodhi[1], Derek Parsonage[2], P. Andrew Karplus[4],

Leslie B. Poole[2], Yuan Jiang[3], and Claudia S. Maier[1]

Department of Chemistry, Oregon State University;

Department of Biochemistry, Wake Forest University School of Medicine, Medical Center Boulevard, Winston-Salem, NC 27157, USA;

Department of Statistics, Oregon State University;

Department of Biochemistry and Biophysics, Oregon State University, Corvallis, OR 97331, USA;

Abbreviations

Alkyl hydroperoxide reductase C-22 (AhpC); Peroxiredoxin,Prx; *Salmonella typhimurium* AhpC (*St*AhpC); wt, wild-type; C46S mutant, Cysteine-46 Serine mutants; Human peroxiredoxin2 (Prx2).

4.1 Introduction

Peroxiredoxins (Prxs) are ubiquitous cysteine based peroxidases that function as antioxidant enzymes in many organisms. These are highly abundant protein systems that reduce peroxide substrates using conserved reactive cysteine residue to regulate peroxide levels in the cells. They are important for developing new drug targets as many pathogens use Prxs as a defenses mechanism to counteract the peroxide exposure generated by the host immune system [1-3]. Prxs were initially known only for their antioxidant protection but later found to be involved in peroxide mediated signaling pathways [4, 5]. There are diverse classes of Prxs that are grouped into several families and sub classes based on the location of the peroxidatic cysteine (C_P) and the resolving cysteine (C_R), and the types of disulfide bonding that link the subunits. Several reviews describing the chemistry, function and structural changes of Prxs are available [6-8]. Our primary focus is on typical 2-Cys Prxs [6, 9]. Typical 2-Cys Prxs are homo-dimers and a disulfide bond is formed between the conserved C_P of the active site loop of one subunit and C-terminal end C_R of the second subunit of a dimer. The catalytic cycle involves three major steps: peroxidation, resolution, recycling and a side step reaction called overoxidation [10]. Peroxidation occurs in the fully folded confirmation but the active site loop needs to undergo a partial unfolding for the resolution to occur. Delay of the resolution step can lead to the overoxidation of the active site to form cysteine sulfinic acid [8].

Overoxidation or hyperoxidation is an oxidative inactivation step observed as a competing side reaction with resolution among several Prxs. The Cys-sulfenic acid (Cys-S_P-OH) upon reaction with a second molecule of peroxide forms Cys-sulfinic acid (Cys-S_PO_2H) and can further react with a third peroxide to yield Cys-sulfonic acid (Cys-S_PO_3H). This overoxidation was thought to be a permanent inactivation step but later a sulfiredoxin enzyme was found to reverse the inactivation back to the

peroxidatic cysteine. This oxidative inactivation and reversal among eukaryotic Prxs has suggested a role for Prxs in peroxide-mediated cellular signaling. Prxs with higher propensity towards oxidative inactivation are referred as “sensitive” Prxs. All eukaryotic Prxs are sensitive to overoxidation [11, 12]. Prxs that are not sensitive towards overoxidation are characterized as “robust” Prxs. Many bacterial Prxs are robust [4] towards overoxidation. It was proposed that sensitivity of eukaryotic Prxs was probably due to the presence of the following specific structural features: the GGLG and YF motifs [9]. These motifs contribute to the delay of the unfolding of the C_P and C_R active site loops to form a disulfide bond which allows the C_P residue of reacting with second and third molecules of peroxide substrates resulting in the oxidation inactivation of eukaryotic Prxs. The decameric form of the protein tends to be catalytically active in reducing peroxides.

Functionality of a protein is directly related to its structure and there are several studies describing the eukaryotic and bacterial Prxs [13]. Most of the high resolution structural information of Prxs is provided by X-ray crystallography, but the atomically resolved structures are confined in a static crystal environment which is not completely representative of the physiological environment. The dynamics of a protein in a physiologically relevant solution phase can be studied by applying an alternative technique such as hydrogen deuterium exchange mass spectrometry (HDX-MS). HDX-MS enabled us to compare the conformational dynamics of sensitive and robust Prxs in solution phase. As part of this study we performed HDX-MS experiments of robust peroxirdoxins, i.e. the *Salmonella typhimurium St*AhpC ($Wt_{S\text{-}S}$) (LU, locally folded) and the a C46S mutant of *St*AhpC aswhich mimics the Wt_{SH} (FF, fully folded) form and as representative of the sensitive peroxiredoxins, the human Prx2 in its thiol form.

4.2 Materials

Deuterium oxide (99.999 atom% D), biochemical grade potassium phosphate monobasic (KH_2PO_4) and potassium phosphate dibasic anhydrous (K_2HPO_4) were purchased from Sigma Aldrich Co (St.Louis, MO) and tris(2-carboxy-ethylphosphine) hydrochloride (TCEP.HCl) was obtained from Thermo/Pierce (Rockford, IL).

The wild-type protein, C46S mutant of StAhpC and Human Peroxiredoxin-2 (Prx2) were prepared and purified in Dr. Poole's laboratory (Wake Forest University) according to published protocols [19] and stored at −80 ºC. Reduced proteins were prepared by adding 0.5 µL 0.01M TCEP.HCl (in 25mM phosphate buffer, pH 7) to 0.5µL protein stock solution (10mg/mL in 25mM potassium phosphate buffer containing 1mM EDTA, pH7). Deuteriated phosphate buffer solution (0.01 M pH 7) was prepared in D_2O, lyophilizing it and reconstituting the residue in D_2O twice. Quench buffer contained phosphate buffer solution (0.1 M pH 2.5) and 0.01 M TCEP.HCl; 18 M concentrated HCl was used to adjust the pH of the quench buffer solution to pH 2.5.

4.2.1 Hydrogen deuterium exchange labeling

The protein stock solution was equilibrated at room temperature for 30 min. HDX labeling reaction was initiated by adding 10 µL of deuterated phosphate buffer solution (0.01 M pH 7) to 0.5 µL of the protein stock solution. Labeling was carried out for different reaction time points (0.5, 1, 2, 5, 10, 15, 30, 60, 120 min). Labeling reaction was then arrested by adding pre-cooled ice cold quench buffer and then flash frozen in liquid nitrogen (-80 ºC) until further analysis. Three replicates of each sample were prepared for all the time points. Three control samples were also prepared with undeuterated buffer solution for peptide identification. Each of three proteins, i.e. wild type FF ($Wt_{S\text{-}S}$) (10 mg/mL),

C46S mutant LU (3.6 mg/mL) of *St*AhpC and Prx2 proteins (10 mg/mL), was labeled using the same protocol [14].

Frozen deuterated protein samples were thawed, centrifuged quickly and injected into sample loop of the HDX-chiller module integrated with nanoAcquity UPLC for online pepsin digestion. MS grade water with 0.1 % formic acid was used as binary solvent manager (BSM) solvent A, acetonitrile with 0.1 % formic acid was used as BSM solvent B and water with 0.1% formic acid was used as auxiliary solvent manager (ASM) solvent A throughout the UPLC run. To minimize the back exchange analytical solvents were precooled in ice buckets. Once the process was manually triggered, a constant flow rate of 100 µL/min of ASM A solvent pushes the deuterated sample from the sample loop and carries the protein solution through the pepsin column for non-specific proteolytic digestion. A separate chamber for pepsin column was maintained at 9 ºC appropriate for peptic proteolytic digestion. The rest of the HDX chiller module system was maintained at 0 ºC to minimize back exchange. The eluted peptic peptides were trapped on a UPLC BEH C18 (0.1 µ, 1mm) guard column and washed for 3 min to remove the buffers and other salts. Trapping was followed by analytical separation of peptic peptides in an Acquity UPLC BEH C18 (1.7 µ, 1.0 mm x 100 mm) reverse phase column. A 12 min short gradient (starts with 8% of solvent B and ramps to 40% in 6 min and by 7 min it ramps to 85% and stays at 85% until 9 min and finally by 10 min it linearly ramps down to 8% and stays there for 2 min) with a constant flow rate of 40 µL/min was used for analytical separation of peptic peptides. The separated peptides were eluted into the electrospray ionization (ESI) source of the Waters Synapt G1 HDMS mass spectrometer for subsequent mass analysis.

4.2.2 ESI-MS Analysis

Eluted peptides were sprayed using an ESI source operated at 3 kV. The source cone was maintained at 40 V. The mass spectrometry data was acquired over a mass range of m/z 100 to 2000. Ions were fragmented using MS^E tandem mass spectrometry method. MS^E is a non-selective fragmentation method used for fragmenting all the ions in the trap chamber. MS^E is also referred to as "hi low" as it uses two MS functions in an alternating fashion. At low energy a survey scan at 10 eV was performed enabling conditions in which almost no fragmentation of the precursor ions was observed. Whereas, at elevated energy (25 eV) the precursor ions were fragmented in the gas cell (referred as trap). For mass calibration, 250 pmols/µL Glu^1 fibrinopeptide B (prepared in 30% ACN with 0.05% formic acid) with a constant flow rate of 10 µL/min was used as a reference lock mass solvent and sprayed every 30 sec. The lock mass sample cone was maintained at 37 V, trap CE (collision energy) at 10 V and the scan time was 0.3 sec.

4.2.3 Data Analysis

4.2.3.1 PLGS

The raw data acquired for the undeuterated control samples were processed using ProteinLynx Global SERVER (PLGS) V2.5.2 for peptide identification and sequence assignment. PLGS considers the low energy and elevated energy data including their properties such as mass to charge ratio, retention time and ion intensity derived from the area calculated from chromatographic and mass spectrometric peaks for each ion. PLGS produces a precursor and product ion list. The peak apexes are located and data calibrated and then lock mass corrected. PLGS deconvolutes precursor and product ions and matches the precursor products and peptide fragments. It scores the peptides and calculates the false positive rate. The final peptide list is created as an ion accounting file in .CSV format. It includes protein

list, peptide ion list and their product ion list. The peptide list includes properties of each peptide such as intensity, charge, m/Z, retention time, sum of product ion intensity etc.

4.2.3.2 DynamX

Multiple PLGS results obtained by processing the three replicates of undeuterated raw data files were imported to DynamX software. DynamX software aggregates the peptides from multiple search results and generates a grand peptide list. Peptides can be filtered from the grand list by applying a threshold on several parameters (minimum intensity of a peptide, minimum sequence length in a peptide, minimum number of product ions identified, minimum number of product ions identified per amino acid residue, minimum number of consecutive product ions identified, minimum total intensity of all identified product ions, minimum score and maximum MH+ error (ppm)) to generate more reliable and desired peptide list. Replication thresholds can be set to include the peptides with higher replication. Mass spectrometric raw data files of deuterated and control samples were imported to the DynamX software. User defines each raw data file with the respective labeling time and the state of the protein for the HDX analysis. Software scans for detected ions and searches them across the peptide list to match its properties and finalizes the peptide spectra for all raw data files in each state. DynamX calculates the average deuterium uptake as a difference between the centroid mass of deuterated and undeuterated peptide spectra with observed standard deviation calculated from the replicates. Results can be viewed for each peptide as a function of labeling time. A separate window can be opened to view the stacked spectra for all time points. There is a provision for viewing the spectra of other charge states available for the same peptide in the stacked spectra window. Each peptide was manually cross checked before considering it for deuterium uptake information. The deuterium uptake data for the finalized peptides can be exported as a .CSV file to the desired location. The final data can also be viewed as a

butterfly plot to compare the differences among two states of the protein. It also provides the coverage information from the overlapping peptides.

4.2.3.3 Kinetic modeling of HDX-MS data

Several methods available have been described for extracting the rate constants "k" values from the HDX data [15-18]. A fixed-rate-constant binning model was used to fit the peptide kinetic data using R statistical software by minimizing the sum of squared error (SSE). Six rate constants (k = 100, k = 10, k = 1, k = 0.1, k = 0.001, k = 0.0001) were selected. Each dataset of three replicates were fit together and the fitted curves were displayed with average values and their standard deviation as error bars. In this study we have used a fixed rate binning model as this allowed us to assign the exchangeable backbone amide hydrogens into six different groups based on their exchange rate constants which enabled a comparative evaluation of the three different protein systems analyzed in this study. A compilation of the results obtained using the fixed-rate constant binning model for human Prx2 HDX-MS data is presented (Table 4). The curve fitting plots for specific peptides belonging to human Prx2 are presented (Figure 4-8).

4.3 Results and Discussion

4.3.1 Peptide level HDX-MS analysis of C46S mutant and Wild-type Prxs:

To study the redox dependent oligomeric changes observed in *St*AhpC, we compared the peptide level deuterium uptake data of $Wt_{S\text{-}S}$ LU with C46S mutant mimicing the Wt_{SH} FF form. The C46S mutant represents the fully folded form of Prxs in the thiolate form (WtSH).

We used HDX-MS to study the conformational dynamics of $Wt_{S\text{-}S}$ LU form and the C46S FF form of *St*AhpC. The filtered peptide list was obtained from DynamX software for both protein states. Common peptides available among both protein states were selected from the filtered list. A subset of common peptides was selected to cover the protein sequence. The common peptides allowed us to compare the peptide deuterium uptake of $Wt_{S\text{-}S}$ LU form and the C46S FF form of the protein. Overlapping peptides were only used if more information was needed at specific regions. In the entire study, back exchange correction was not performed on the deuterium uptake data. Relative deuterium uptake obtained from the DynamX software for each peptide was normalized to compare them among different peptides in the same protein state. Normalized relative deuterium uptake (%) of a peptide was calculated by dividing the relative deuterium uptake with number of exchangeable backbone amide hydrogens in each peptide. Normalized values were calculated for both protein states. The average normalized values and their standard deviations were calculated from their replicate. Number of exchangeable backbone amide hydrogens in each peptide was given by number of amino acids subtracted by the N-terminal amino acid (i.e., 1) and number of prolines present in a peptide.

The normalized deuterium uptake profiles of C46S mutant Prx was presented in a bar graph (Figure 2) with peptic peptides arranged in a sequential order. Peptides with higher deuterium uptake represent higher flexibility in the region whereas the ones with lower deuterium uptake represent higher protection from solvent accessibility or lower flexibility.

It is clearly evident from Figure 2 that the peptides encompassing the active site C46 loop and the C-terminal end exhibited highest deuterium uptake. No significant change was observed in the deuterium uptake among both peptides over different labeling times (30 s or 15 min or 60 min) (Figure 2.a). Higher deuterium uptake observed for the peptide encompassing the C-terminal end represents higher flexibility in the region and this is in compliance with the fact that the C-terminal region is known

to be more flexible without secondary structural elements. The peptide 123-132 that covers the partial sequence of β8 and β9 strands and the peptide 148-156 encompassing the α7 helix region exhibited lowest deuterium uptake (<10%) and indicating the highest degree of protection in these regions of the C46S mutant.

We compared the HDX-MS data with the B-factors data extracted from the crystal structures. Whereas the active site loop represented by the peptide 44-50 exhibited relatively higher uptake, as it was expected to be representing the Wt_{SH} FU fully folded form of the protein.

4.3.2 Statistical Analysis

Two Way ANOVA:

In order to identify region that showed significant differences in deuterium levels we performed a statistical analysis of two-way-Anova on the deuterium levels observed for *St*AhpC and its single point mutant C46S representing the disulfide-reduced form of *St*AhpC. The resulting p-values (for wild type and C26S mutant *St*AhpC protein forms over a series of time points) are summarized in table 3. Peptides with p-values less than 0.05 are considered to be significantly different and differences for peptides with p-values greater than 0.05 were considered as not significant. In this study we used the p-values as mean to evaluate the degree of significant difference between the peptide derived from the two protein forms. In general, as smaller the p-value below 0.05 as greater the significance in deuterium levels observed between the peptides derived from the two proteins investigated. Peptides were divided into two groups based on their p-values. Peptides with p-values from 0.005 to 0.05 were considered significantly different, whereas the peptides less than 0.005 were categorized as highly significant in their difference. Peptides covered in our current HDX-MS study with their respective p-values are compiled in Table 1.

The mutation at the cysteine 46 residue by the amino acid serine eliminates the possibility of disulfide bond formation between C_P and C_R in the C46S mutant. This makes the C46S mutant attain a fully folded closed conformation. The HDX differences between these two forms are apparent in figure 3.c. When deuterium uptake data of $Wt_{S\text{-}S}$ LU form and C46S mutant Prx were compared most of the peptides exhibited significant difference. It was clearly evident from the differential deuterium level data (Figure 3) that the C46S mutant exhibited higher protection against the deuterium labeling compared to the wild type protein. Specifically, C46S peptides covering regions 51-60 and156-182 exhibited the highest level of protection against exchange. The absence of the disulfide bond allows the C-terminal regions to adopt a closed conformation and this is confirmed by the higher protection observed in the peptide 156-182. The peptide 51-60 being adjacent to the C46S mutation site showed higher protection compared to the peptide 44-50 which indicated that the conformational mobility was in regions distant from the point mutation and immediate vicinity. The regions encompassing the peptides 123-132 and 148-156 were the only ones that exhibited higher flexibility in the C46S mutant compared to its wild type counterpart.

A fully deuterated $Wt_{S\text{-}S}$ *St*AhpC was prepared as reference for evaluating the potential loss of deuterium labeling information due to back exchange during the analytical workflow. The same protocol was used to acquire the kinetic HDX-MS data maintaining all the experimental conditions and parameters constant. The maximum deuterium incorporation observed for the peptic peptides was 70%. This indicates that the online pepsin digestion integrated with UPLC separation and ESI-MS data acquisition contributed to 30% back exchange (carried out in Waters HDX chiller module integrated in Waters nanoAcquity UPLC with Synapt HDMS G1 setup).

4.3.3 Human Prx2:

The human Prx2 is sensitive to overoxidation [4, 11]. We attempted to gain further structural insights into its sensitivity towards overoxidation by studying the structural and conformational dynamics of Prx2 using HDX-MS. The peptide level HDX-MS analysis was performed on the human Prx2 protein in the reduced form with no disulfide bond. From the finalized peptide list a subset of peptides that covered the entire protein sequence was selected for the deuterium uptake analysis. Overall, the highest deuterium uptake observed in this protein was much less compared to the deuterium uptake data that we had obtained for the bacterial Prxs studied. Within the Prx 2 (thiol form) HDX-MS data set the active site Cys-51 region represented by the peptide 47-55 exhibited the highest deuterium uptake (~28%) compared to the other peptides covering entire protein sequence. The peptides 16-27, 35-56, 48-57, 86-104, 141-156, 164-181, and 182-193 also exhibited high deuterium uptake compared to the rest of the protein. Peptide encompassing regions 28-37, 78-84, 119-130, 133-140, 157-163 exhibited very low deuterium uptake and the rest of the peptides 2-15, 16-25, 42-48, 58-65, 65-73, 85-104, 105-118, 146-156 had a medium deuterium uptake.

Peptides were categorized into three groups based on their deuterium uptake (Table 1). The kinetic profiles of the deuterium uptake over different labeling times were different for several peptides. Peptide level deuterium uptake of the regions 4-15, 16-27, 28-37, 133-140, had a very small incremental change in deuterium uptake over the labeling period. Peptide 182-193 encompassing the C-terminal end of the protein was the only peptide that exhibited no significant change in its kinetic profile over the labeling period. The rest of the peptides exhibited a significant change in deuterium uptake over time. The rate constants obtained by fitting the kinetic HDX-MS data are compiled in Table 4.

4.3.4 Comparison of Human Prx2 *versus* C46S mutant *St*AhpC Prxs

Human Prx2 and *St*AhpC are proteins with high structural similarity with different amino acid sequence that exhibit reverse tendency towards overoxidation. To investigate their inverse tendency towards overoxidation, we propose to compare the deuterium uptake data acquired from the HDX-MS studies of human Prx2 and *St*AhpC that represents the structural conformations and dynamics of proteins. Different amino acid sequence of Prx2 and *St*AhpC shuns the direct comparison of their deuterium uptake data. Human Prx2 and wild type *St*AhpC were sequence aligned based on their structural similarity as described in Wood et al [4]. As the current human Prx2 studied is in reduced form, HDX-MS data of C46S mutant *St*AhpC was also included in the comparison as it mimics the reduced form of *St*AhpC. The aligned deuterium uptake data of human Prx2, wild type and C46S mutant *St*AhpC is presented in a line plot (Figure 6).

When aligned deuterium uptake profiles were compared, it became apparent that deuterium uptake of Prx2 and *St*AhpC exhibited similar trends with higher deuterium uptake observed at the active site loop region (C_P), A-interface region and C-terminal end (C_R) regions. A significantly lower deuterium uptake was observed in those regions of the human Prx2 protein compared to its bacterial counterpart. Remaining regions of the Prx2 also exhibited a lower deuterium uptake compared to *St*AhpC. Relatively low deuterium uptake of Prx2 confirms the lower flexibility and higher protection towards solvent accessibility. We speculate a closed and compact structural conformation for Prx2.

To understand this further, the B-factors of Prx2 and *St*AhpC were extracted from their respective crystal structures. B-factor values were sequence aligned based on their structural similarity and presented in a line plot (Figure 7). B-factors data of Prx2 and *St*AhpC also exhibited similar trend along their sequence compared to the deuterium uptake data.

Overall, the HDX-MS seem to indicate that human Prx2 attains a relatively closed and solvent-protected conformation compared to the C46S mutant *St*AhpC. From our initial results we speculate that Prx2 attains a relatively closed and compact overall conformation which seems to be concurrent with the apparent rigidity that also seemed to be reflected in the B-factor values that were observed in the X-ray structure (pdb file 1QMV). Further studies are needed to unravel the conformational properties of Prx 2. In particular a comparative study of the thiol form of PRX (current study) with the disulfide-linked form of the Prx2 is suggested to deepen our understanding regarding the conformational aspects that contribute to the sensitivity of human Prxs.

4.4 References

1. Chen, L., Q.W. Xie, and C. Nathan, *Alkyl hydroperoxide reductase subunit C (AhpC) protects bacterial and human cells against reactive nitrogen intermediates.* Mol Cell, 1998. **1**(6): p. 795-805.
2. Fang, F.C., *Perspectives series: host/pathogen interactions. Mechanisms of nitric oxide-related antimicrobial activity.* J Clin Invest, 1997. **99**(12): p. 2818-25.
3. Seaver, L.C. and J.A. Imlay, *Alkyl hydroperoxide reductase is the primary scavenger of endogenous hydrogen peroxide in Escherichia coli.* J Bacteriol, 2001. **183**(24): p. 7173-81.
4. Wood, Z.A., L.B. Poole, and P.A. Karplus, *Peroxiredoxin evolution and the regulation of hydrogen peroxide signaling.* Science, 2003. **300**(5619): p. 650-3.
5. Cox, A.G., C.C. Winterbourn, and M.B. Hampton, *Mitochondrial peroxiredoxin involvement in antioxidant defence and redox signalling.* Biochem J, 2010. **425**(2): p. 313-25.
6. Hall, A., P.A. Karplus, and L.B. Poole, *Typical 2-Cys peroxiredoxins--structures, mechanisms and functions.* FEBS J, 2009. **276**(9): p. 2469-77.
7. Parsonage, D., P.A. Karplus, and L.B. Poole, *Substrate specificity and redox potential of AhpC, a bacterial peroxiredoxin.* Proc Natl Acad Sci U S A, 2008. **105**(24): p. 8209-14.
8. Parsonage, D., et al., *Analysis of the link between enzymatic activity and oligomeric state in AhpC, a bacterial peroxiredoxin.* Biochemistry, 2005. **44**(31): p. 10583-92.
9. Hall, A., et al., *Structure-based insights into the catalytic power and conformational dexterity of peroxiredoxins.* Antioxid Redox Signal, 2011. **15**(3): p. 795-815.
10. Karplus, P.A. and L.B. Poole, *Peroxiredoxins as molecular triage agents, sacrificing themselves to enhance cell survival during a peroxide attack.* Mol Cell, 2012. **45**(3): p. 275-8.

11. Yang, K.S., et al., *Inactivation of human peroxiredoxin I during catalysis as the result of the oxidation of the catalytic site cysteine to cysteine-sulfinic acid.* J Biol Chem, 2002. **277**(41): p. 38029-36.

12. Poole, L.B., *The catalytic mechanism of peroxiredoxins.* Subcell Biochem, 2007. **44**: p. 61-81.

13. Rhee, S.G., et al., *Peroxiredoxin functions as a peroxidase and a regulator and sensor of local peroxides.* J Biol Chem, 2012. **287**(7): p. 4403-10.

14. Nirudodhi, S., et al., *Conformational studies of the robust 2-Cys peroxiredoxin Salmonella typhimurium AhpC by solution phase hydrogen/deuterium (H/D) exchange monitored by electrospray ionization mass spectrometry.* Int J Mass Spectrom, 2011. **302**(1-3): p. 93-100.

15. Yan, X., et al., *Hydrogen/deuterium exchange and mass spectrometric analysis of a protein containing multiple disulfide bonds: Solution structure of recombinant macrophage colony stimulating factor-beta (rhM-CSFbeta).* Protein Sci, 2002. **11**(9): p. 2113-24.

16. Frantom, P.A., et al., *Mapping of the allosteric network in the regulation of alpha-isopropylmalate synthase from Mycobacterium tuberculosis by the feedback inhibitor L-leucine: solution-phase H/D exchange monitored by FT-ICR mass spectrometry.* Biochemistry, 2009. **48**(31): p. 7457-64.

17. Miller, D.E., et al., *HDXFinder: automated analysis and data reporting of deuterium/hydrogen exchange mass spectrometry.* J Am Soc Mass Spectrom, 2012. **23**(2): p. 425-9.

18. Orban, T., et al., *Conformational dynamics of activation for the pentameric complex of dimeric G protein-coupled receptor and heterotrimeric G protein.* Structure, 2012. **20**(5): p. 826-40.

19. Schroder, E., et al., *Crystal structure of decameric 2-Cys peroxiredoxin from human erythrocytes at 1.7 A resolution.* Structure, 2000. **8**(6): p. 605-15.

Figure Legends

Figure 1 HDX-MS profile of wild-type *St*AhpC protein: Summary of normalized deuterium uptake percentages of peptic peptides acquired over a series of labeling reaction time points (0.5, 1, 2, 5, 10, 15, 30, 60, 120 min) arranged in a sequential order in a (a) bar graph, (b) Heat Map colored from blue to red refers to low to high deuterium uptake or low to high flexibility. All the time points are arranged one below the other. (c) Deuterium uptake data was overlaid on the crystal structure of wild-type *St*AhpC (1YEP).

Figure 2 HDX-MS profile of C46S mutant of *St*AhpC protein: Summary of normalized deuterium uptake percentages of peptic peptides acquired over a series of labeling reaction time points (0.5, 1, 2, 5, 10, 15, 30, 60, 120 min) arranged in a sequential order in a (a) bar graph, (b) Heat Map colored from blue to red refers to low to high deuterium uptake or low to high flexibility. All the time points are arranged one below the other. (c) Deuterium uptake data was overlaid on the crystal structure of C46S mutant of *St*AhpC (1N8J).

Figure 3 Comparative HDX-MS profile of wild-type and C46S mutant of *St*AhpC. (a) Differential HX-MS profile, Wt-C46S mutant, difference between the deuterium uptake data of wild-type and the C46S mutant is presented as a bar graph. Positive bars indicate regions that showed higher deuterium incorporation levels in the wild-type protein whereas the negative bars represent regions with lower deuterium uptake in wild-type protein. (b) Deuterium exchange-in data is overlaid on the X-ray structure of C46S mutant (1N8J). Red regions show higher deuterium uptake in the wild-type protein relative to the C46S mutant, i.e., more flexible and more solvent accessible in wild-type. Blue regions represent regions that show lower deuterium uptake, i.e., are more protected against exchange-in, in the C46S

mutant relative to the wild-type protein. (c) Differential deuterium uptake data was overlaid on the decameric form of C46S mutant (1N8J) for better representation.

Figure 4 Fully deuterated wild-type *St*AhpC data was presented in a bar graph format. Peptic peptides are arranged in a sequential order.

Figure 5 HDX-MS profile of human Prx2 protein: Summary of normalized deuterium uptake percentages of peptic peptides acquired over a series of labeling reaction time points (0.5, 1, 2, 5, 10, 15, 30, 60, 120 min) arranged in a sequential order in a (a) bar graph, (b) Heat Map colored from blue to red refers to low to high deuterium uptake or low to high flexibility. All the time points are arranged one below the other. (c) Deuterium uptake data was overlaid on the crystal structure of human Prx2 (1QMV).

Figure 6 Deuterium uptake data of wild-type *St*AhpC, C46S mutant of *St*AhpC and human Prx2 is assigned to each aminoacid and arranged in a line graph.

Figure 7 B-factors of wild-type *St*AhpC, C46S mutant of *St*AhpC and human Prx2 arranged according to their structure based sequence alignment in a line graph as described in Wood et al.

Table 1 High, Medium and Low Exchanging peptides: Peptides with high deuterium uptakes were associated with higher flexibility and lower protection. Medium exchanging peptides are moderately flexible and were associated with medium protection and the low exchange peptides have highest protection against exchange being very less solvent accessible. Peptides with gradual increase in the deuterium uptake over time: Some protected regions of the protein tend to breath and flex as part of their routine dynamics in the solution state. Regular breathing and flexing of the protein may increase the solvent accessibility to these protected regions tending to be more flexible over time.

Table 2 A statistical two-way ANOVA analysis was performed on the peptide level deuterium uptake of wild-type and C46S mutant of *St*AhpC proteins. Peptides were divided into three groups based on their p-values obtained.

Table 3 p-values obtained from the statistical two-way ANOVA performed on the peptide level deuterium uptake of wild-type and C46S mutant of *St*AhpC proteins are listed in the table. Red colored peptides were highly significant, orange were significant and the non-colored peptides were not significant in their difference.

Table 4 The HDX-MS data was fitted with a fixed-rate-constant binning model. All the exchangeable amide hydrogens are assigned to 6 binning groups as listed in the table.

Figure 1 28 HDX-MS profile of wild-type StAhpC

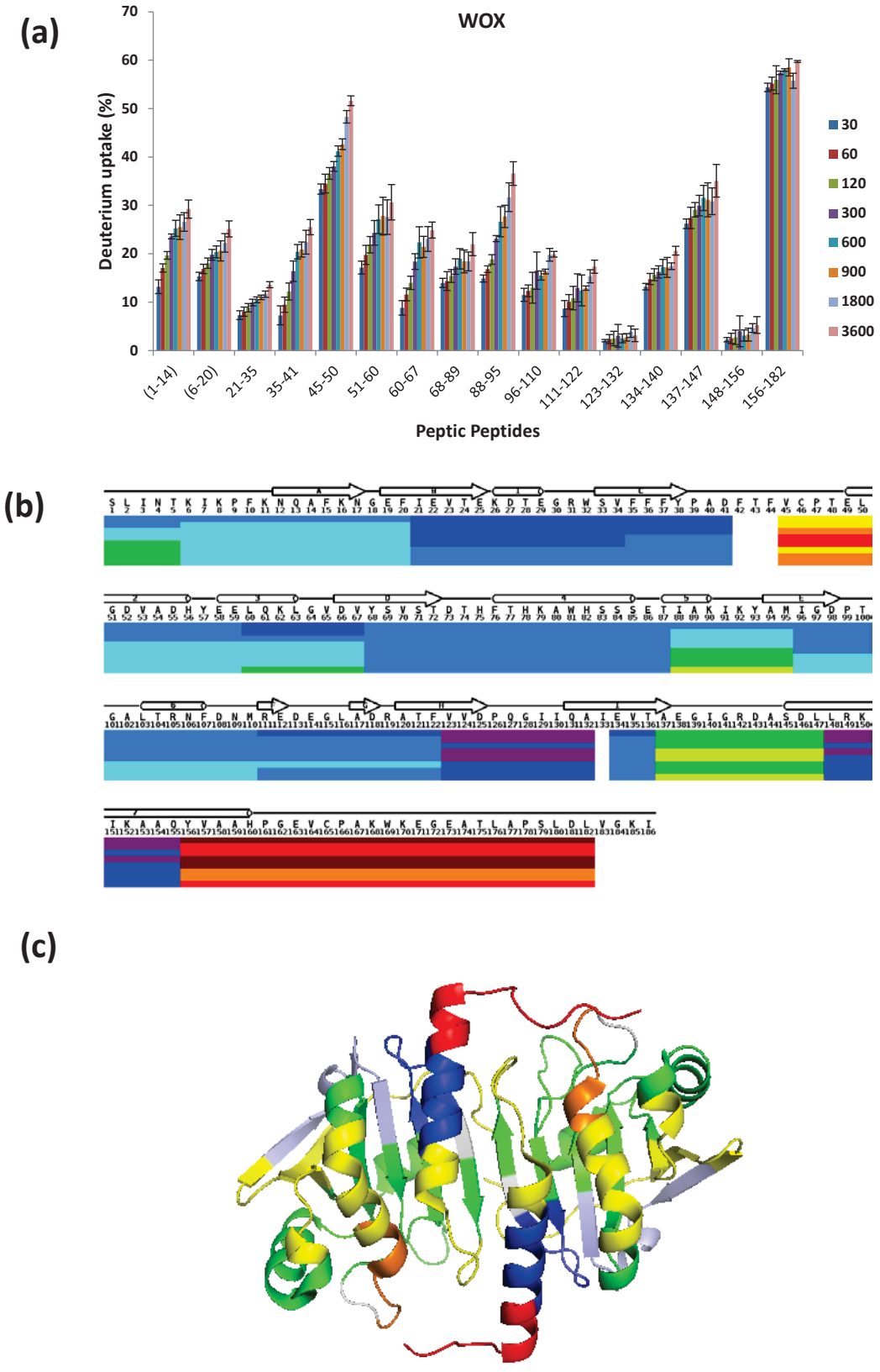

Figure 2 29 HDX-MS profile of C46S mutant of StAhpC

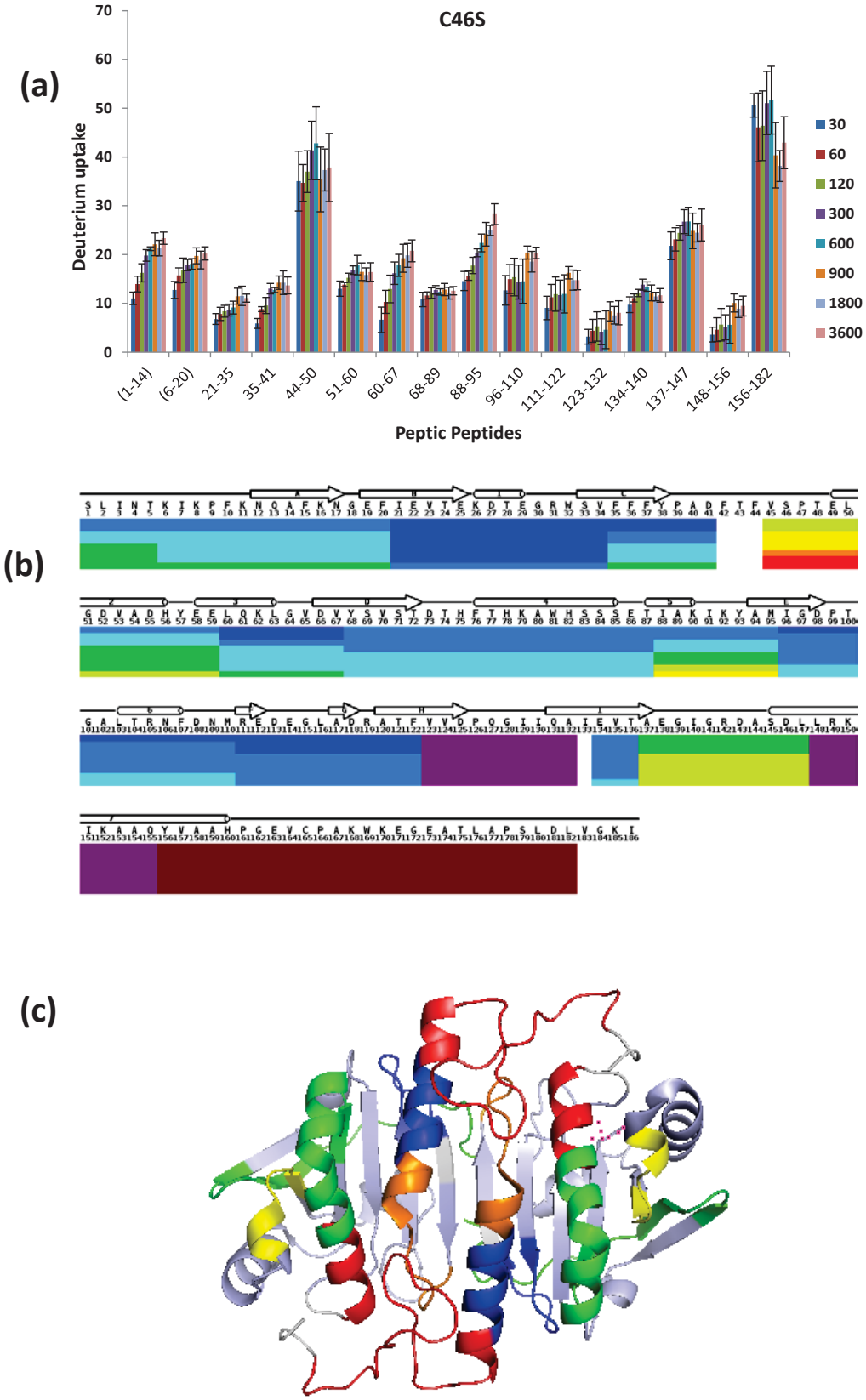

Figure 3

(a)

30 **Comparative HDX-MS profile of wild-type and C46S mutant of StAhpC**

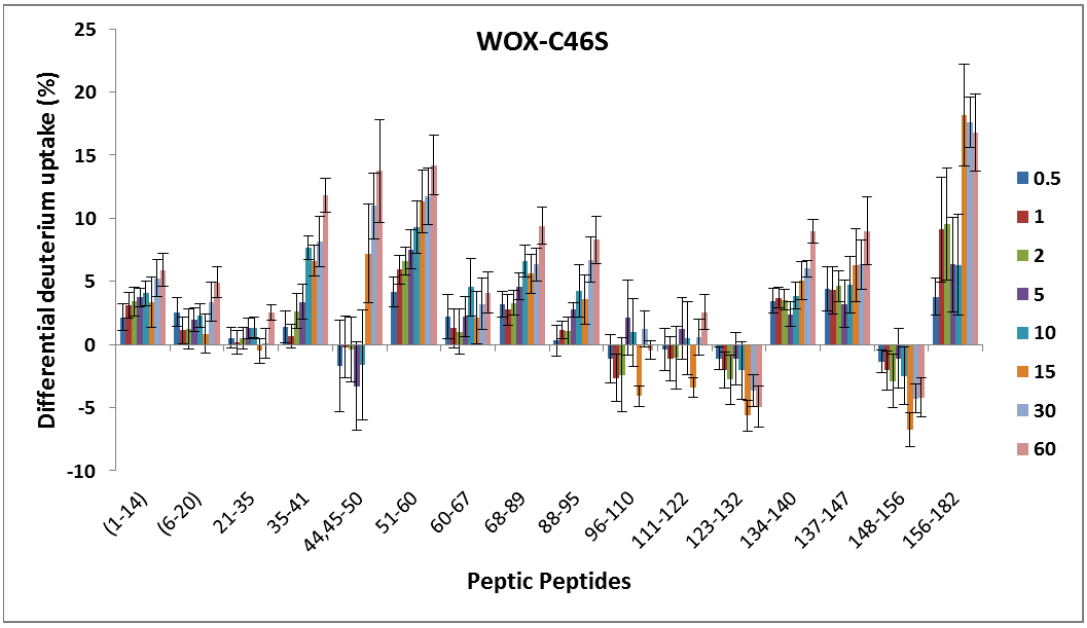

(b)

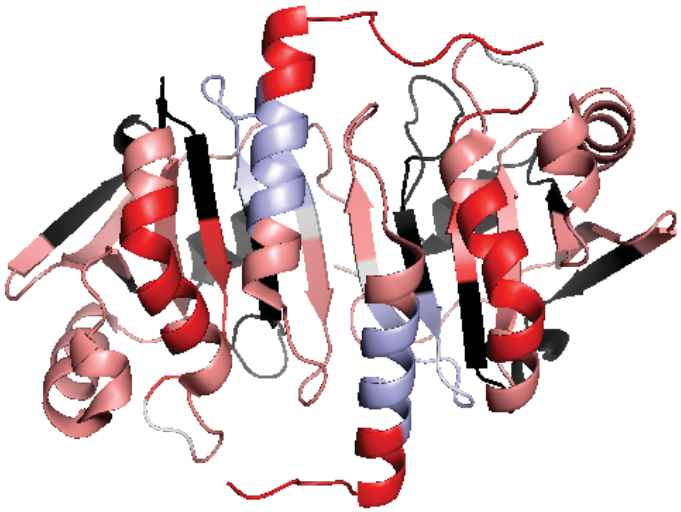

(c)

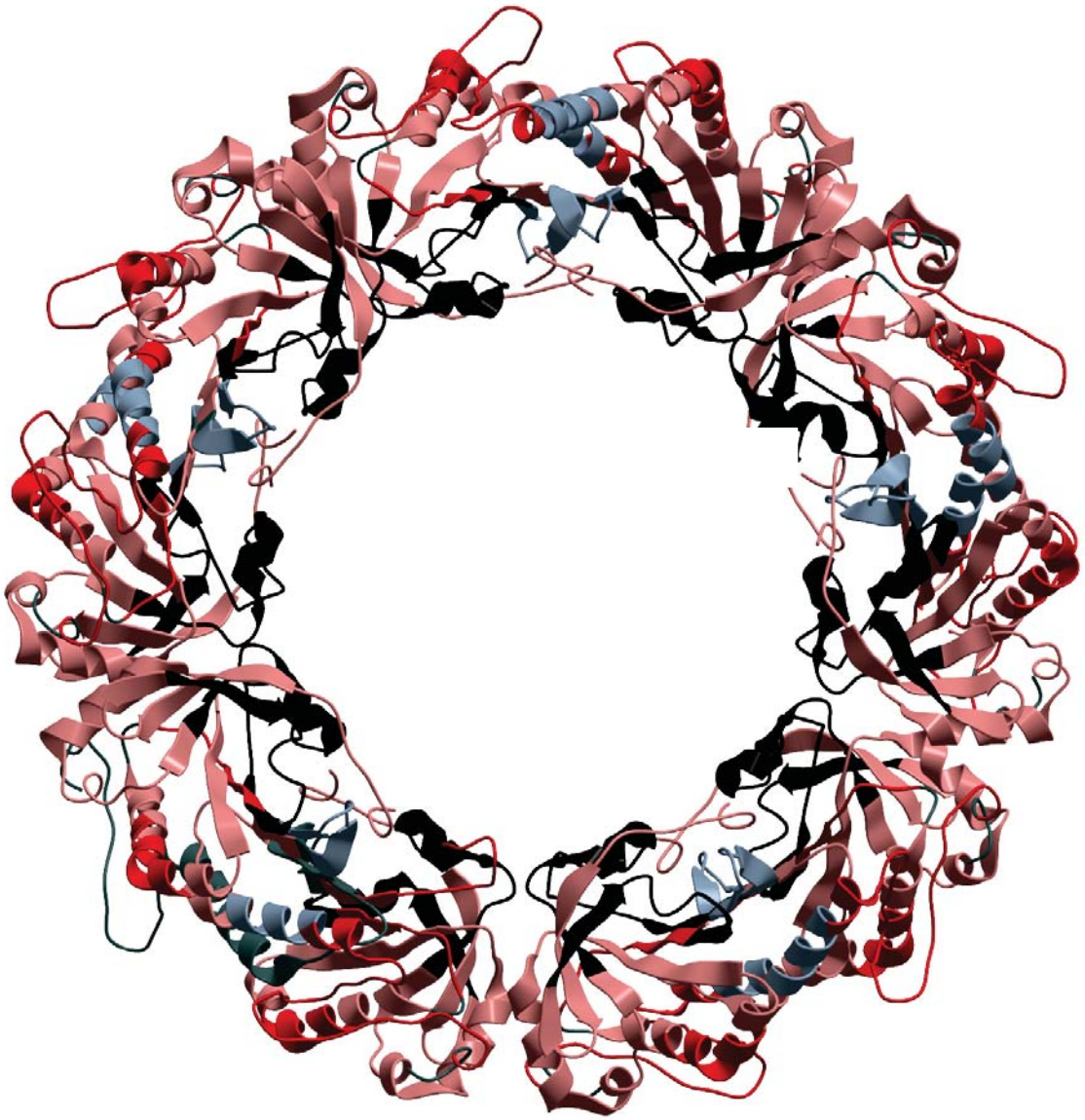

Figure 4

31 Fully deuterated wild-type StAhpC data in a bar graph

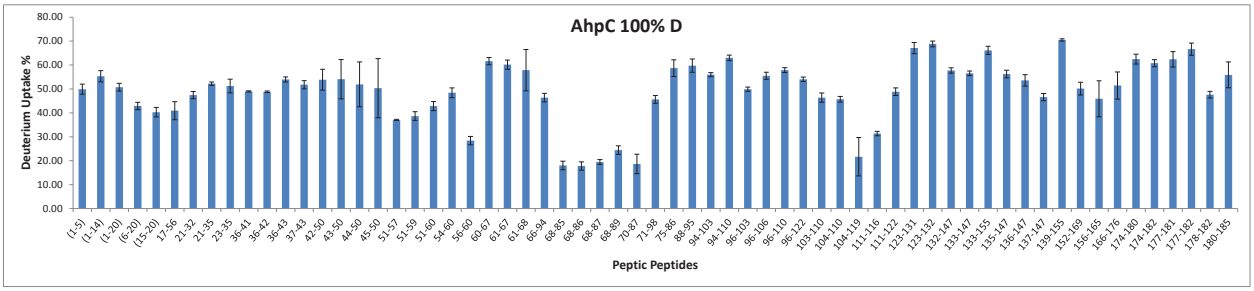

100% deuterated $Wt_{S\text{-}S}$ *St*AhpC HDX-MS data was presented in a bar graph with peptides arranged sequentially.

Figure 5 32 HDX-MS profile of human Prx2 protein

(a)

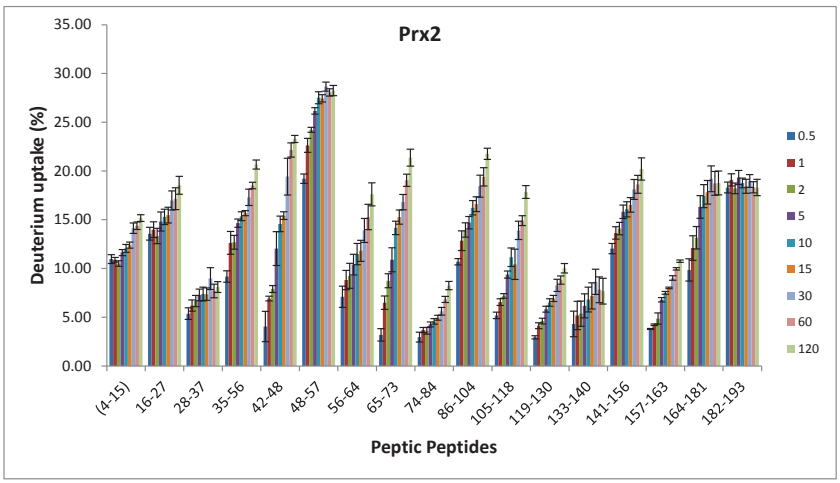

(b)

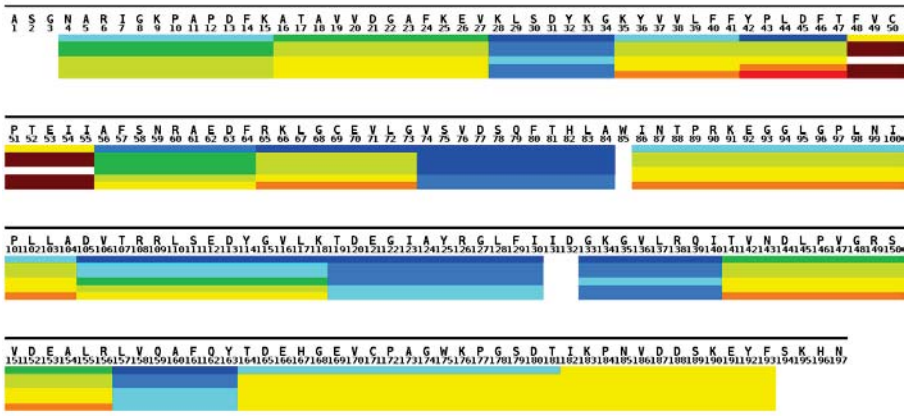

(c)

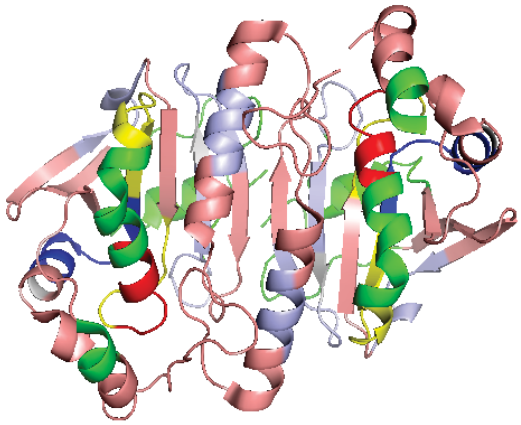

Figure 6

33 **Deuterium uptake data of wild-type StAhpC, C46S mutant of StAhpC and human Prx2**

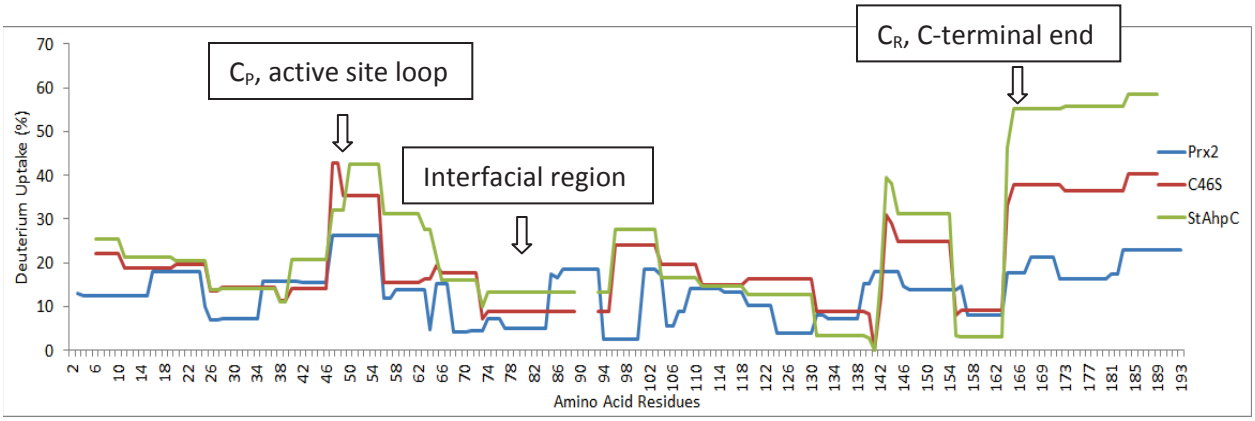

Figure 7

34 **B-factors of wild-type StAhpC, C46S mutant of StAhpC and human Prx2**

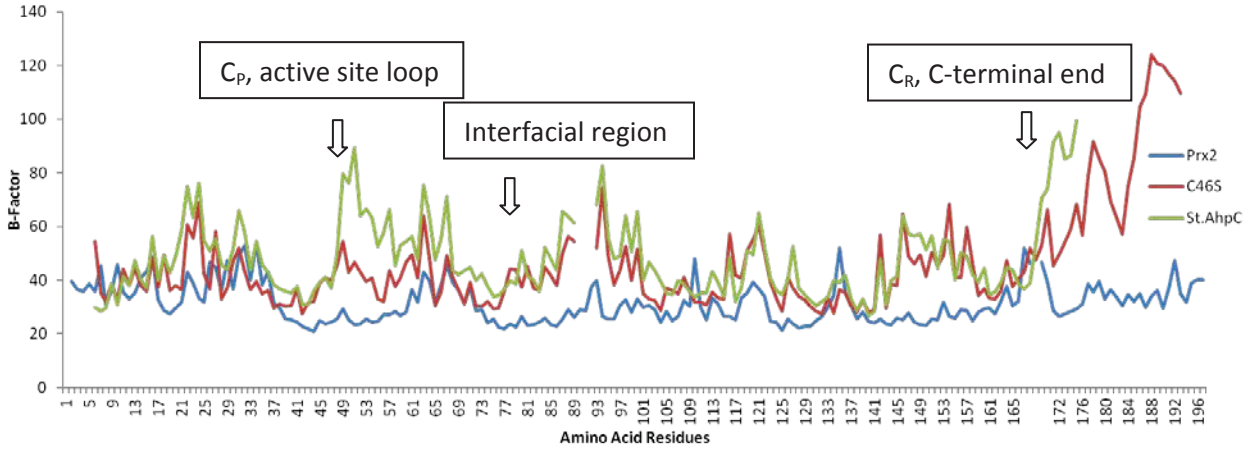

Table 1

2 **Peptides divided into High, Medium and Low Exchanging peptides**

	High exchange peptides		Medium exchange peptides		Low exchange peptides	
Gradual increase over time	**Small or No Incremental increase**	**Significant increase**	**Small or No Incremental increase**	**Significant increase**	**Small or No Incremental increase**	**Significant increase**
C46S	44-50, 156-182		51-60, 96-110, 137-147	1-14, 6-20, 60-67, 88-95	21-35, 68-89, 111-122, 123-132, 134-140, 148-156	35-41,
WOX	137-147, 156-182	45-50,	68-89, 134-140	1-14, 6-20, 35-41, 51-60, 60-67, 88-95, 96-110,	21-35, 123-132, 148-156	111-122,
Prx2	16-27, 182-193	35-56, 48-57, 86-104, 141-156, 164-181	4-15	42-48, 56-64, 65-73, 105-118	28-37, 133-140	78-84, 119-130, 157-163

Table 2

3 **Peptides separated based on statistical two-way ANOVA analysis**

	Not significant p >0.05	Significant p = 0.05 to 0.005	Highly Significant p = <0.005
Wt_{S-S} Vs C46S Difference in deuterium uptake	61-67, 96-106, 96-110, 111-122,	21-35, 45-50, 103-110, 123-131, 123-132, 137-147, 147-155, 148-155, 148-156, 156-169, 156-176,	1-14, 6-14, 6-20, 21-32, 23-32, 35-41, 51-57, 51-60, 60-67, 61-87, 68-85, 68-86, 68-89, 69-87, 88-95, 134-140, 135-147, 136-147, 156-165, 156-174, 156-182, 157-176, 166-176

Table 3

4 **p-values obtained from the statistical two-way ANOVA of wild type and C46S mutant *St*AhpC.**

	pvalues.bin
(1-14)	0.000219
(6-14)	0.000642
(6-20)	0.002175
21-32	0.000241
21-35	0.049901
23-32	0.003688
35-41	0.000666
44,45-50	0.030096
51-57	1.51E-11
51-60	8.04E-07
60-67	0.001224
61-67	0.679625
61-87	0.004631
68-85	6.99E-06
68-86	2.97E-06
68-89	3.55E-06
69-87	5.64E-05
88-95	0.000106
96-106	0.548459
96-110	0.941426
103-110	0.046317
111-122	0.78321
123-131	0.021743
123-132	0.009461
134-140	0.000108
135-147	0.004518
136-147	0.004832
137-147	0.005775
147-155	0.024007
148-155	0.029535
148-156	0.010681
156-165	0.000997
156-169	0.027679
156-174	0.000135
156-176	0.031259
156-182	6.25E-06
157-176	5.90E-05
166-176	1.30E-05

Table 4

5 **HDX-MS data of human Prx2 was fitted with a fixed-rate-constant binning model**

Sequence	Bin 1	Bin 2	Bin 3	Bin 4	Bin 5	Bin 6
ASGNARIGKPAPDF	2	1	0	0	0	8
KATAVVDGAFKE	2	1	0	0	0	8
VKLSDYKGKYVVL	1	1	0	0	0	10
FYPLDFT	0	1	0	0	2	2
IAFSNRAED	0	2	0	0	0	6
FRKLGCEVL	1	0	1	0	0	6
GVSVDSQFTHL	1	0	1	0	0	8
AWINTPRKEGGLGPLNIPLL	3	1	0	0	0	12
ADVTRRLSED	1	1	0	0	0	7
YGVLKTDEGIAYRGLF	1	2	0	1	0	11
FIIDGKGVLRQ	1	0	0	0	4	5
ITVNDLPVGRSVDEA	2	2	0	0	0	9
LRLVQAFQ	0	1	0	0	0	6
YTDEHGEVCPAGWKPGSD	1	3	0	0	0	11
TIKPNVDDSKEYF	2	2	0	0	0	7

5 Chapter

Conformational changes in the dynamics of CUL1 proteins upon neddylation studied by solution-phase hydrogen deuterium exchange mass spectrometry

Sasidhar N Nirudodhi[1], Haibin Mao[2], Yuan Jiang[3], Ning Zheng[2], and Claudia S. Maier[1]

Department of Chemistry, Oregon State University;

School of Medicine, Department of Pharmacology, University of Washington

Department of Statistics, Oregon State University;

Corresponding author: Claudia S. Maier

Email: claudia.maier@oregonstate.edu

Phone: 541-737-9533

Fax: 541-737-2062

Abbreviations

Cullin-RING ubiquitin ligases (CRLs), Really interesting new gene (RING), Ring box-1 (RBX1), Ubiquitin-like proteins (UBLs), Hydrogen deuterium exchange mass spectrometry (HDX-MS).

5.1 Introduction

Protein ubiquitination is an essential post-translational modification in eukaryotic cells that regulates the diversity of biological processes including cell cycle progression, gene transcription, signal transduction, DNA replication, DNA repair, and even viral and bacterial infections [1-3]. Ubiquitin is a highly conserved small eukaryotic protein consisting of 76 amino acids. Ubiquitination refers to the covalent attachment of ubiquitin carboxyl terminus to the lysine residues of substrate proteins or other ubiquitin molecules. This process requires a three-enzyme enzymatic cascade consisting of an ubiquitin-activating enzyme (E1), a ubiquitin-conjugating enzyme (E2) and a ubiquitin ligases (E3)[4]. First, the active site cysteine of E1 forms a thioester bond with the C-terminal glycine residue of ubiquitin in an ATP-dependent manner. The activated ubiquitin is then transferred to the catalytic cysteine of the E2. Last, the E3 recognizes and recruits both the ubiquitin-charged E2 and target substrate and catalyzes the transfer of the ubiquitin to a lysine residue of the substrate or substrate-conjugated ubiquitin.

E3 ubiquitin ligases play a central role in identifying target substrates and thus conferring specificity to the ubiquitination pathway. There are two major groups of E3 ubiquitin ligases: the HECT E3s and the RING E3s. HECT E3s contain a *H*omologous to *E*6-Associated Protein *C*arboxyl *T*erminus (HECT) domain with a catalytic cysteine residue that forms a thioester bond with Ub before transfers it to the substrate lysine [5]. About 30 HECT E3s have been identified in mammals to date. The majority of E3 ubiquitin ligases belong to the RING E3s [6], which contain a *R*eally *I*nteresting *N*ew *G*ene (RING) domain that interacts with an appropriate E2 enzyme and activates the E2 [7]. In contrast to HECT E3s, RING E3s act as scaffold proteins that bring together ubiquitin-charged E2 and substrate protein to facilitate the direct transfer of ubiquitin from E2 to the substrate [6, 8, 9].

Cullin-RING Ligases (CRLs) are a superfamily of multi-subunit RING E3 ligases that control about 20% of the proteasome-dependent cellular protein degradation [10]. Crystal structures of several CRLs are currently available [11-15], which revealed an overall similar modular architecture of CRLs. For example, SCF (Skp1-CUL1-F box proteins), the archetype and the founding member of all CRLs, consists of the CUL1 protein, the RING protein RBX1, the adaptor protein SKP1, and a substrate receptor F-box protein. CRLs are assembled around a cullin scaffold protein. The C-terminal domain (CTD) of cullin tightly interacts with a RING protein, either RBX1 or RBX2, to recruit the E2 ubiquitin-conjugating enzyme. At the other end, the N-terminal domain (NTD) of cullin interacts with one of many substrate receptors, either directly or via an adaptor protein, to recruits specific substrates. Most significantly, the central scaffold cullin protein adopts a rigid elongated arc-shaped structure, which brings about a 50 Å gap between the substrate-binding site of the CRL and the active site of the E2. This conformation represents catalytically inactive state of CRLs. The human genome contains six closely related cullin proteins: CUL1, 2, 3, 4A, 4B and 5. A total of around 500 CRLs family members are generated by selective combination of different Cullin proteins with various adaptor proteins and substrate receptors [16].

However, the 50 Å gap raised the question of how ubiquitin is transferred from E2 to the substrate on a CRL complex. For isopeptide bond formation between the lysine side chain of the substrate and the ubiquitin carboxyl terminus at the active site of the E2, these two parts must be very close to each other. It is known that activation of CRLs requires cullin neddylation, which refers to the covalent attachment of NEDD8 to a conserved lysine residue in the CTD of cullins. Nedd8 is an ubiquitin-like protein that is 57% identical to ubiquitin [17]. NEDD8 conjugation stimulates the ubiquitin-ligase activity of CRL both *in vitro* and *in vivo*. Neddylation increases the affinity between SCF and ubiquitin-loaded E2 enzyme UBC4 [18], and further significantly stimulates ubiquitin transfer from SCF-bound E2 to the substrate [19]. Interestingly, a bacterial effector protein, CIF, deamidates the conserved

glutamine 40 residue of NEDD8 to glutamate (Q40E) and directly impairs the E3 ligase activity of the neddylated CRLs [20].

Structural studies performed by Duda *et al* provided new insights into how neddylation activates CRL function [19, 21]. Crystallization of both neddylated and unmodified forms of a full length CRL has been proved extremely difficult. They only obtained crystal structure data of $CUL5^{CTD}$-RBX1 and neddylated $CUL5^{CTD}$-RBX1. Comparing those two structures, they found neddylation induced a drastic conformational change of CUL5 CTD, thus released the RING domain from its Cullin-binding site. Since the RING domain no longer binds CUL5, it can freely to adopt multiple conformations. As a result, RBX1 and its bound ubiquitin-loaded E2 can be positioned in close proximity to the substrate, thus stimulating the transfer of ubiquitin to the substrate. Therefore, neddylation confers great structural flexibility on CRLs to bridge the 50 Å gap[21].

However, the lack of the NTD of the Cullin scaffold protein in the above-mentioned structures raises a major concern as the NTD plays an important role in modulating the activity of the E3 ligases. To fill in the gap, we applied an alternate technique, hydrogen/deuterium exchange mass spectrometry, to study the dynamic conformational changes induced by the neddylation on full length CUL1-RBX1 complex. In this initial study, we analyzed the CUL1-RBX1, NEDD8 modified CUL1-RBX1 and NEDD8 Q40E modified CUL1-RBX1 complexes. Conformational changes were evaluated by comparing the exchange-in data of Nedd8-modified and Nedd8 Q40E-modified CUL1-RBX1 protein complexes with the goal to gain insights into the mechanisms associated with the activation of CRLs linked to neddylation of the cullins.

HDX involves the exchange of the backbone amide hydrogen with deuterium. HDX depends on the solvent accessibility and is sensitive to small structural changes that disrupt the intramolecular hydrogen bonds and facilitate the exchange of backbone amide hydrogen with deuterium in deuterating solutions. Deuterium incorporation can be measured as increase in mass by mass spectrometry. Using

HDX in conjuction with proteolytic pepsin digestion in combination with mass spectrometry we localized regions that underwent structural and conformational changes in this large protein complex upon covalent attachment of Nedd8 on the CUL1-RBX1 complex.

5.2 Materials and Methods

5.2.1 Materials

Deuterium oxide (99.999 atom% D) was purchased from Sigma Aldrich Co (St.Louis, MO), 1.5 M TRIS-HCl buffer (pH 8.8) was purchased from Bio-Rad Laboratories (Hercules, CA), phosphoric acid (85%) was purchased from Mallinckrodt Chemicals (Phillipsburg NJ).

5.2.2 Protein expression and purification

APPBP1-UBA3 and UBC12 were prepared as described previously [22]. NEDD8 was ligated into a modified pGEX4T1 (Amersham Biosciences) containing a GST tag followed by a Tobacco Etch Virus (TEV) protease cleavage site. TEV cleavage leaves three extra residues (Ser-Gly-Gly) at the N-terminus of NEDD8. GST-NEDD8 was purified by glutathione affinity and anion exchange chromatography. In this study, we used a truncated version of NEDD8 terminating at Gly 76, representing its mature form.

Both $CUL1^{13-776}$ and $RBX1^{16-108}$ were fused with an N-terminal hexa-Histidine tag followed by a TEV cleavage site and coexpressed in BL21(DE3). TEV cleavage leaves one extra serine residue at the N-terminus of both CUL1 and RBX1. The complex was first purified by a Ni sepharose (GE Healthcare) affinity column, then neddylated with GST-NEDD8 as previously reported [21]. The free CUL1-RBX1 was separated from neddylated CUL1-RBX1 by a glutathione affinity column. After TEV cleavage to remove all the tags, the NEDD8-CUL1-RBX1 were further purified by cation exchange (Source 15S, GE healthcare)

and gel filtration, then concentrated to 5-6 mg/ml in 20 mM Tris-HCl, 200 mM NaCl, 5 mM DTT, pH 8.0, aliquoted, flash-frozen, and stored at -80 ^{o}C. NEDD8 Q40E modified CUL1-RBX1 was purified using the same protocol, except that the wild type NEDD8 was replaced by NEDD8 Q40E.

5.2.3 Solution-phase hydrogen deuterium exchange mass spectrometry

For the HDX-MS experimental workflow previously reported protocols for H/D exchange-in analysis were followed [23-36] but several modifications were necessary to enable the analysis of the current large protein complexes [23-36]. Protein stock solution (6 mg/mL) was equilibrated at room temperature for 30 min prior to the labeling reaction. Deuterium labeling reaction was triggered by mixing 0.5 µL of protein with 11 µL of deuterated 0.01 M (pH 7) TRIS buffer. Labeling reaction was carried out for different time points (0.5min, 1min, 2min, 5min, 10min, 15min, 30min, 60min, 120min) and three replicates were prepared for each time point. The labeled samples were quenched by adding 13 µL of pre cooled 0.42% phosphoric acid (pH 2.5) and then flash frozen in liquid nitrogen until further analysis [24-26, 28, 37-39]. Three undeuterated samples were prepared as controls using the same protocol by replacing the deuterated pH 7 TRIS buffer with undeuterated buffer [25, 29, 40-42]. The frozen samples were thawed and injected into Waters HDX chiller module integrated with the nano-Acquity UPLC for online digestion, trapping and analytical separation. The HDX chiller module system has separate chambers to maintain ambient temperature of 9 ^{o}C for digestion and 0 ^{o}C for rest of the system to minimize back exchange [39]. Analytical solvents were pre-cooled and kept in the ice baskets throughout the data acquisition process to minimize back exchange. As solvent A 0.1% formic acid in 100% MS grade water and as solvent B 0.1% formic acid in acetonitrile was used as mobile phase. A 100 µL/min flow rate of solvent A was used to push the protein sample from the sample loop through the ABI Poroszyme immobilized pepsin cartridge (2.1 mm x 30 mm) to execute the protein digestion step.

Proteolytic peptides were eluted and trapped onto an Acquity UPLC BEH C_{18} (0.1 µ 1mm) guard column. The trapped peptides were desalted with a 40 µL/min constant flow rate of solvent A for 3 min to waste. By using a switching valve the peptic peptides were diverted onto an Acquity UPLC BEH C_{18} (1.7 µ, 1.0 mm x 100 mm) analytical column for peptide separation. A constant flow rate of 40 µL/min with a short 12 min gradient was used to separate the peptic peptides. The gradient design was as follows: start with 8% of solvent B; ramp to 40% in 6 min and by 7 min ramp to 85%; stay at 85% until 9 min and finally by 10 min linearly ramp down to 8%; stays at 8% for 2 min. Peptides eluted from the nanoAcquity UPLC were passed on to a divert valve (Rheodyne MX Series II 6-port valve) to minimize that impurities enter the ESI source.

Separated peptic peptides were eluted into a Waters Synapt HDMS electrospray ionization mass spectrometer for mass analysis. A voltage of 3 KV was applied to the electrospray emitter; 35 V was applied on a separation cone; Source and desolvation temperatures were maintained at 90 and 180 ^{o}C; Mass spectra were acquired over a mass range of m/z 200 – 2000. The MS^{E} (hi low) method was used for the tandem mass analysis of the ionized peptic peptides [43, 44]. The MS^{E} acquisition mode, sometimes also referred to as “hi lo” was applied; a low energy regime for the survey scan (10 eV) and a high energy regime (25 eV) for fragmenting all the ions in the gas cell was applied in an alternative fashion. A 250 pmol/µL of Glu^{1}-fibrinopeptide B in 30% ACN and 70% MS-grade water with 0.05% formic acid was used as a reference lock mass solution. Lock spray solution was sprayed at an interval of 30 sec with a flow rate of 10 µL/min. The sample cone was maintained at 37 V, trap CE (collision energy) at 24 V and the scan time was 0.3 sec.

5.2.4 PLGS Database Search

Undeuterated raw data files were processed using PLGS 2.5.2 for peptide identification and the protein sequence coverage. PLGS first produces a precursor and product ion list. The peak apexes are located and data calibrated and then lock mass corrected. The precursor and product ions spectra were deconvoluted and matched with the precursor products and peptide fragments. PLGS scores the peptides and calculates the false positive rate. The final peptide list is created as an ion accounting file in .CSV format.

5.2.5 Data Analysis

PLGS processes the raw data of the control samples and produces a peptide list (as.CSV output file) which includes the following parameters: m/z, retention time, peptide score, product ions matched, average mass, charge, sum of matched product intensity. The DynamX software uses PLGS results to create a peptide list. Raw data files of different exchange-in time points and protein states were added to the software and their exposure times were manually added. After identifying the files, DynamX software scans each file for detected ions. It searches the ions to determine which isotope cluster belongs to each peptide in an experiment, and then calculates the deuterium uptake. The DynamX main window, allows to view the deuterium uptake as a function of exposure time for each available charge state of a peptide. No back exchange corrections were implemented due to the comparative nature of this study. We also have not performed any substrative methods to avoid over interpretation of the exchange-in study due to the recently raised concerns that back-exchange rates of peptides are governed by the nature of the peptide and potential interactions with the stationary phase of the reversed-phase LC column [45]. We manually examine each spectrum and modify peptide assignments wherever deemed necessary.

5.2.5.1 HDExaminer

Peptide list with m/z values and corresponding retention times were added to the HDExaminer 1.0 [46-48]. When RAW data files were added to the HDExaminer, it starts searching for the ion peaks at the same retention time in the raw data files and processes the data to display deuterated peaks for each peptide for the entire spectrum of time points. We manually reviewed the isotope patterns of the deuterated peptides and selected the ones with good intensity to compile a list of peptides to be included in the analysis. HDExaminer also allows to displays plots that depict the time evolution of deuterium uptake as Deuterium level versus time. . All exchange data can be transferred into a .CSV file for further analysis.

5.2.5.2 Kinetic Modeling of HDX Exchange-in Data

Several methods have been described for extracting the rate constants “k” values from the HDX data [27, 49-51]. A fixed-rate-constant binning model was used to fit the peptide kinetic data using R statistical software by minimizing the sum of squared error (SSE). Six rate constants (k = 100, k = 10, k = 1, k = 0.1, k = 0.001, k = 0.0001) were selected. Each dataset of three replicates were fit together and the fitted curves were displayed with average values and their standard deviation as error bars. In this study we have used a fixed rate binning model as this allowed us to assign the exchangeable back bone amide hydrogens into six different groups based on their exchange rate constants which enabled a comparative evaluation of the three different protein systems analyzed in this study. A compilation of the rate constants obtained for each peptide analyzed is presented in the supplementary section (Table S2). The curve fitting plots of CUL1-RBX1, Nedd8 modified- CUL1-RBX1 and Nedd8 Q40E modified CUL1-

RBX1 protein state for each peptide was plotted in a single graph. All the curve fitting plots were presented in the supplementary section (Figure S3).

5.3 Results and Discussion

Previous studies have reported the crystal structure of CUL1 [13]. However, the crystal structure of the Nedd8-modified full length CUL1 has not yet been obtained. Duda *et al* studied the Nedd8-CUL1^{CTD}-RBX1 and CUL1^{CTD}-RBX1 using small-angle X-ray scattering (SAXS) analysis which revealed an open conformation for the Nedd8- CUL1^{CTD}-RBX1 assembly [21]. Due to the difficulties in preparing the diffraction quality crystals of Nedd8-CUL1-RBX1 no study has become possible yet that enabled studying the conformational changes that occur on the full length protein upon neddylation.

The current study is the first attempt to determine the conformational changes caused by neddylation of full length CUL1-RBX1. To understand the conformational changes associated with the neddylation of the CUL1-RBX1 full length protein in solution, we performed hydrogen/deuterium exchange-in experiment on the following three protein states: CUL1-RBX1, Nedd8 modified and Nedd8 Q40E modified CUL1-RBX1. As part of our HDX method to attain better spatial resolution, proteins were subjected to pepsin digestion. We obtained a combined peptide list from three replicates of the undeuterated samples for each protein state. These peptic peptides were filtered by considering several parameters such as intensity of the spectra, quality of peptide spectra, minimum products per amino acid, minimum sum intensity of the products, replication of peptide among all control files and peptide scores.

5.3.1 HDX-MS analysis of CUL1

We selected 90 overlapping peptic peptides common to all three protein states. These 90 peptides provided 73% sequence coverage for the CUL1 protein and this enabled us to study the structural changes throughout the protein. From these peptides a subset of 45 non-overlapping peptides were finally chosen for evaluating the structural plasticity of CUL1-RBX1 upon neddylation. Deuterium uptake values for the peptides were extracted as described in the method section and their corresponding normalized deuterium exchange-in percentages were calculated as described previously [41].

The deuterium uptake data of CUL1-RBX1, Nedd8 modified- CUL1-RBX1 and Nedd8 Q40E modified CUL1-RBX1 was presented in a bar graph format (Figure S1.1), overlaid on the CUL1 crystal structure (Figure S1.2) and also presented as heat maps (Figure S1.3). We did not discuss this data in the results but all the data is provided in the supplementary information for reference. Focus of our research is to study the conformational changes accompanied by the neddylation of CUL1-RBX1. We presented the differential deuterium uptake data obtained from comparing the CUL1-RBX1 protein with neddylated CUL1-RBX1 protein complexes in a bar graph format (Figure 1.a) and overlaid on the CUL1 crystal structure (PDB code-1LDK) (Figure 1.b) for better visual representation. The dissection of the differential CUL1 peptide-level exchange-in data sets reveals that overall change in the deuterium uptake levels in the N-terminal region of CUL1 were less as observed for the peptides that encompassed the C-terminal half upon neddylation. This disparate exchange-in behavior is consistent with the notion that neddylation induces conformational plasticity.

5.3.2 CUL1 HDX-MS Deuterium Uptake

We statistically evaluated the differences in peptide deuterium uptake values using two-way Anova: (i) CUL1-RBX1 and Nedd8 modified CUL1-RBX1; (ii) CUL1-RBX1 and Nedd8 Q40E-modified CUL1-RBX1 and (iii) Nedd8-modified CUL1-RBX1 and Nedd8 Q40E-modified CUL1-RBX1 protein complexes. The resulting p-values (for the binding factor over a period of various time points) were corrected using most conservative method of Bonfferoni correction and compiled in Table S1). In statistics, corrections are commonly used while analyzing multiple comparisons tests to control family wise error rate. Based on the Bonfferoni corrected p-values, peptic peptides were divided into four groups: (i) peptides with p-values less than 1.0E-7 had very high significant change; (ii) peptides with p-value between 1.0E-4 to 1.0E-7 had moderate significant change; (iii) peptides with p-value between 0.05 and 0.0001 had less significant change; (iv) peptides with p-value greater than 0.05 had no observed change upon respective neddylation related modifications (Table 1).

5.3.3 Comparing CUL1-RBX1 Vs Nedd8-CUL1-RBX

Differential deuterium uptake data of the CUL1-RBX1 and Nedd8-CUL1-RBX1 is presented in a bar graph (Figure 1.a). All CUL1 peptides that exhibited significant change upon Nedd8 modification are listed in the Table 1. Among all the peptides that exhibited significant change, 238-243 and 755-762 are the only ones that had lower deuterium uptake upon neddylation. All other peptides had higher deuterium uptake after neddylation. The increase in the deuterium uptake observed among peptic peptides is associated with the higher flexibility and lower protection against deuterium exchange and decrease in the deuterium uptake is associated with the lower flexibility and higher protection. Most of the CUL1 peptides exhibited flexibility upon neddylation with an exception in 238-243 and 755-762

peptide encompassing regions being more protected. This portrays that CUL1 adopts an open conformation upon neddylation with a few exceptions being more closed.

CUL1 is a large scaffold protein that adopts an elongated structure to fulfill varied functions at opposite ends; as discussed earlier NTD involves in recruiting substrate proteins directly or through an adaptor protein binding to substrate receptors whereas CTD interacts with RBX1 and that recruits an E2-ubiquitin. CTD and NTD of CUL1 are very different structurally and functionally. Impact of the neddylation at the conserved lysine residue of CUL1 will be discussed in two separate sections below: (i) Section 5.3.3.1 discusses changes in conformational dynamics of CUL1-CTD, the region of ligase binding site, and (ii) allosteric changes observed in the CUL1-NTD are outlined in section 5.3.3.2.

Differences in deuterium uptake percentages observed between CUL1-RBX1 and neddylated CUL1-RBX1 are overlaid on the CUL1 crystal structure (1LDK) (Figure 1.b). Red colored regions represent major increase in deuterium uptake percentage depicting high flexible regions upon nedd-ylation. Light red regions represent the moderate increase in deuterium uptake percentage that indicates some flexibility in these regions upon neddylation. Whereas blue colored regions are more stabilized as a decrease in deuterium uptake was observed upon neddylation. While black colored regions had no significant change in the deuterium uptake after Nedd8 modification. The pictorial comparison of the color-coded regions of CUL1 in (Figure 1.b) makes it evident that red colored regions are more dominant in CUL1-CTD. This signifies that the CTD region became more flexible and adopted a relatively open conformation upon neddylation. Peptide 755-762 region bearing the blue color was structurally close to the K720 site of Nedd8 modification and this might have contributed for the stabilization of the C-terminus of the protein being more protected towards exchange-in reaction.

As CUL1 is a very large scaffold protein with 776 amino acid residues, we decided to divide the protein into two regions CUL1-CTD, CUL1-NTD and discuss the differential deuterium uptake profiles separately.

5.3.3.1 CUL1-CTD

The CUL1-CTD can be divided into three regions as described by Zheng *et al* [13]:

(i) A four helix bundle that connects the CTD to NTD and forms a bridge between them. Amino acid residues 418 to 493 form part of this region. The helices H20, H23 form the two ends of the four helix bundle connecting to other regions. No significant change in deuterium uptake was observed in these regions, whereas the regions H21 and part of H22 exhibited large flexibility upon neddylation (Table 2.i).

(ii) an α/β domain that interacts with the N-terminal of the RBX1 protein. This region has the maximum number of β sheets in the entire protein. Amino acid residues from 500-604, 680-700 are considered part of this region. The structural features H24, H25, S2, S3, S4, S8, and the first half of H29 exhibit higher flexibility, whereas the flexibility of S1 and the second part of H29 seem to remain unchanged upon neddylation (Table 2.ii).

(iii) and the winged helix motif which has two subdomains. Amino acid residues from 605-679, and 715-776 are described as part of this region. All regions in the winged helix A, B (WHA, WHB) exhibited higher flexibility with the single exception of H26 that remained unchanged upon neddylation (Table 2.iii).

All three regions in the CTD structurally organize in a V-shaped groove to bind the N-terminal strand of RBX1.

5.3.3.2 CUL1-NTD

The five helices of the cullin-repeat-motif were labeled A to E as described by Zheng *et al* [13]. The three cullin repeats were labeled as 1, 2, and 3.

First Repeat: In the first cullin-repeat-motif A1 to E1, we observed higher flexibility in the regions encompassing first half of the A1 and E1 helices whereas for the rest of the motif no significant change was observed upon neddylation (Table 3.a).

Second Repeat: No significant change was observed in the A2, second half of D2, and the E2 helices whereas the rest of the motif exhibited higher flexibility upon neddylation (Table 3.b).

Third Repeat: All the helices exhibited higher flexibility upon neddylation with the single exception of the D3 helix. First half of the D3 helix exhibited higher protection whereas for the second part no significant change was observed upon neddylation (Table 3.c).

5.3.4 Differential deuterium uptake upon neddylation of CUL1

When the HDX-MS results of Nedd8-modified and unmodified CUL1 proteins were compared a major increase in the deuterium uptake was observed in the Nedd8-modified protein indicating higher conformational flexibility for the Nedd8-modified CUL1 protein.

Major increase in the deuterium uptake was observed in the CTD of the Nedd8-modified CUL1 whereas the CUL1-NTD exhibited a fewer uptake. The loop region in the CUL1-CTD encompassing the peptides 672-682, 683-705 exhibited the highest increase in the deuterium uptake after neddylation. A major decrease in the deuterium uptake was also observed in the Nedd8-modified CUL1-CTD encompassing the peptide 755-762 and the reduced deuterium incorporation observed for this region can be explained by its close proximity to the neddylation site. Most of the peptides encompassing the

following partial sequences 430-442, 443-450, 451-465, 489- 498, 498-504, 508-535, 536-552, 553-559, 570-582, 582-589, 595-605, 661-668, and 736-756 exhibited a medium increase in the deuterium uptake after neddylation. Regions encompassing the peptides 410-422, 470-488, 560-566, 612-619, and 620-630 exhibited very low increase in the deuterium uptake after neddylation. The region encompassing the peptide 706-714 had no significant change in the deuterium uptake after neddylation and this site was in close vicinity to lysine-720 that was covalently bonded to the Nedd8.

Most of the peptides 25-37, 129-138, 164-171, 172-184, 201-208, 229-237, 280-287, 294-307, 308-322, 326-351, 372-382, and 383-391 in N-terminal part of CUL1 exhibited minimal increase in deuterium uptake whereas a medium increase in the deuterium uptake was observed in the regions encompassing the peptides 12-24, 82-91, 104-109, 185-200, 244-251, 352-365, and 389-405 for Nedd8-modified CUL1-NTD. While no or little change in deuterium uptake was observed for the partial sequences 89-103 and 269-279, a significant decrease in deuterium incorporation was found for peptide 238-243 and only a very minimal decrease was observed for peptide 77-86.

5.3.5 Nedd8 Q40E-modified CUL1

As discussed earlier the Q40E mutant of Nedd8 was designed because the deamidation of the Glu-40 in the Nedd8 and ubiquitin inactivates ubiquitin and ubiquitin like protein Nedd8 and attenuates the ubiquitination process both in vitro and in vivo [20]. By studying the deuterium uptake data of the Q40E-mutant of Nedd8-modified CUL1-RBX1 in comparison to the Nedd8-modified CUL1-RBX1 protein complex we hoped to gain better insights regarding the conformational determinants of the inactive state of the deamidated Nedd8- CUL1-RBX1 complex which, in turn, will foster our understanding on which conformational determinants constitute the active state of the Nedd8- CUL1-RBX1 complex.

Deuterium uptake of CUL1 peptides in Nedd8-CUL1-RBX1 and Nedd8 Q40E-modified CUL1-RBX1 was compared and their differential deuterium uptake data was presented as a bar graph in Figure 3. The differential deuterium uptake plot shows that very few CUL1 peptides exhibited a change in deuterium exchange characteristics and thus conformational dynamics. Upon two way ANOVA statistical analysis, the CUL1 peptides that exhibited significant change were 25-37, 352-365, 443-450, 453-465, 498-504, 595-605, 683-705, 706-714, 736-756, and 755-762 ($p>0.05$). Among these peptides ($p>0.05$), the CUL1 peptides 452-465 and 595-605 exhibited decreased deuterium uptake whereas the rest of the CUL1 peptides exhibited higher deuterium uptake in the Nedd8 Q40E-modified CUL1-RBX1 complex. It can be stated that the Q40E mutation in Nedd8 has made very few significant changes to the conformation of the CUL1 protein. The major significant increase in deuterium uptake is observed among the regions encompassing the peptides 706-714 and 736-756. The peptides 706-714 and 736-756 of CUL1 are structurally close to the neddylation site. Higher flexibility observed in this region displays changes in the regional conformation of CUL-CTD. The identical HDX-MS behavior of Nedd8- modified CUL1-Rbx1 and Nedd8 Q40E- modified CUL1-Rbx1, suggests that Nedd8 Q40E mutation does not induce large structural and conformation change but it rather suggests that small regional changes in the surface properties of CUL1 may affect the binding of Ub-charged E2.

5.3.6 HDX-MS analysis of RBX1

We used the same criteria as described earlier for CUL1 to select the peptic peptides that represent the RBX1 protein. Eight overlapping peptic peptides, that were common among all three protein states, were selected. These peptides had around 50% sequence coverage for the RBX1 protein. The RBX1 deuterium uptake data acquired from CUL1-RBX1, Nedd8 modified- CUL1-RBX1 and Nedd8 Q40E modified CUL1-RBX1 is presented in a bar graph format (Figure S2), overlaid on the CUL1 crystal

structure (Figure S2) and also displayed as heat maps (Figure S3). We did not discuss this data in the results but all the data is provided in the supplementary information for reference as our primary focus is to study the conformational changes upon neddylation of the CUL1-RBX1 complexes.

5.3.6.1 Differential deuterium uptake of RBX1 upon neddylation of CUL1-RBX1

RBX1 differential deuterium uptake data presented in a bar graph format were obtained by comparing deuterium uptake levels of CUL1-RBX1 *vs* Nedd8 modified- CUL1-RBX1 (Figure 4.1.a), CUL1-RBX1 *vs* Nedd8 Q40E modified- CUL1-RBX1 (Figure 4.2) and Nedd8 modified- CUL1-RBX1 *vs* Nedd8 Q40E modified- CUL1-RBX1 (Figure 4.3). For better visual understanding the differential deuterium uptake data of CUL1-RBX1 *vs* Nedd8 modified- CUL1-RBX1 was overlaid on the RBX1 crystal structure (1LDK) (Figure 4.1.b). The structural visualization of the differential deuterium uptake data provided some insight into the change in dynamics of the RBX1 protein upon Nedd8 -binding.

When the HDX-MS results of RBX1 from CUL1-RBX1 and Nedd8-modified CUL1-RBX1 complexes were compared peptides encompassing the region 72-81 and 91-102 in the RBX1-CTD did not exhibit a significant change in deuterium uptake after neddylation, whereas the peptide 15-32 of the RBX1-NTD exhibited a medium increase in deuterium uptake after neddylation. The rest of the peptides 37-43 and 44-52 exhibited a major increase in deuterium uptake after neddylation. The regions with the major change in the deuterium uptake exhibited higher flexibility after neddylation and thus adopt a relatively open conformation. A major conformational change leading to the open conformation of the activated CUL1-CTD-RBX1 by Nedd8-modification was proposed by the structural analyses performed on CUL1-CTD-RBX1, Nedd8-modified by Duda et al. SAXS, disulphide engineering probes and several other analysis were performed on the CUL1-CTD-RBX1A but a high resolution crystal structure of the Nedd8-modified complexes has not yet become available. Based on our HDX-MS results, we speculate that the Nedd8-modified full length CUL1-RBX1 protein complex engages in a structural and conformational

reorientation that resulted in higher flexibility of the region 37-53 of RBX1 leading to more open conformation as proposed by Duda et al [21]. These regions became more flexible after neddylation and this supports the general assumption of the field that neddylation enables the unwinding of RBX1 from the CUL1-CTD.

Taken together, these finding suggest that neddylation seems to significantly enhance the conformational flexibility in the C-terminal region of CUL1. We may speculate that cullin's gain in conformational flexibility upon needylation may enable a more flexible positioning of the ubiquitin E2 ligase thereby leading to stimulation of CRL activity.

5.4 Acknowledgements

This study was made possible in parts by grants from the National Institute of Health S10RR025628 and P30 ES00210.

5.5 Supporting Information Available

5.6 References:

1. **Hershko, A. and A. Ciechanover, *The ubiquitin system.* Annu Rev Biochem, 1998. 67: p. 425-79.**
2. **Xu, G. and S.R. Jaffrey, *The new landscape of protein ubiquitination.* Nat Biotechnol, 2011. 29(12): p. 1098-100.**
3. **Wu, G., et al., *Structure of a beta-TrCP1-Skp1-beta-catenin complex: destruction motif binding and lysine specificity of the SCF(beta-TrCP1) ubiquitin ligase.* Mol Cell, 2003. 11(6): p. 1445-56.**
4. **Pickart, C.M., *Mechanisms underlying ubiquitination.* Annu Rev Biochem, 2001. 70: p. 503-33.**
5. **Scheffner, M., U. Nuber, and J.M. Huibregtse, *Protein ubiquitination involving an E1-E2-E3 enzyme ubiquitin thioester cascade.* Nature, 1995. 373(6509): p. 81-3.**
6. **Deshaies, R.J. and C.A. Joazeiro, *RING domain E3 ubiquitin ligases.* Annu Rev Biochem, 2009. 78: p. 399-434.**
7. **Furukawa, M., T. Ohta, and Y. Xiong, *Activation of UBC5 ubiquitin-conjugating enzyme by the RING finger of ROC1 and assembly of active ubiquitin ligases by all cullins.* Journal of Biological Chemistry, 2002. 277(18): p. 15758-15765.**
8. **Kamura, T., et al., *VHL-box and SOCS-box domains determine binding specificity for Cul2-Rbx1 and Cul5-Rbx2 modules of ubiquitin ligases.* Genes Dev, 2004. 18(24): p. 3055-65.**
9. **Mahrour, N., et al., *Characterization of Cullin-box sequences that direct recruitment of Cul2-Rbx1 and Cul5-Rbx2 modules to Elongin BC-based ubiquitin ligases.* J Biol Chem, 2008. 283(12): p. 8005-13.**
10. **Soucy, T.A., et al., *An inhibitor of NEDD8-activating enzyme as a new approach to treat cancer.* Nature, 2009. 458(7239): p. 732-U67.**
11. **Angers, S., et al., *The KLHL12-Cullin-3 ubiquitin ligase negatively regulates the Wnt-beta-catenin pathway by targeting Dishevelled for degradation.* Nat Cell Biol, 2006. 8(4): p. 348-57.**

12. **Goldenberg, S.J., et al.,** ***Structure of the Cand1-Cul1-Roc1 complex reveals regulatory mechanisms for the assembly of the multisubunit cullin-dependent ubiquitin ligases.*** **Cell, 2004. 119(4): p. 517-28.**

13. **Zheng, N., et al.,** ***Structure of the Cul1-Rbx1-Skp1-F boxSkp2 SCF ubiquitin ligase complex.*** **Nature, 2002. 416(6882): p. 703-9.**

14. **Schulman, B.A., et al.,** ***Insights into SCF ubiquitin ligases from the structure of the Skp1-Skp2 complex.*** **Nature, 2000. 408(6810): p. 381-6.**

15. **Zheng, N., et al.,** ***Structure of a c-Cbl-UbcH7 complex: RING domain function in ubiquitin-protein ligases.*** **Cell, 2000. 102(4): p. 533-9.**

16. **Zimmerman, E.S., B.A. Schulman, and N. Zheng,** ***Structural assembly of cullin-RING ubiquitin ligase complexes.*** **Curr Opin Struct Biol, 2010. 20(6): p. 714-21.**

17. **Whitby, F.G., et al.,** ***Crystal structure of the human ubiquitin-like protein NEDD8 and interactions with ubiquitin pathway enzymes.*** **Journal of Biological Chemistry, 1998. 273(52): p. 34983-34991.**

18. **Kawakami, T., et al.,** ***NEDD8 recruits E2-ubiquitin to SCF E3 ligase.*** **EMBO J, 2001. 20(15): p. 4003-12.**

19. **Saha, A. and R.J. Deshaies,** ***Multimodal activation of the ubiquitin ligase SCF by Nedd8 conjugation.*** **Mol Cell, 2008. 32(1): p. 21-31.**

20. **Cui, J., et al.,** ***Glutamine deamidation and dysfunction of ubiquitin/NEDD8 induced by a bacterial effector family.*** **Science, 2010. 329(5996): p. 1215-8.**

21. **Duda, D.M., et al.,** ***Structural insights into NEDD8 activation of cullin-RING ligases: conformational control of conjugation.*** **Cell, 2008. 134(6): p. 995-1006.**

22. **Walden, H., M.S. Podgorski, and B.A. Schulman,** ***Insights into the ubiquitin transfer cascade from the structure of the activating enzyme for NEDD8.*** **Nature, 2003. 422(6929): p. 330-334.**

23. **Burke, J.E., et al.,** ***Interaction of group IA phospholipase A2 with metal ions and phospholipid vesicles probed with deuterium exchange mass spectrometry.*** **Biochemistry, 2008. 47(24): p. 6451-9.**

24. **Marcsisin, S.R., et al.,** ***On the solution conformation and dynamics of the HIV-1 viral infectivity factor.*** **J Mol Biol, 2011. 410(5): p. 1008-22.**

25. **West, G.M., et al.,** ***Ligand-dependent perturbation of the conformational ensemble for the GPCR beta2 adrenergic receptor revealed by HDX.*** **Structure, 2011. 19(10): p. 1424-32.**

26. **West, G.M., et al.,** ***Protein Conformation Ensembles Monitored by HDX Reveal a Structural Rationale for Abscisic Acid Signaling Protein Affinities and Activities.*** **Structure, 2013. 21(2): p. 229-35.**

27. **Yan, X., et al.,** ***Hydrogen/deuterium exchange and mass spectrometric analysis of a protein containing multiple disulfide bonds: Solution structure of recombinant macrophage colony stimulating factor-beta (rhM-CSFbeta).*** **Protein Sci, 2002. 11(9): p. 2113-24.**

28. **Zhang, J., et al.,** ***Hydrogen/deuterium exchange reveals distinct agonist/partial agonist receptor dynamics within vitamin D receptor/retinoid X receptor heterodimer.*** **Structure, 2010. 18(10): p. 1332-41.**

29. **Zhang, Q., et al.,** ***Nucleotide-induced conformational changes of tetradecameric GroEL mapped by H/D exchange monitored by FT-ICR mass spectrometry.*** **Sci Rep, 2013. 3: p. 1247.**

30. **Zhang, X., et al.,** ***Dynamics of the beta2-adrenergic G-protein coupled receptor revealed by hydrogen-deuterium exchange.*** **Anal Chem, 2010. 82(3): p. 1100-8.**

31. **Chung, K.Y., et al.,** ***Conformational changes in the G protein Gs induced by the beta2 adrenergic receptor.*** **Nature, 2011. 477(7366): p. 611-5.**

32. **Houde, D. and S.J. Demarest, *Fine details of IGF-1R activation, inhibition, and asymmetry determined by associated hydrogen /deuterium-exchange and peptide mass mapping.* Structure, 2011. 19(6): p. 890-900.**

33. **Orban, T., et al., *Substrate-induced changes in the dynamics of rhodopsin kinase (G protein-coupled receptor kinase 1).* Biochemistry, 2012. 51(16): p. 3404-11.**

34. **Dai, S.Y., et al., *Prediction of the tissue-specificity of selective estrogen receptor modulators by using a single biochemical method.* Proc Natl Acad Sci U S A, 2008. 105(20): p. 7171-6.**

35. **Chalmers, M.J., et al., *Probing protein ligand interactions by automated hydrogen/deuterium exchange mass spectrometry.* Anal Chem, 2006. 78(4): p. 1005-14.**

36. **Kim, M.Y., et al., *Conformational changes in chemically modified Escherichia coli thioredoxin monitored by H/D exchange and electrospray ionization mass spectrometry.* Protein Sci, 2002. 11(6): p. 1320-9.**

37. **Zhang, Z. and D.L. Smith, *Determination of amide hydrogen exchange by mass spectrometry: a new tool for protein structure elucidation.* Protein Sci, 1993. 2(4): p. 522-31.**

38. **Englander, S.W., et al., *Hydrogen exchange: the modern legacy of Linderstrom-Lang.* Protein Sci, 1997. 6(5): p. 1101-9.**

39. **Houde, D., et al., *Characterization of IgG1 conformation and conformational dynamics by hydrogen/deuterium exchange mass spectrometry.* Anal Chem, 2009. 81(7): p. 2644-51.**

40. **Sperry, J.B., et al., *Hydrophobic Peptides Affect Binding of Calmodulin and Ca as Explored by H/D Amide Exchange and Mass Spectrometry.* Int J Mass Spectrom, 2011. 302(1-3): p. 85-92.**

41. **Nirudodhi, S., et al., *Conformational studies of the robust 2-Cys peroxiredoxin Salmonella typhimurium AhpC by solution phase hydrogen/deuterium (H/D) exchange monitored by electrospray ionization mass spectrometry.* Int J Mass Spectrom, 2011. 302(1-3): p. 93-100.**

42. **Yan, X. and C.S. Maier, *Hydrogen/deuterium exchange mass spectrometry.* Methods Mol Biol, 2009. 492: p. 255-71.**

43. **Silva, J.C., et al., *Quantitative proteomic analysis by accurate mass retention time pairs.* Anal Chem, 2005. 77(7): p. 2187-200.**

44. **Plumb, R.S., et al., *UPLC/MS(E); a new approach for generating molecular fragment information for biomarker structure elucidation.* Rapid Commun Mass Spectrom, 2006. 20(13): p. 1989-94.**

45. **Sheff, J.G., M. Rey, and D.C. Schriemer, *Peptide-column interactions and their influence on back exchange rates in hydrogen/deuterium exchange-MS.* J Am Soc Mass Spectrom, 2013. 24(7): p. 1006-15.**

46. **Horn, J.R., et al., *The role of protein dynamics in increasing binding affinity for an engineered protein-protein interaction established by H/D exchange mass spectrometry.* Biochemistry, 2006. 45(28): p. 8488-98.**

47. **Englander, J.J., et al., *Protein structure change studied by hydrogen-deuterium exchange, functional labeling, and mass spectrometry.* Proc Natl Acad Sci U S A, 2003. 100(12): p. 7057-62.**

48. **Hamuro, Y., et al., *Hydrogen/deuterium-exchange (H/D-Ex) of PPARgamma LBD in the presence of various modulators.* Protein Sci, 2006. 15(8): p. 1883-92.**

49. **Frantom, P.A., et al., *Mapping of the allosteric network in the regulation of alpha-isopropylmalate synthase from Mycobacterium tuberculosis by the feedback inhibitor L-leucine: solution-phase H/D exchange monitored by FT-ICR mass spectrometry.* Biochemistry, 2009. 48(31): p. 7457-64.**

50. **Miller, D.E., et al., *HDXFinder: automated analysis and data reporting of deuterium/hydrogen exchange mass spectrometry.* J Am Soc Mass Spectrom, 2012. 23(2): p. 425-9.**

51. **Orban, T., et al.,** ***Conformational dynamics of activation for the pentameric complex of dimeric G protein-coupled receptor and heterotrimeric G protein.*** **Structure, 2012. 20(5): p. 826-40.**

52. **Kavan, D. and Man, P. ,** ***MSTools - Web based application for visualization and presentation of HXMS data*****. Int. J. Mass Spectrom. 2011, 302: 53-58.**

Figure Legends

Figure 1

Comparative HDX-MS study of CUL1-RBX1 and Nedd8-modified CUL1-RBX1 proteins complex: (a) Summary of differential deuterium uptake percentages of the peptic peptides acquired over a series of exchange time points (0.5, 1, 2, 5, 10, 15, 30, 60 and 120 min) arranged in the sequential order. Difference between the deuterium uptake percentages of the peptic peptides of Nedd8-modified and unmodified CUL1-RBX1 is presented in a bar graph. The peptides with positive bars above the axis represent regions that showed higher deuterium incorporation levels in the Nedd8-modified protein whereas the negative bars below the axis represent regions with lower deuterium uptake in Nedd8-modified protein. In the bar graph each vertical block represents a peptide and different colored bars represent deuterium exchange-in percentages at different time points. (b) Differential deuterium exchange-in data was overlaid on the X-ray structure of the CUL1-RBX1 protein (1LDK). Red colored regions exhibit increase in deuterium uptake after neddylation whereas the blue colored regions exhibited decrease in deuterium uptake or attains more protection upon neddylation. Grey regions are not covered by the current experiment and the whitish grey color represents the regions that exhibited no significant change upon neddylation.

Figure 2

Differential HDX data of the Nedd8 Q40E-modified and unmodified CUL1-RBX1 complex. Summary of differential deuterium uptake percentages of the peptic peptides acquired over a series of exchange time points (0.5, 1, 2, 5, 10, 15, 30, 60 and 120 min) arranged in the sequential order. Difference between the deuterium uptake percentages of the peptic peptides of Nedd8 Q40E -modified and

unmodified CUL1-RBX1 is presented in a bar graph. The peptides with positive bars above the axis represent regions that showed higher deuterium incorporation levels in the Nedd8 Q40E -modified protein whereas the negative bars below the axis represent regions with lower deuterium uptake in the Nedd8 Q40E -modified protein. In the bar graph each vertical block represents a peptide and different colored bars represent deuterium exchange-in percentages at different time points.

Figure 3

Differential HDX data of the Nedd8 Q40E, Nedd8 modified CUL1-RBX1 complex. Summary of differential deuterium uptake percentages of the peptic peptides acquired over a series of exchange time points (0.5, 1, 2, 5, 10, 15, 30, 60 and 120 min) arranged in the sequential order. Difference between the deuterium uptake percentages of the peptic peptides of Nedd8 Q40E -modified and Nedd8-modified CUL1-RBX1 is presented in a bar graph. The peptides with positive bars above the axis represent regions that showed higher deuterium incorporation levels in the Nedd8 Q40E -modified protein whereas the negative bars below the axis represent regions with lower deuterium uptake in the Nedd8 Q40E -modified protein. In the bar graph each vertical block represents a peptide and different colored bars represent deuterium exchange-in percentages at different time points.

4. Differential HDX-MS peptic peptide profiles of RBX1

Figure 4.1

Difference between the deuterium uptake of the Nedd8-modified and CUL1-RBX1 complex: (A) presented in a bar graph format; and (b) overlaid on the crystal structure of RBX1 of CUL1-RBX1 (pdb 1LDK).

Figure 4.2

Difference between the deuterium uptake of Nedd8 Q40E-modified and CUL1-RBX1 complex is presented in a bar graph format.

Figure 4.3

Difference between the deuterium uptake of Nedd8 Q40E-modified and Nedd8-modified CUL1-RBX1 complex is presented in a bar graph format.

Table 1

Two way ANOVA was performed on the kinetic deuterium uptake data of (a) CUL1-RBX1 *vs* Nedd8-modified CUL1-RBX1; (b) CUL1-RBX1 *vs* Nedd8 Q40E-modified CUL1-RBX1; and (c) Nedd8-modified CUL1-RBX1 *vs* Nedd8 Q40E-modified CUL1-RBX1. Based on the p-values obtained, peptide peptides were divided into four groups. Peptides marked with an asterisk (*) have exhibited a significant decrease in deuterium uptake upon neddylation.

Table 2

CUL1-CTD

The CUL1-CTD can be divided into three regions as described by Zheng *et al* [13]: (i) four-helix bundle (4HB, 418-493) that connects the CTD to NTD and covers the mentioned regions H20 (422-430), H21 (443-450), H22 (453-465, covers turn and H22), H23 (470-488 covering both H22, H23); (ii) an α/β domain (500-604, 680-700) interacts with the N-terminal of the RBX1 and covers H24 (508-520), H25

(560-566 turn and part of helix), S1 (536-540), S2 (570-582, turn and entire β-sheet), S3 (585-590), S4 (595-605, loop and β-sheet), S8, H29 first half (683-705, covers S8, loop, H29, 706-712); and (iii) winged helix motif has with two subdomains (iii.a) WHA (~605-679), H26 (606-611), H27 (620-626, most part of S5 and H27), H28 (631-660 missing), S5 (620-626, most part of S5 and H27), S6 (631-660 missing), S7 (661-668, turn and part of sheet); (iii.b) WHB (715-776), H29 second half (missing region 715-735 also H30), H30 (missing), H31 (covering helix and 3/10 helix), (736-756 covers turn and helix, 755-762 covers 3/10 helix), S9 (missing~721-725), S10 (missing), S11 (missing) S10 and S11 close to C-terminal. All three regions in the CTD structurally organize in a V-shaped groove to bind RBX1 N-terminal strand.

Table 3

CUL1-NTD

The five helices of the cullin-repeat-motif were labeled A to E as described by Zheng *et al* [13]. The three cullin repeats were labeled as 1, 2, 3. Changes in deuterium uptake of cullin-repeat-motif were discussed among 3 states below. Peptides covered by HDX-MS were mentioned.

(a) First Repeat: Helix A.1 (19-24 first half of helix, 25-31 second half of helix); Helix B.1 (46-52 second half of helix); Helix C.1 (82-91 small part of helix, 89-103 most of the helix); Helix D.1 (123-128 small part of helix, 129-138 second half of the helix); Helix E.1 (159-164 first half of helix, 164-170 second half of helix);

(b) Second Repeat: Helix A.2 (172-184 most part of helix); (185-200, end of Helix A.2 and beginning of Helix B.2); Helix B.2 (201-208, entire helix); Helix C.2 (229-237 beginning of Helix, 236-243 center of the helix, 244-251 last part of the helix); Helix D.2 (252-260 beginning of the helix, 269-278 last part of the helix); Helix E.2 (280-287 beginning of the helix, 288-295 second half of the helix)

(c) Third Repeat: Helix A.3 (296-307 first half of the helix); (308-322, end of Helix A.3 and first half of Helix B.3); Helix B.3 (311-322 entire helix); Helix C.3 (328-351 entire helix); Helix D.3 (366-371 first part of helix, 372-382 second half of helix); Helix E.3 (389-405 entire helix)

1

(a)

35 **Comparative HDX-MS study of CUL1-RBX1 and Nedd8-modified CUL1-RBX1 proteins**

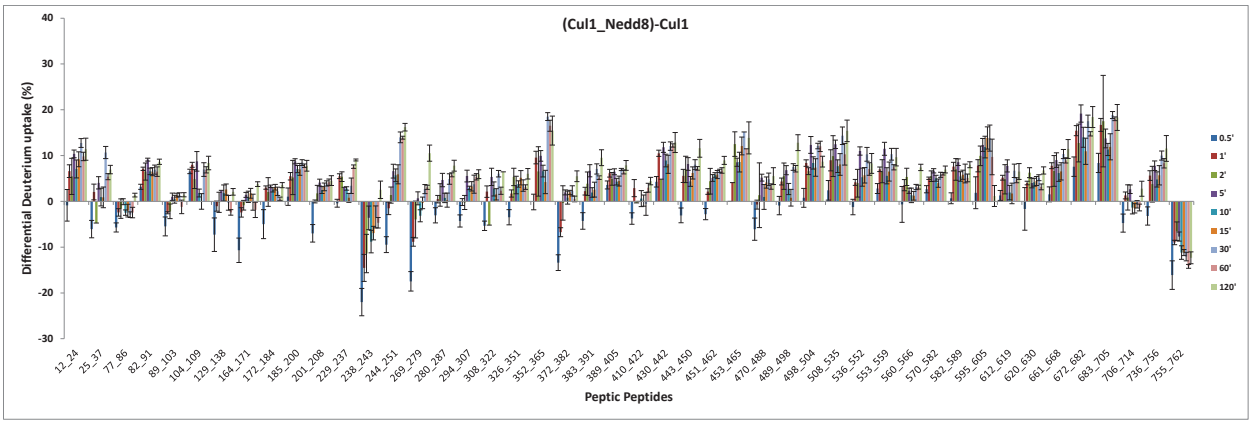

(b)

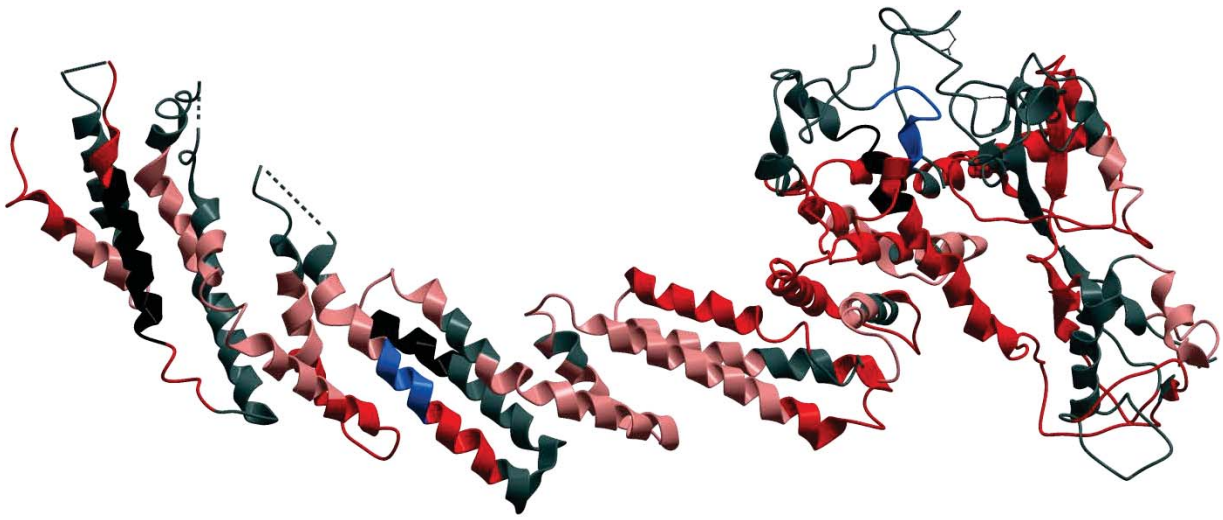

2

36 **Differential HDX data of Nedd8 Q40E-modified and unmodified CUL1-RBX1 complex**

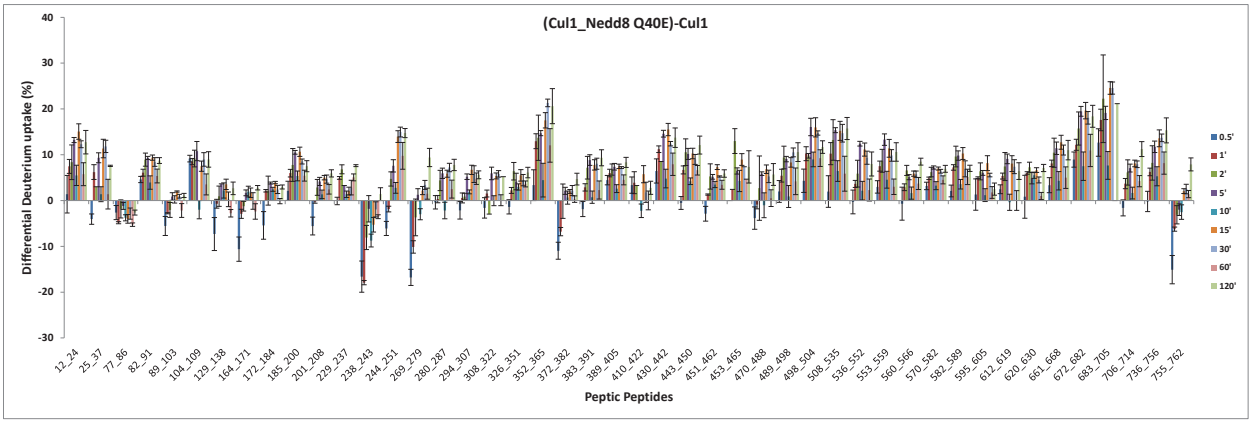

3

37 **Differential HDX data of Nedd8 Q40E, Nedd8 modified CUL1-RBX1 complex**

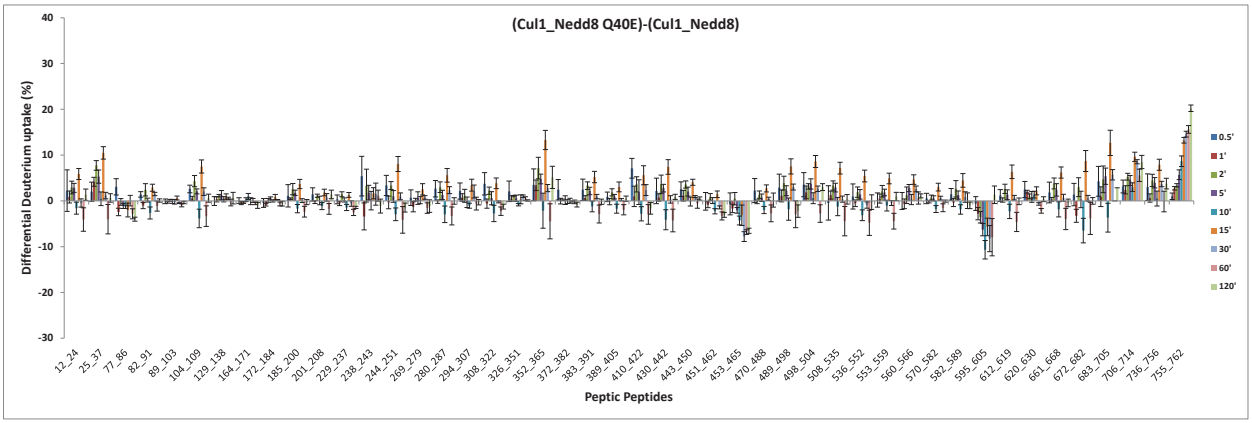

4.1

(a)

38 **Differential deuterium uptake of Nedd8-modified and CUL1-RBX1 complex**

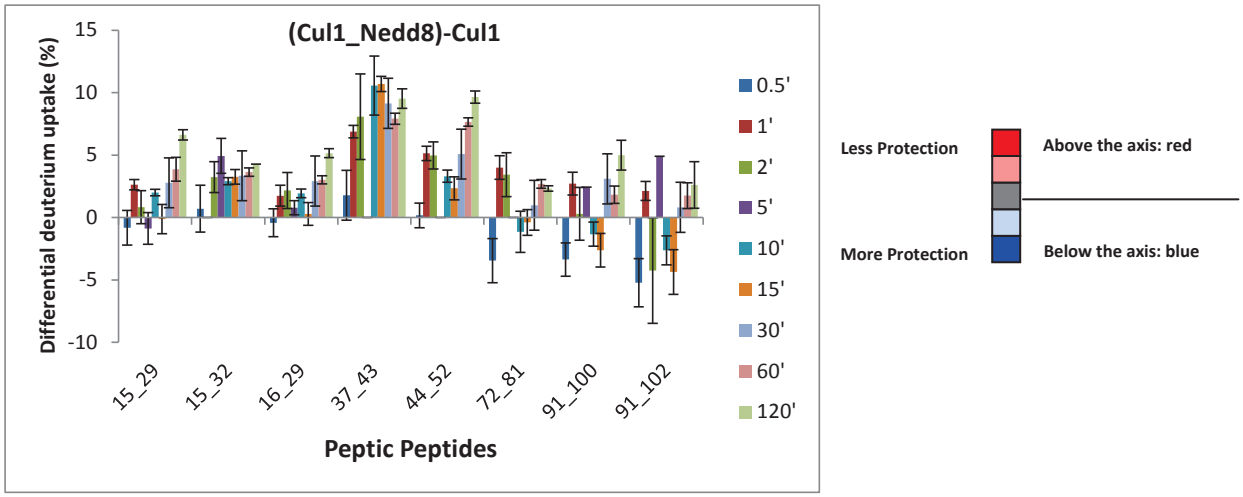

(b)

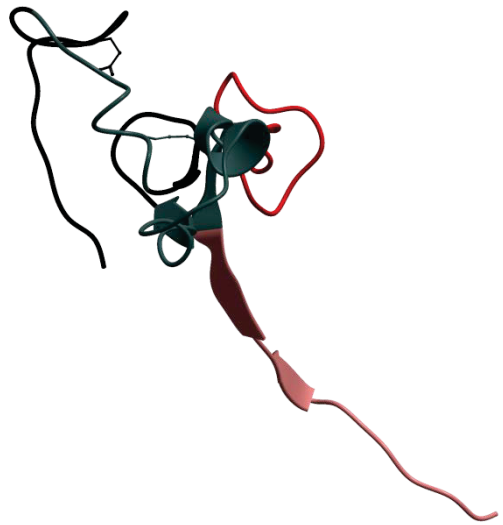

4.2

39 **Differential deuterium uptake of Nedd8 Q40E-modified and CUL1-RBX1 complex**

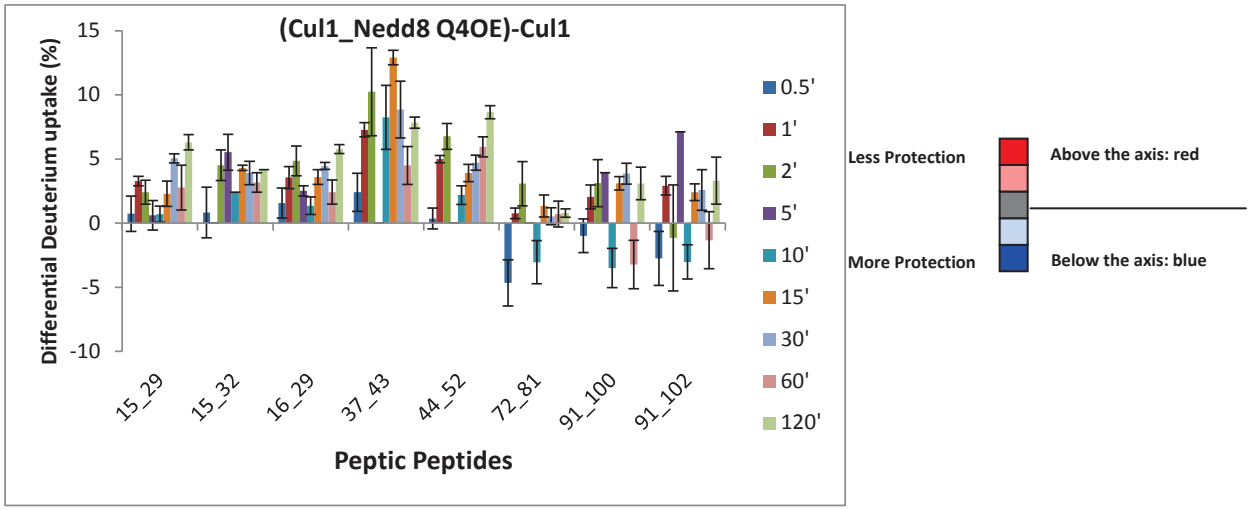

4.3

40 **Differential deuterium uptake of Nedd8 Q40E-modified and Nedd8-modified CUL1-RBX1**

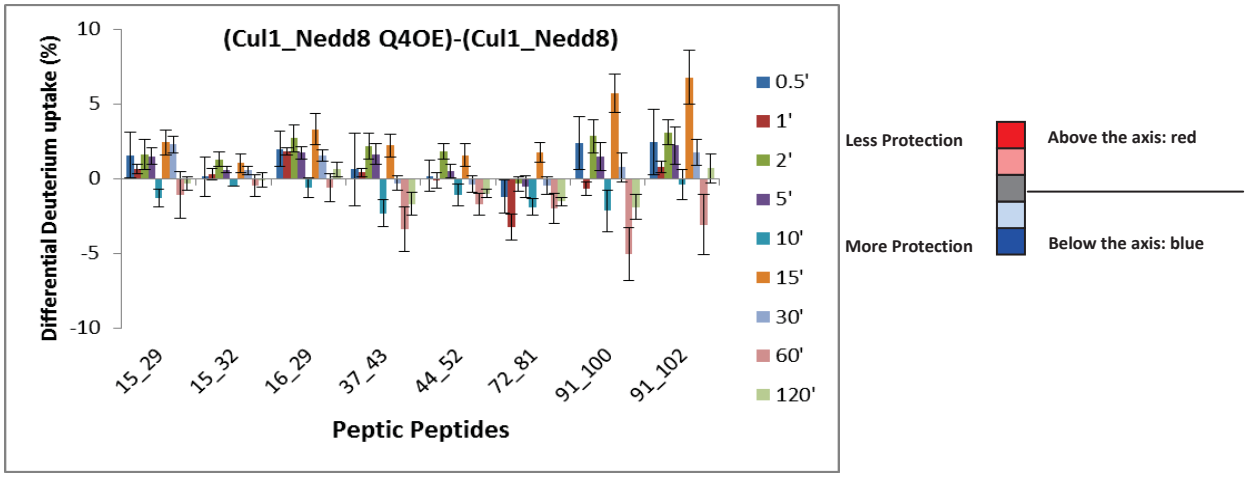

Table 1

6 **Peptides divided based on p-values of Two-way ANOVA analysis**

P-values for comparing the deuterium uptake of two different state of CUL1-RBX1 can be divided into 4 groups				
	< 1.0E-7 Very high significant change	**1.0E-4 to 1.0E-7 moderate significant change**	**0.05 to 0.0001 less significant change**	**> 0.05 no observed change**
CUL1-RBX1 *vs* Nedd8-modified CUL1-RBX1	12-24, 82-91, 104-109, 185-200, 229-237, 244-251, 352-365, 389-405, 430-442, 443-450, 451-462, 453-465, 489-498, 498-504, 508-535, 536-552, 553-559, 570-582, 595-605, 661-668, 672-682, 683-705, 736-756, **755-762***	**238-243***, 294-307, 326-351, 383-391, 612-619, 620-630	25-37, 77-86, 201-208, 280-287, 308-322, 560-566, 582-589	89-103, 129-138, 164-171, 172-184, 269-279, 372-382, 410-422, 470-488, 706-714
CUL1-RBX1 *vs* Nedd8 Q40E - modified CUL1-RBX1	12-24, 25-37, **77-86***, 82-91, 104-109, 185-200, 229-237, 244-251, 294-307, 326-351, 352-365, 383-391, 389-405, 430-442, 443-450, 451-462, 453-465, 489-498, 498-504, 508-535, 536-552, 553-559, 560-566, 570-582, 582-589, 595-605, 612-619, 620-630, 661-668, 672-682, 683-705, 706-714, 736-756	201-208, **238-243***, 280-287, 308-322	410-422	89-103, 129-138, 164-171, 172-184, 269-279, 372-382, 470-488, 755-762
Nedd8 modified - CUL1-RBX1 *vs* Nedd8 Q40E modified CUL1-RBX1	**453-465***, 706-714, 755-762	25-37, 498-504, **595-605***, 683-705, 736-756	352-365, 443-450	12-24, 77-86, 82-91, 89-103, 104-109, 129-138, 164-171, 172-184, 185-200, 201-208, 229-237, 238-243, 244-251, 269-279, 280-287, 294-307, 308-322, 326-351, 372-382, 383-391, 389-405, 410-422, 430-442, 451-462, 470-488, 489-498, 508-535, 536-552, 553-559, 560-566, 570-582, 582-589, 612-619, 620-630, 661-668, 672-682

Table 2.(a)

7 **Comparitive HDX-MS data in CUL1-CTD four-helix bundle**

Four-helix bundle (4HB, 418-493)					
		H20 422-430	**H21 443-450**	**H22 453-465**	**H22, H23 470-488**
CUL1-RBX1 *vs* Nedd8 modified CUL1-RBX1	significant change observed upon nedd8ylation	No	Yes, higher flexibility	Yes, higher flexibility	No, Small increment in flexibility
CUL1-RBX1 *vs* Nedd8 Q40E modified CUL1-RBX1	significant change observed upon Nedd8 Q40E binding	No, Small increment in protection	Yes, higher flexibility	Yes, higher flexibility	No, Small increment in flexibility
Nedd8 modified CUL1-RBX1 *vs* Nedd8 Q40E modified CUL1-RBX1	significant change observed upon Nedd8 Q40E single point mutation	No	Yes, small change, higher flexibility	Yes, higher protection	No

Table 2.(b)

8 **Comparative HDX-MS data of α/β in CUL1-CTD**

α/β domain (500-604, 680-700)									
		H24 508-520	**H25 560-566**	**S1 536-540**	**S2 570-582**	**S3 585-590**	**S4 595-605**	**S8, H29 first half 683-705**	**H29 706-712**
CUL1-RBX1 *vs* Nedd8 modified CUL1-RBX1	significant change observed upon nedd8ylation	Yes, higher flexibility	Yes, higher flexibility	No	Yes, higher flexibility	Yes, higher flexibility	Yes, higher flexibility	Yes, higher flexibility	No
CUL1-RBX1 *vs* Nedd8 Q40E modified CUL1-RBX1	significant change observed upon Nedd8 Q40E binding	Yes, higher flexibility	Yes, higher flexibility	No	Yes, higher flexibility	Yes, higher flexibility	Yes, higher flexibility	Yes, higher flexibility	Yes, higher flexibility
Nedd8 modified CUL1-RBX1 *vs* Nedd8 Q40E modified CUL1-RBX1	significant change observed upon Nedd8 Q40E single point mutation	No	No	No	No	No	Yes, higher protection	Yes, higher flexibility	Yes, higher flexibility

Table 2.(c)

9 **Comparative HDX-MS data in CUL1-CTD winged helix motif**

		WHA (605-679)			WHB (715-776)	
					H31	
		H26 606-611	S5, H27 620-626	S7 661-668	736-756	755-762
CUL1-RBX1 *vs* Nedd8 modified CUL1-RBX1	significant change observed upon nedd8ylation	No	Yes, higher flexibility	Yes, higher flexibility	Yes, higher flexibility	Yes, higher protection
CUL1-RBX1 *vs* Nedd8 Q40E modified CUL1-RBX1	significant change observed upon Nedd8 Q40E binding	No	Yes, higher flexibility	Yes, higher flexibility	Yes, higher flexibility	No, Small change was observed but not significant
Nedd8 modified CUL1-RBX1 *vs* Nedd8 Q40E modified CUL1-RBX1	significant change observed upon Nedd8 Q40E single point mutation	No	No	No	Yes, higher flexibility	Yes, higher flexibility

Table 3.(a)

10 **Comparison of HDX-MS data in the five helices of the Cullin-repeat-motif 1 of CUL1-NTD**

The Five helices of Cullin-repeat-motif 1 (First repeat)										
		A.1		B.1	C.1		D.1		E.1	
		19-24	25-31	46-52	82-91	89-103	123-128	129-138	159-164	164-170
CUL1-RBX1 *vs* Nedd8 modified CUL1-RBX1	significant change observed upon nedd8ylation	Yes, higher flexibility	No	No	Yes, higher flexibility	No	No	No	No	No
CUL1-RBX1 *vs* Nedd8 Q40E modified CUL1-RBX1	significant change observed upon Nedd8 Q40E binding	Yes, higher flexibility	No	No	Yes, higher flexibility	No	No	No	No	No
Nedd8 modified CUL1-RBX1 *vs* Nedd8 Q40E modified CUL1-RBX1	significant change observed upon Nedd8 Q40E single point mutation	Yes, higher flexibility	No	No	No	No	No	No	No	No

Table 3.(b)

11 **Comparison of HDX-MS data in the five helices of the Cullin-repeat-motif 2 of CUL1-NTD**

The Five helices of Cullin-repeat-motif 2 (Second repeat)										
		A.2	**B.2**	**C.2**			**D.2**		**E.2**	
		172-184	**201-208**	**229-237**	**236-243**	**244-251**	**252-260**	**269-278**	**280-287**	**288-295**
CUL1-RBX1 *vs* Nedd8 modified CUL1-RBX1	significant change observed upon nedd8ylation	No, Small increment in flexibility	Yes, higher flexi-bility	Yes, higher flexi-bility	Yes, higher flexibility	Yes, higher flexibility	Yes, higher flexibility	No	Yes, higher flexibility	No
CUL1-RBX1 *vs* Nedd8 Q40E modified CUL1-RBX1	significant change observed upon Nedd8 Q40E binding	No, Small increment in flexibility	Yes, higher flexi-bility	Yes, higher flexi-bility	Yes, higher flexibility	Yes, higher flexibility	Yes, higher flexibility	No	Yes, higher flexibility	No, Small increment in protection
Nedd8 modified CUL1-RBX1 *vs* Nedd8 Q40E modified CUL1-RBX1	significant change observed upon Nedd8 Q40E single point mutation	No	No	No	No	No	No	No	No	No, Small increment in protection

Table 3.(c)

12 **Comparison of HDX-MS data in the five helices of Cullin-repeat-motif 3 of CUL1-NTD**

The Five helices of the Cullin-repeat-motif 3 (Third repeat)								
		A.3	**A.3, B.3**	**B.3**	**C.3**	**D.3**		**E.3**
		296-307	**308-322**	**311-322**	**328-351**	**366-371**	**372-382**	**389-405**
CUL1-RBX1 *vs* Nedd8 modified CUL1-RBX1	significant change observed upon nedd8ylation	Yes, higher flexibility	Yes, higher flexibility	Yes, higher flexibility	Yes, higher flexibility	Yes, higher protection	No	Yes, higher flexibility
CUL1-RBX1 *vs* Nedd8 Q40E modified CUL1-RBX1	significant change observed upon Nedd8 Q40E binding	Yes, higher flexibility	Yes, higher flexibility	Yes, higher flexibility	Yes, higher flexibility	Yes, higher protection	No	Yes, higher flexibility
Nedd8 modified CUL1-RBX1 *vs* Nedd8 Q40E modified CUL1-RBX1	significant change observed upon Nedd8 Q40E single point mutation	No	No	No	No	No, Small increment in protection	No	No

SUPPLEMENTARY DATA

Conformational Changes in the Dynamics of Cul1 Proteins upon Neddylation Studied by Solution-Phase Hydrogen Deuterium Exchange Mass Spectrometry

Sasidhar N Nirudodhi[1], Haibin Mao[2], Yuan Jiang[3], Ning Zheng[2], and Claudia S. Maier[1]

Department of Chemistry, Oregon State University;

School of Medicine, Department of Pharmacology, University of Washington

Department of Statistics, Oregon State University;

Corresponding author: Claudia S. Maier

Email: claudia.maier@oregonstate.edu

Phone: 541-737-9533

Fax: 541-737-2062

S1. HDX-MS peptic peptide profiles of CUL1

Figure 1.1

Summary of deuterium uptake percentages of the peptic peptides acquired over a series of exchange time points (0.5, 1, 2, 5, 10, 15, 30, 60 and 120 min) is presented in a bar graph. Vertical blocks represent different peptic peptides and different colored bars represent deuterium uptake percentages at different time points arranged in a sequential order. (a) Derived from the HDX MS data for the CUL1-RBX1 protein complex. (b) Derived from HDX MS data for the Nedd8-CUL1-RBX1 protein complex. (c) Derived from the HDX MS data for the Nedd8 Q40E-CUL1-RBX1 protein complex.

Figure 1.2

Deuterium uptake data was overlaid on the X-ray structure of CUL1-RBX1 protein (1LDK): (a) Derived from the HDX-MS study of the CUL1-RBX1 protein complex. (b) Derived from the HDX-MS study of the Nedd8-CUL1-RBX1 protein complex. (C) Derived from the the HDX-MS study of the Nedd8 Q40E-CUL1-RBX1 protein complex.

Figure 1.3

Deuterium uptake data was normalized and presented in a heat map format: (a) HDX-MS data of CUL1-RBX1 protein complex. (b) HDX-MS data of the Nedd8-CUL1-RBX1 protein complex. (C) HDX-MS data of Nedd8 Q40E-CUL1-RBX1 protein complex. The average deuterium uptake percentages from three replicates were used for the heat map and all 9 (0.5, 1, 2, 5, 10, 15, 30, 60 and 120 min) exchange time points were aligned one below the other

S2. HDX-MS peptic peptide profiles of RBX1

Figure 2.1

Summary of deuterium uptake percentages of the peptic peptides acquired over a series of exchange time points (0.5, 1, 2, 5, 10, 15, 30, 60 and 120 min) is presented in a bar graph. Vertical blocks represent different peptic peptides and different colored bars represent deuterium uptake percentages at different time points arranged in a sequential order. (a) HDX-MS data of CUL1-RBX1 protein complex. (b) HDX-MS data of Nedd8-CUL1-RBX1 protein complex. (C) HDX-MS data of Nedd8 Q40E-CUL1-RBX1 protein complex.

Figure 2.2

Deuterium uptake data acquired at an exchange time point of 15 min was overlaid on the X-ray structure of CUL1-RBX1 protein (1LDK): (a) HDX-MS data of CUL1-RBX1 protein complex. (b) HDX-MS data of Nedd8-CUL1-RBX1 protein complex. (C) HDX-MS data of Nedd8 Q40E-CUL1-RBX1 protein complex.

Figure 2.3

Deuterium uptake data was normalized and presented in a heat map format: (a) HDX-MS data of CUL1-RBX1 protein complex. (b) Derived from the Nedd8-CUL1-RBX1 protein complex. (C) HDX-MS data of Nedd8 Q40E-CUL1-RBX1 protein complex. The average deuterium uptake percentages from three replicates were used for the heatmap and all 9 (0.5, 1, 2, 5, 10, 15, 30, 60 and 120 min) exchange time points were aligned one below the other. Heat map were drawn by using a web based application [52]. Heat maps were drawn for each protein by arranging the peptide level HDX-MS data at all exchange time points in a specific order as described in the website http://www.hxms.com/mstools/.

Figure S3.1

Peptide level deuterium uptake data of CUL1-RBX1, Nedd8-CUL1-RBX1 and Nedd8 Q40E-CUL1-RBX1 obtained from the HDX-MS study are curve fitted and presented in the same plots for few peptides.

Table S1

p-values obtained from the Two Way Anova statistical analysis by comparing the peptic peptides of three sets of CUL1-RBX1 complexes were bonferroni corrected and presented.

Figure S1.1

(a)

41 **Summary of deuterium uptake percentages of CUL1-RBX1 protein**

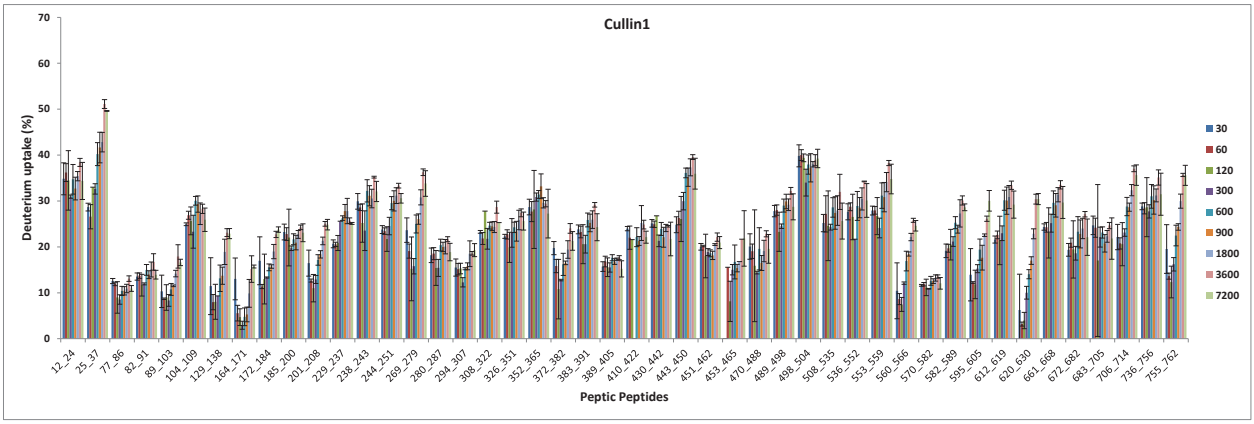

(b)

42 **Summary of deuterium uptake percentages Nedd8-CUL1-RBX1**

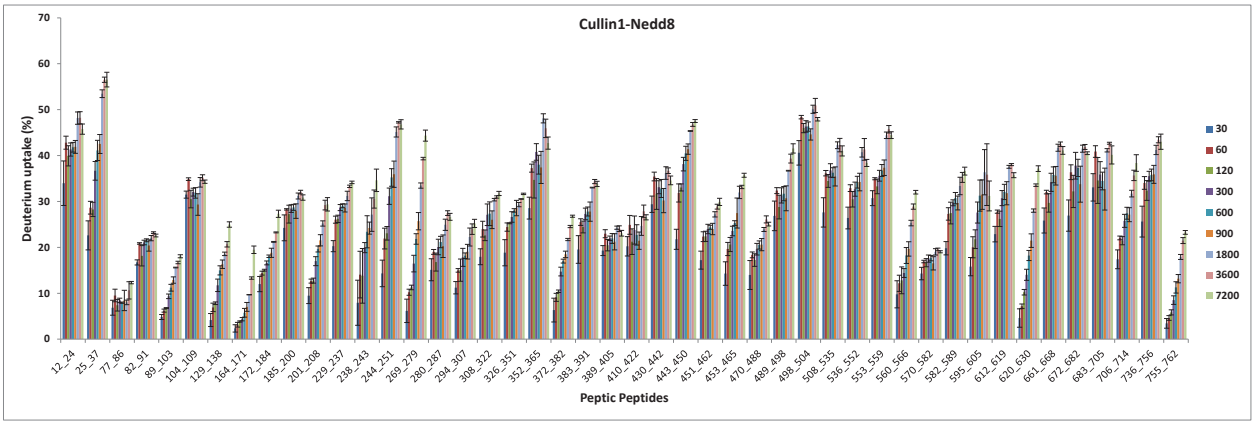

(c)

43 **Summary of deuterium uptake percentages Nedd8 Q40E-CUL1-RBX1**

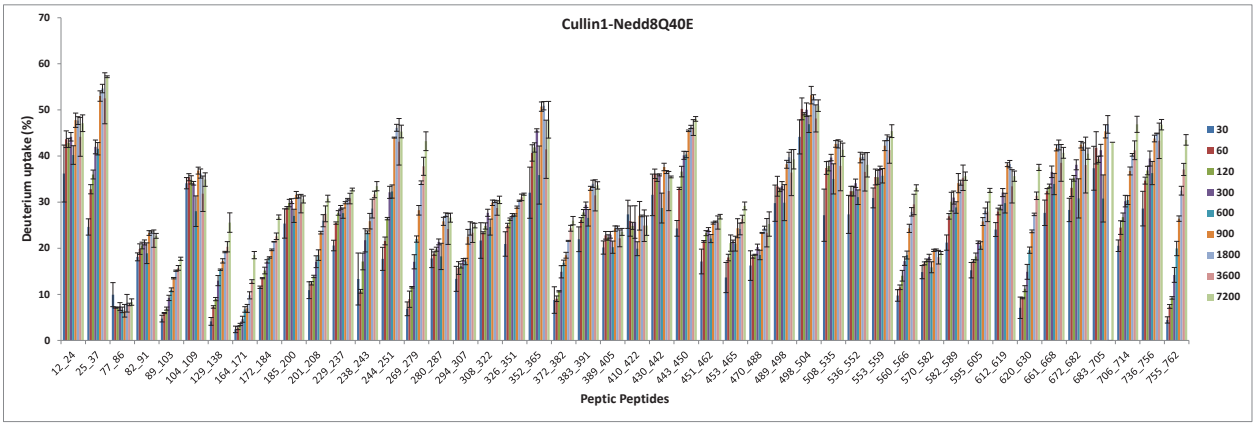

Figure S1.2

(a)

44 **Deuterium uptake data of CUL1-RBX1 was overlaid on the X-ray structure of CUL1-RBX1 protein (1LDK)**

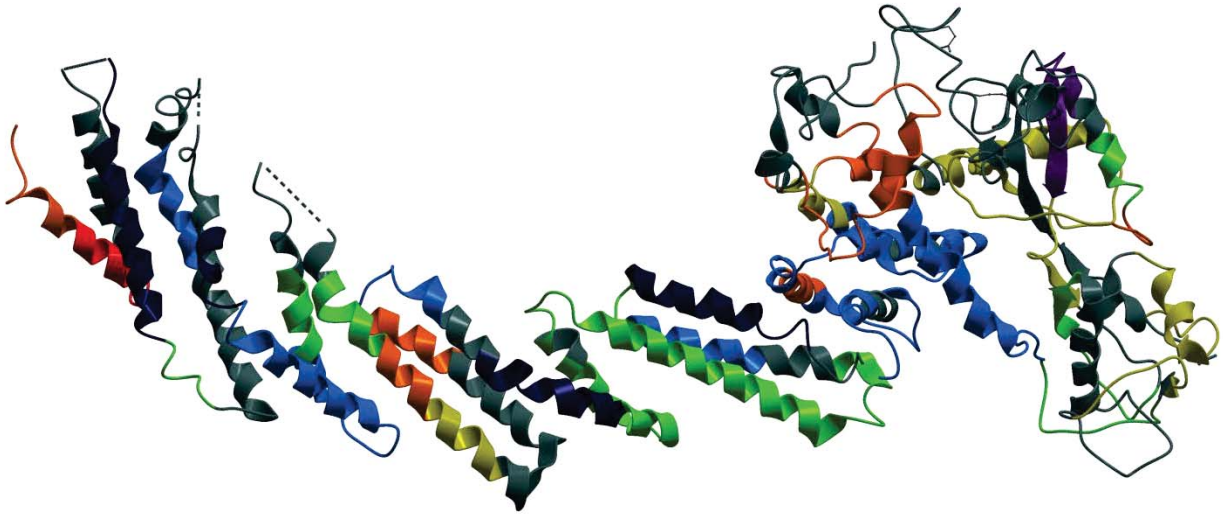

(b)

45 **Deuterium uptake data of Nedd8-CUL1-RBX1 was overlaid on the X-ray structure of CUL1-RBX1 protein (1LDK)**

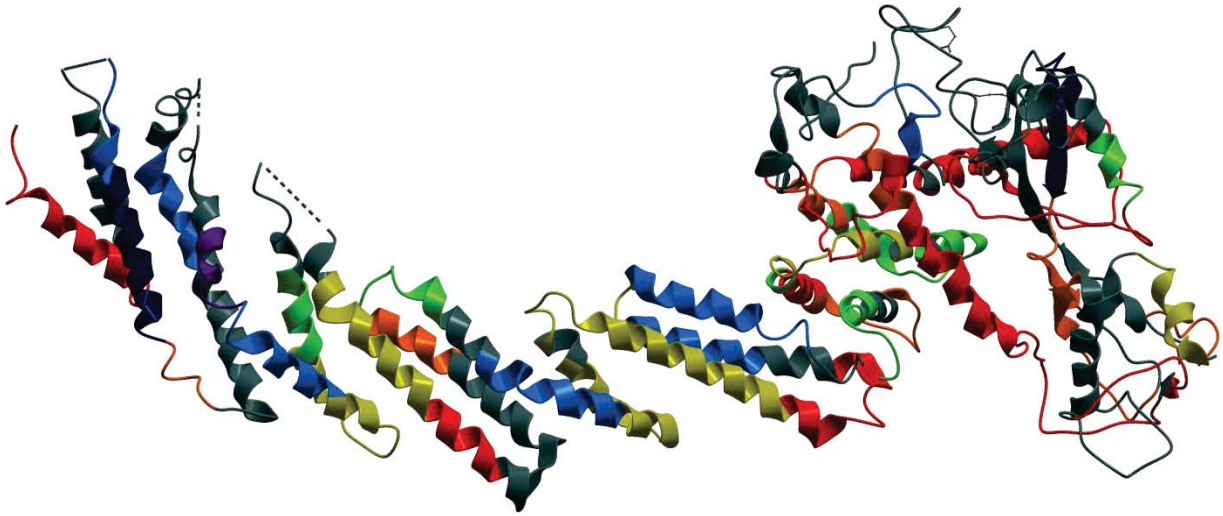

(c)

46 **Deuterium uptake data of Nedd8 Q40E-CUL1-RBX1 was overlaid on the X-ray structure of CUL1-RBX1 protein (1LDK)**

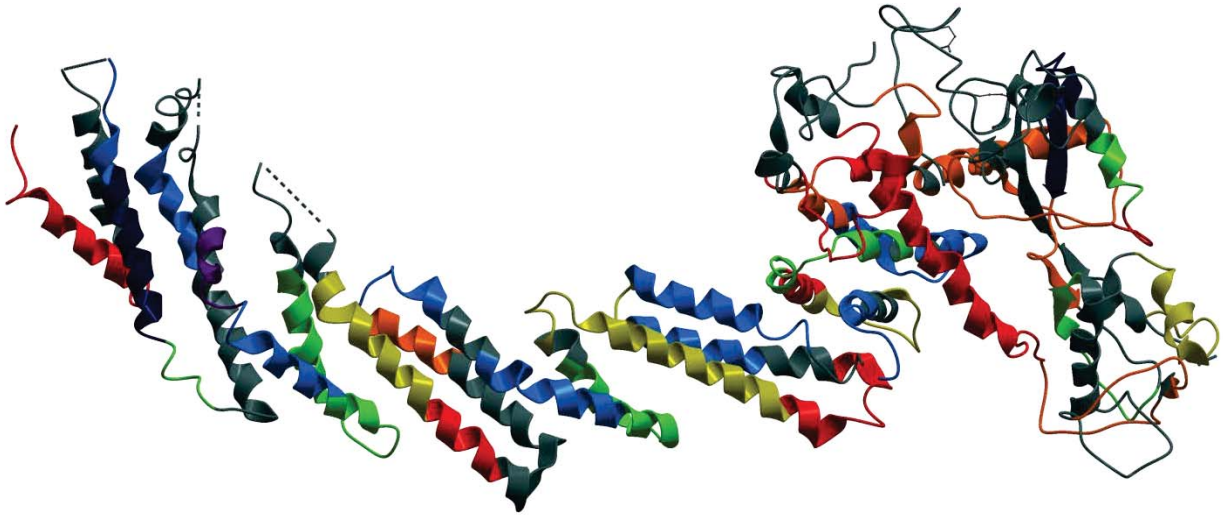

Figure S1.3 (a)

47 Heat Map of CUL1-RBX1 protein

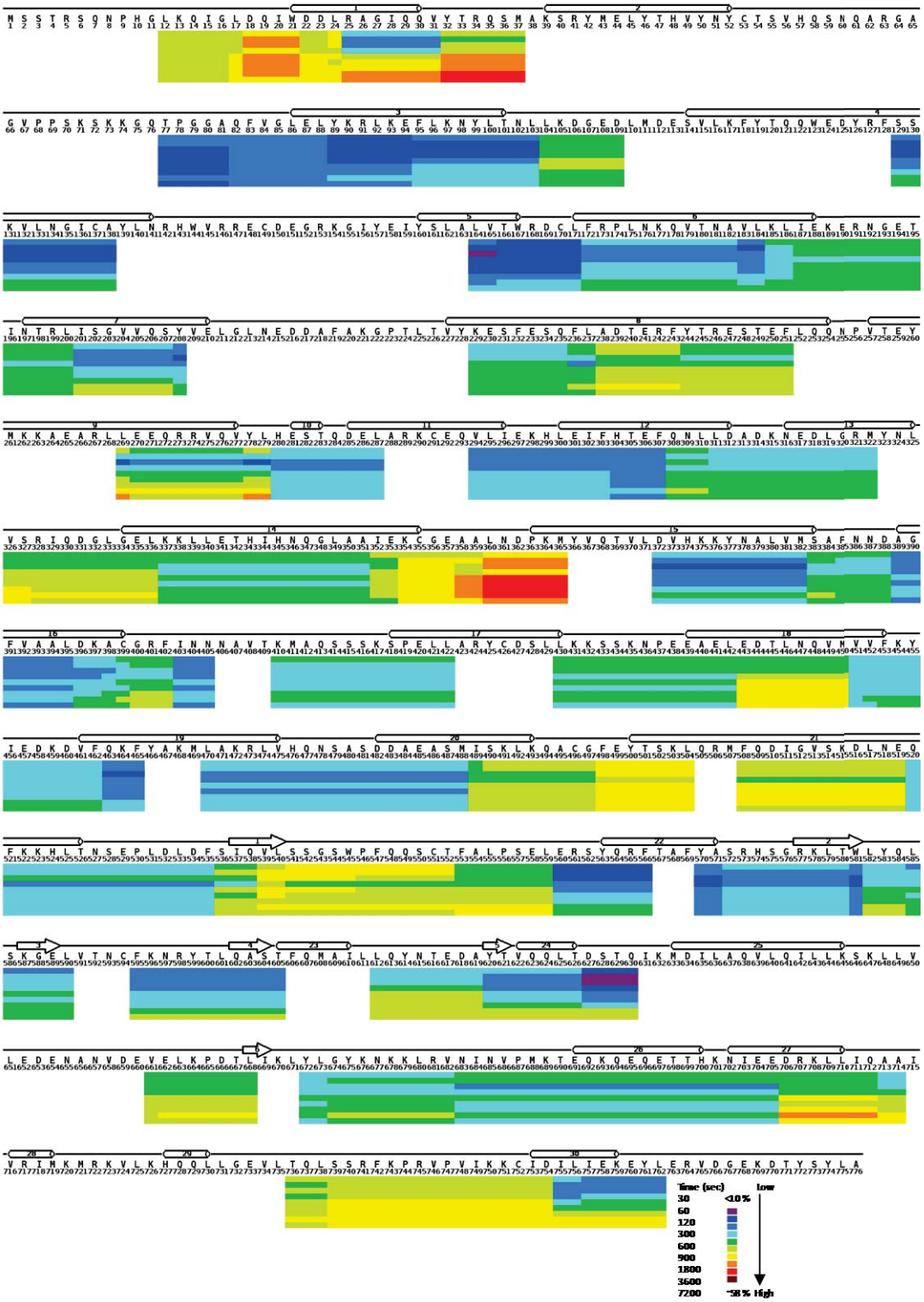

(b) 48 **Heat Map of Nedd8-CUL1-RBX1 protein**

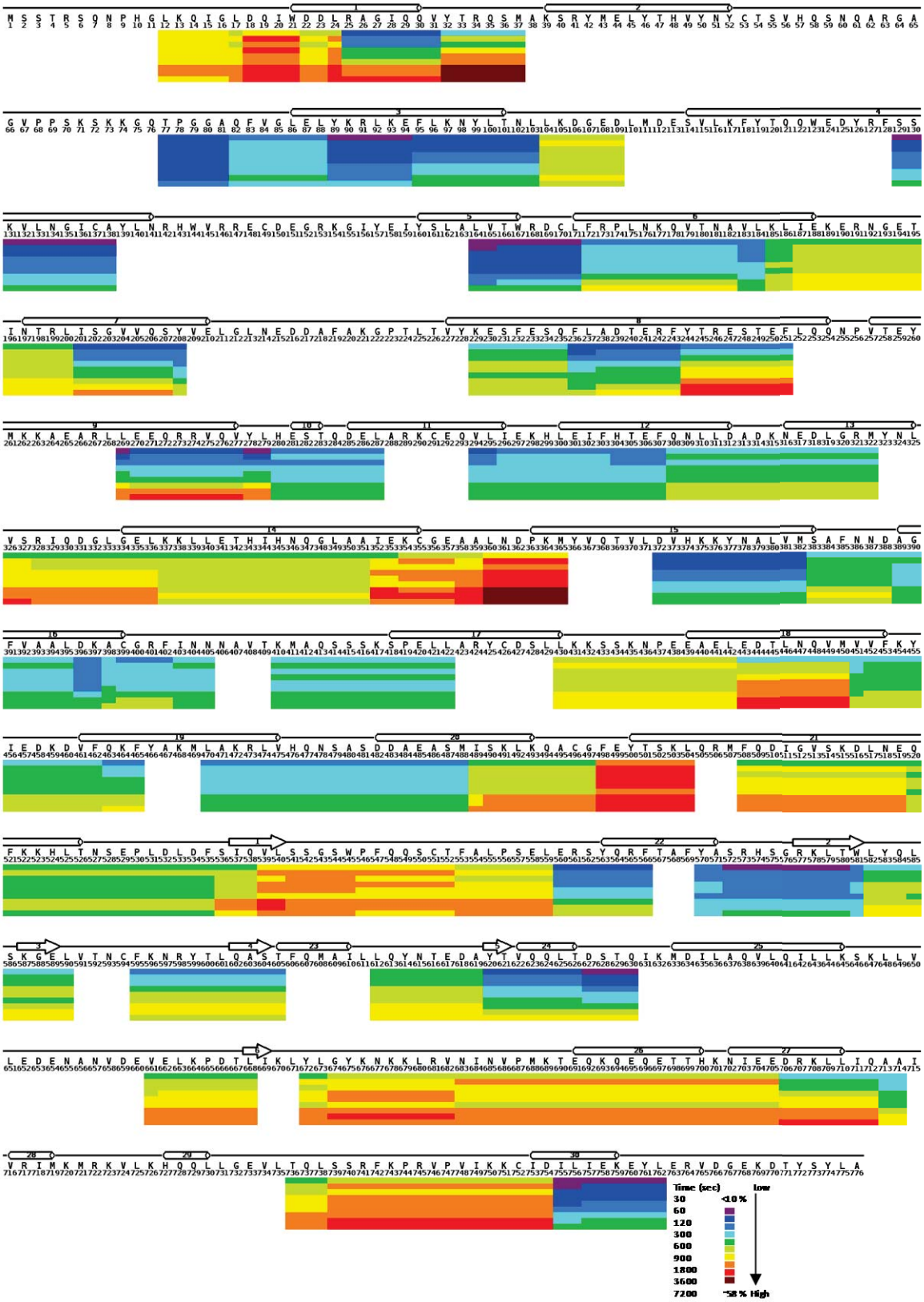

(c) 49 **Heat Map of Nedd8 Q40E-CUL1-RBX1 protein**

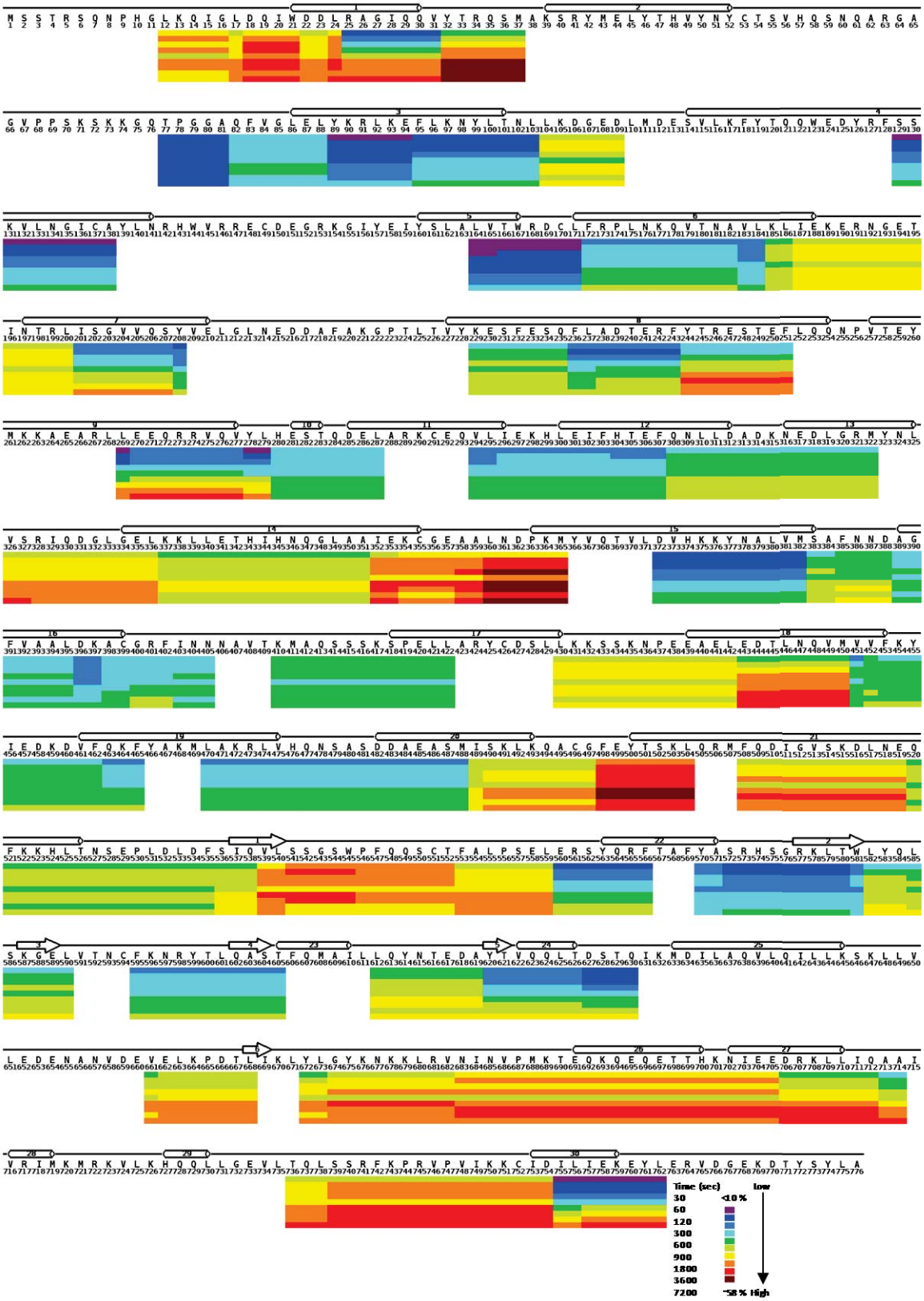

Figure S2.1

(a)

50 **HDX-MS profile of RBX1 in CUL1-RBX1**

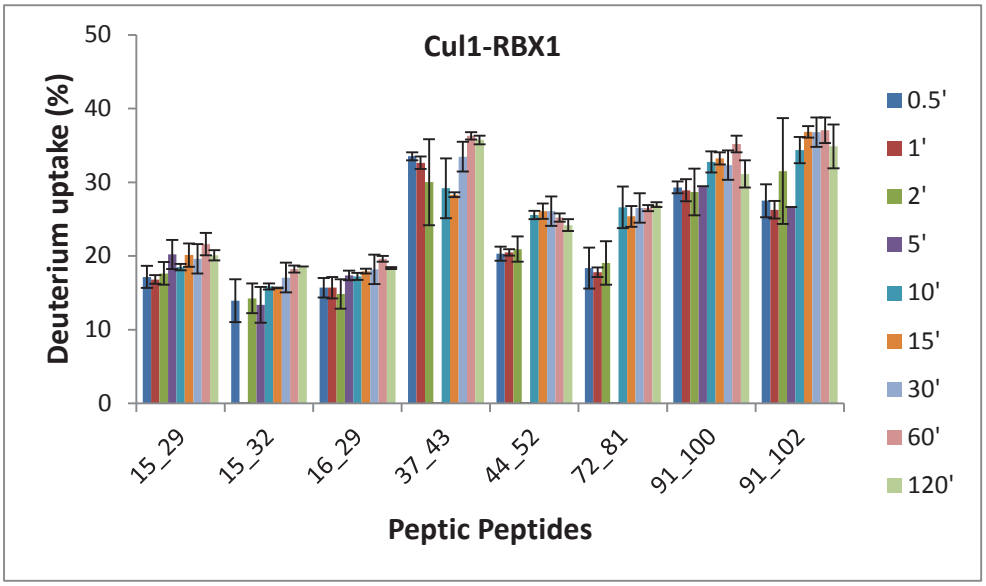

(b)

51 **HDX-MS profile of RBX1 in Nedd8-CUL1-RBX1**

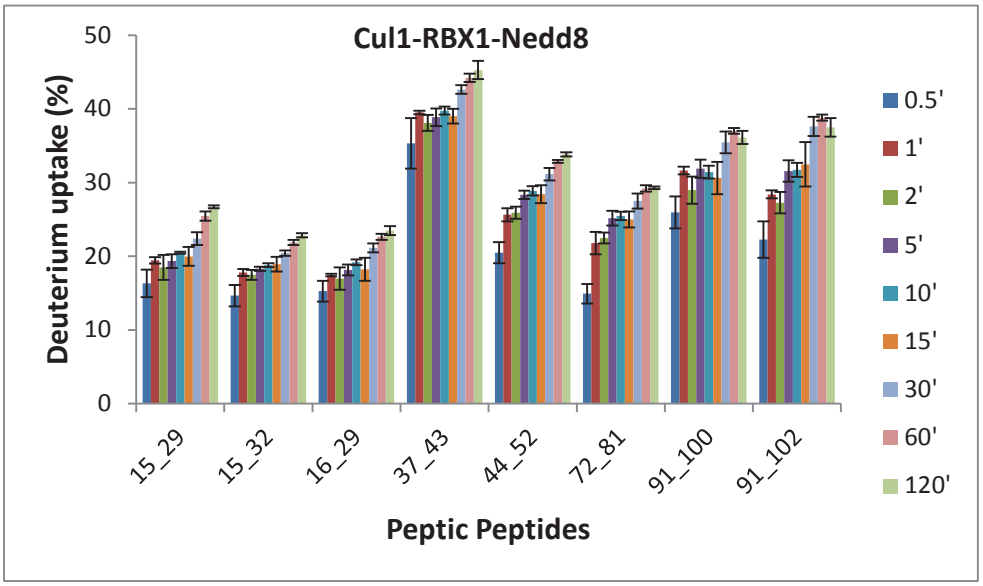

(c)

52 **HDX-MS profile of RBX1 in Nedd8 Q40E-CUL1-RBX1**

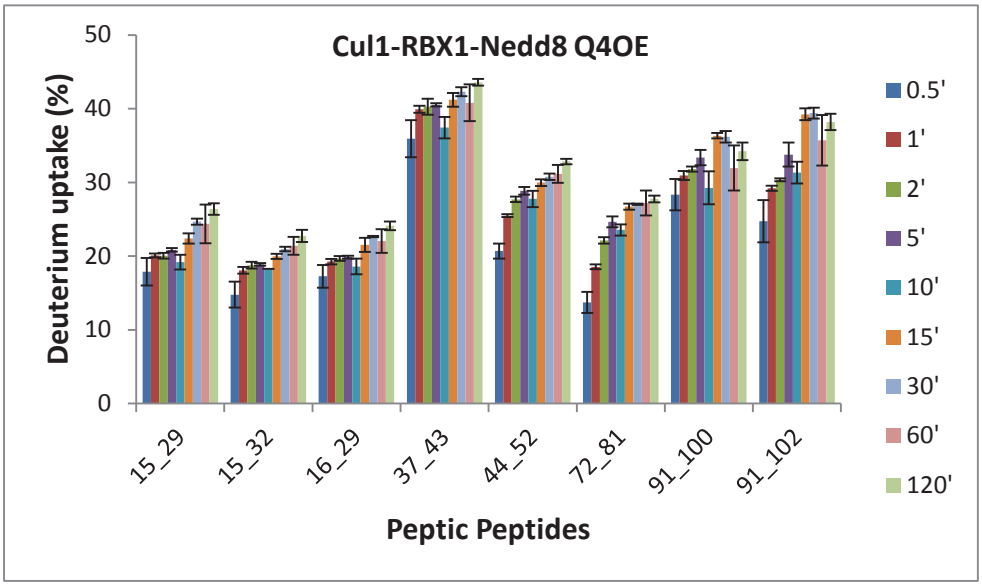

Figure S2.2

(a)

53 **RBX1 HDX-MS data of CUL1-RBX1 overlaid on Crystal structure of RBX1**

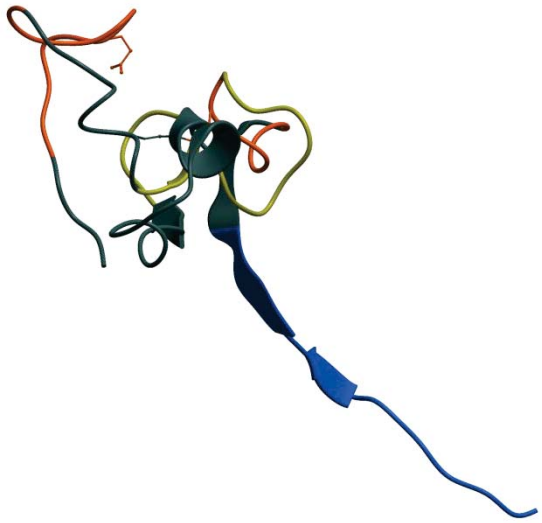

(b)

54 **RBX1 HDX-MS data of Nedd8-CUL1-RBX1 overlaid on Crystal structure of RBX1**

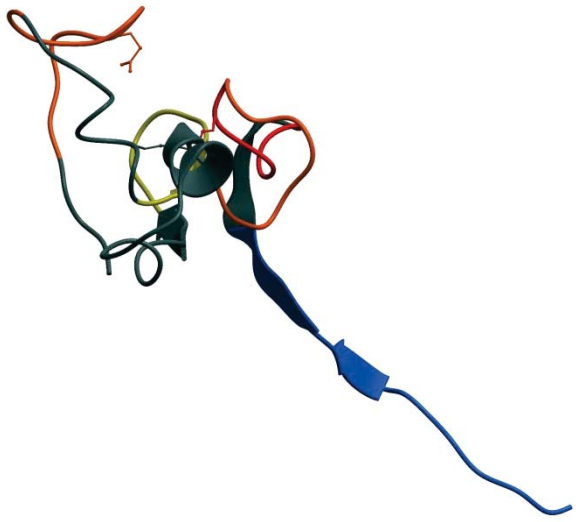

(c)

55 **RBX1 HDX-MS data of Nedd8 Q40E-CUL1-RBX1 overlaid on Crystal structure of RBX1**

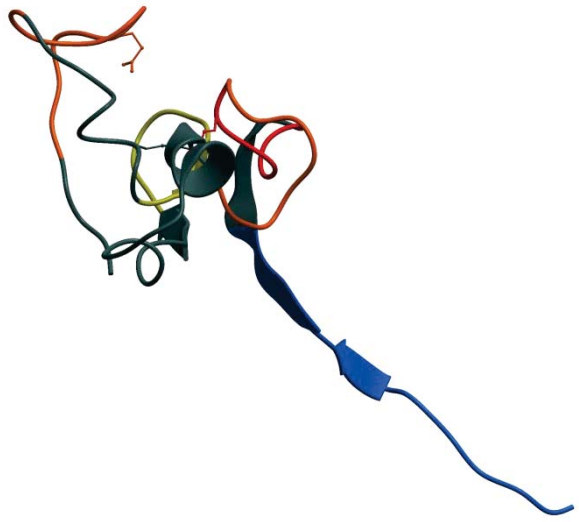

Figure S2.3

(a)

56 **Heat map of RBX1 in CUL1-RBX1**

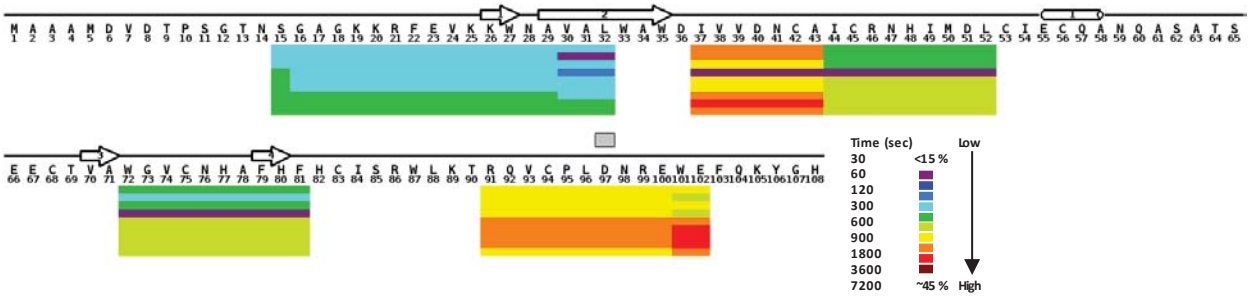

(b)

57 **Heat map of RBX1 in Nedd8-CUL1-RBX1**

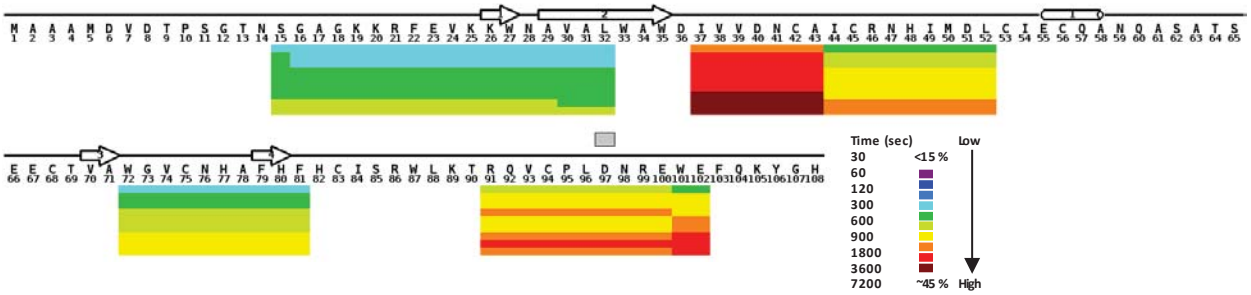

(c)

58 **Heat map of RBX1 in Nedd8 Q40E-CUL1-RBX1**

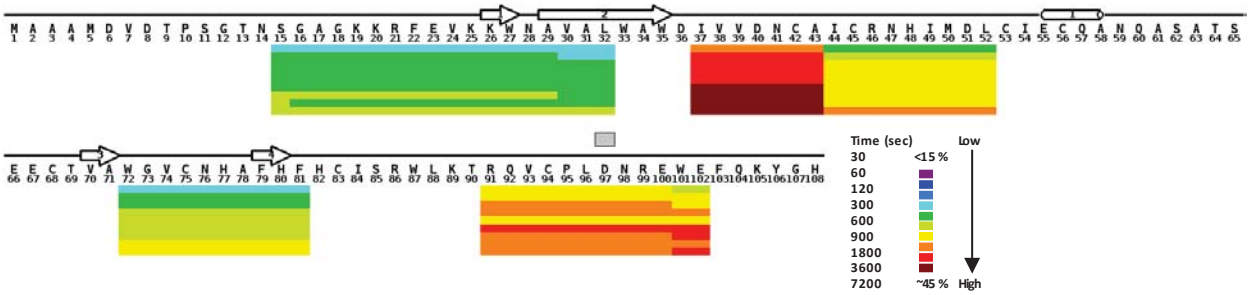

Figure S3.1

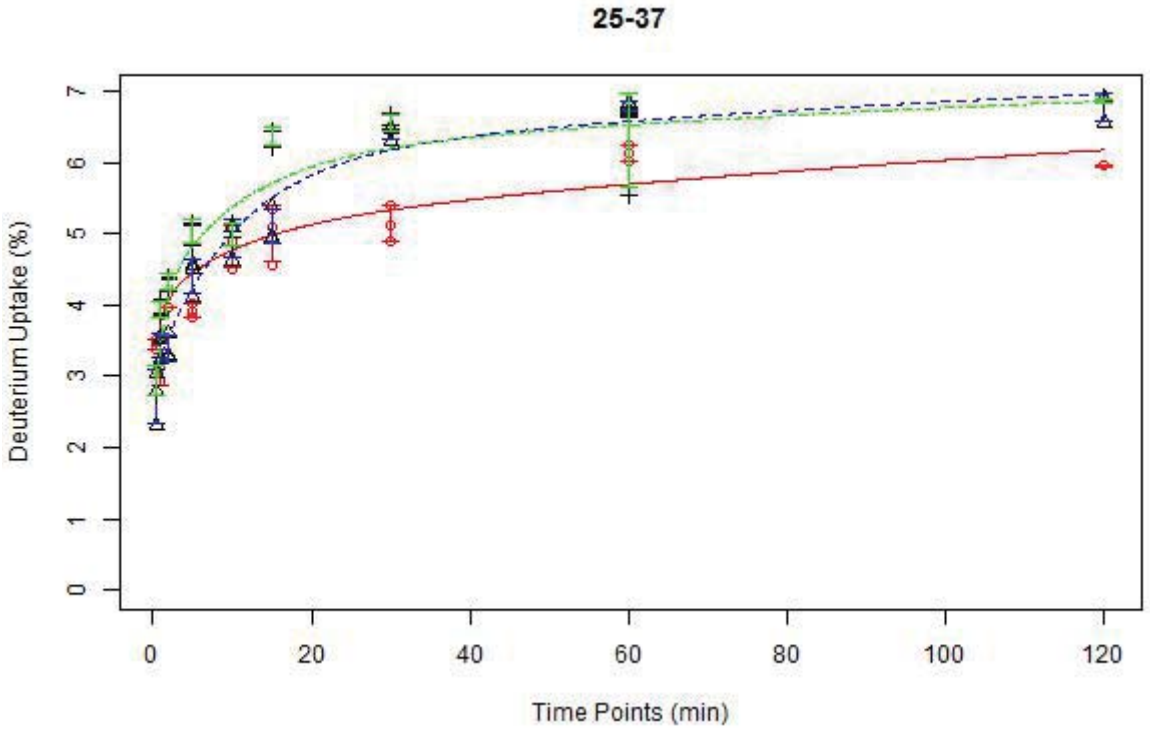
25-37
Deuterium Uptake (%)
0
1
2
3
4
5
6
7
0
20
40
60
80
100
120
Time Points (min)

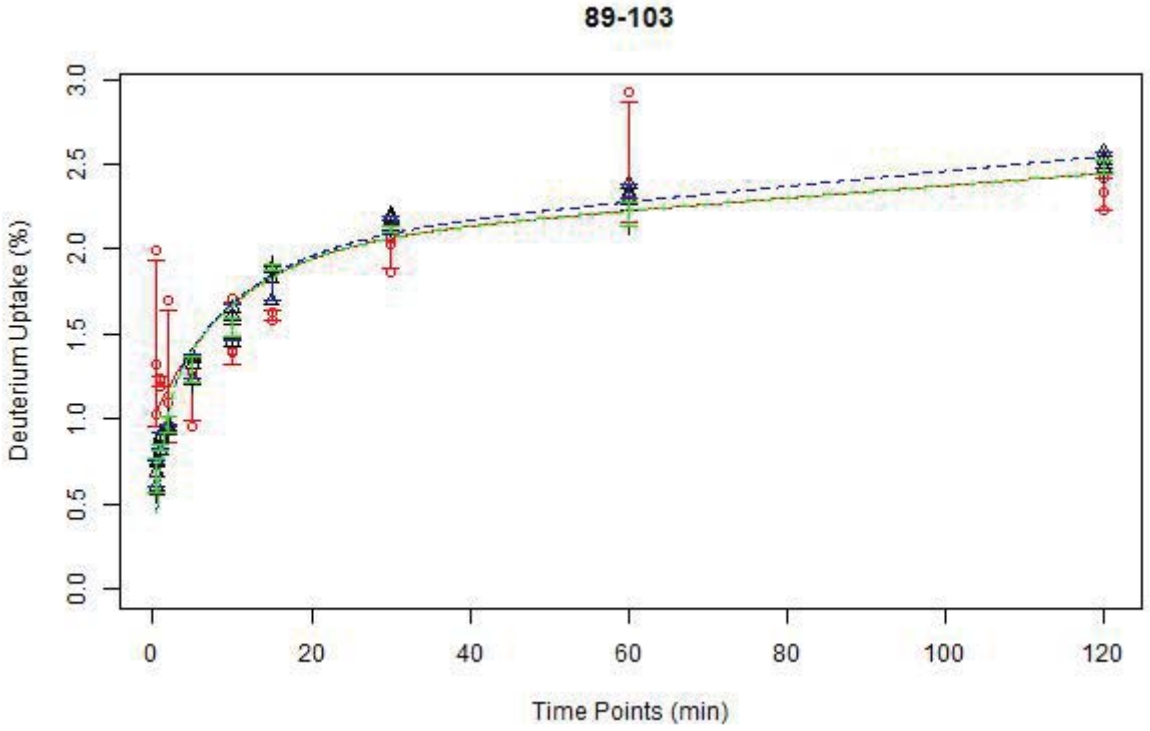
89-103
Deuterium Uptake (%)
0.0
0.5
1.0
1.5
2.0
2.5
3.0
0
20
40
60
80
100
120
Time Points (min)

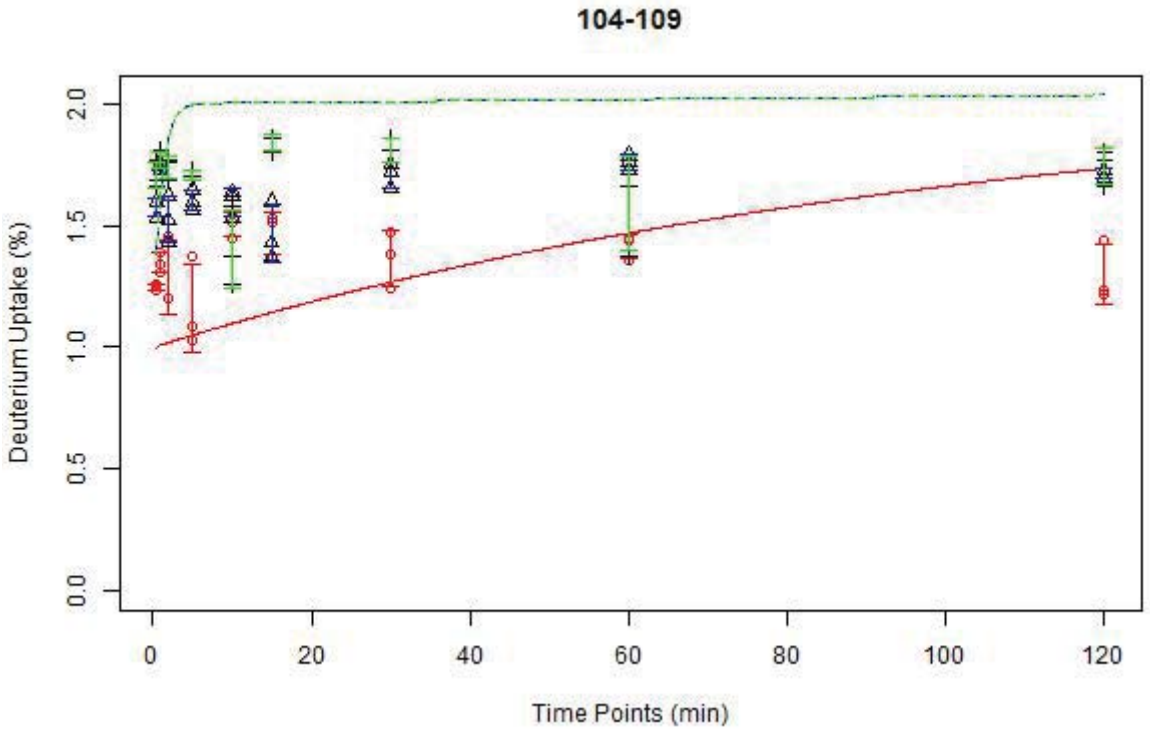
104-109
Deuterium Uptake (%)
0.0
0.5
1.0
1.5
2.0
0
20
40
60
80
100
120
Time Points (min)

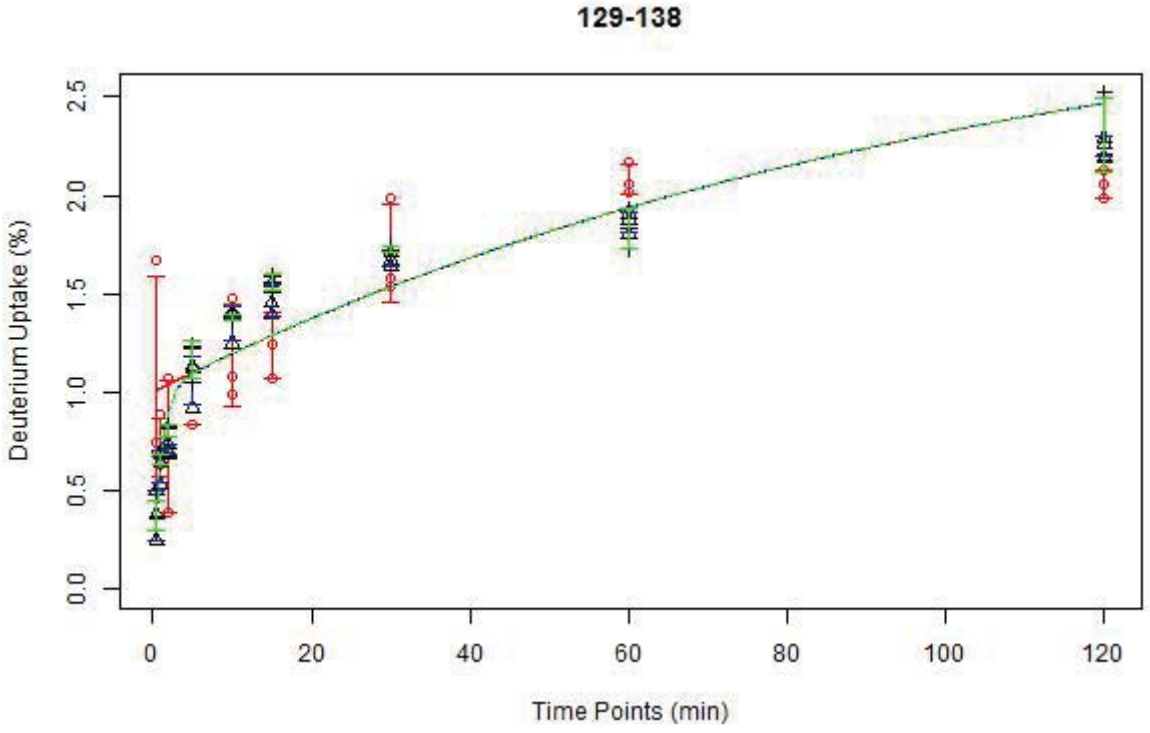
129-138
Deuterium Uptake (%)
0.0
0.5
1.0
1.5
2.0
2.5
0
20
40
60
80
100
120
Time Points (min)

Table S1

13 **p-values obtained from the Two Way Anova statistical analysis for all CUL1-RBX1 protein states**

	p.bind.bonferroni		
Peptic peptides	C1_C1N8	C1_C1N8Q	C1N8_C1N8Q
(12-24)	3.93E-11	1.96E-11	1
25-37	0.004091	4.92E-10	8.18E-05
77-86	0.000118	5.21E-09	0.081834
82-91	7.01E-21	1.80E-20	1
89-103	1	1	1
104-109	7.93E-13	1.14E-13	0.136274
129-138	1	1	1
164-171	1	1	1
172-184	0.113512	0.16101	1
185-200	4.60E-15	5.86E-16	1
201-208	0.000422	2.72E-05	1
229-237	6.61E-15	6.18E-14	1
238-243	1.90E-06	4.08E-06	1
244-251	1.28E-12	8.27E-14	1
269-279	0.211728	0.332625	1
280-287	0.000179	7.20E-07	1
294-307	2.02E-05	3.67E-08	1
308-322	0.001786	6.78E-05	1
326-351	1.41E-06	7.51E-09	1
352-365	1.92E-14	3.50E-15	0.005338
372-382	1	1	1
383-391	2.14E-07	9.62E-10	0.395739
389-405	2.67E-19	5.26E-20	1
410-422	1	0.005793	0.926728
430-442	1.64E-19	8.64E-19	1
443-450	6.87E-12	1.64E-15	0.000742
451-462	1.55E-12	8.34E-10	0.129843
453-465	7.16E-17	4.51E-11	8.34E-08
470-488	0.381799	0.175458	1
489-498	4.93E-10	1.41E-10	1
498-504	3.34E-20	5.65E-21	5.45E-05
508-535	8.47E-13	1.11E-12	1
536-552	1.92E-10	4.97E-09	1
553-559	1.21E-14	1.58E-14	1
560-566	0.00025	6.93E-09	0.053638
570-582	2.28E-21	7.13E-22	1

582-589	0.000125	3.06E-15	0.433998
595-605	3.43E-11	3.67E-08	3.66E-06
612-619	1.01E-07	1.19E-08	1
620-630	1.95E-06	2.96E-08	0.320416
661-668	4.26E-13	4.88E-14	1
672-682	9.14E-19	3.96E-18	1
683-705	1.17E-15	1.39E-19	6.29E-05
706-714	1	2.10E-11	5.50E-16
736-756	9.56E-09	4.86E-13	6.43E-05
755-762	7.51E-21	0.132367	1.07E-28

6 Chapter -Summary and Future Direction

This thesis dissertation primarily focusses on investigating the structural and conformation dynamics of large protein oligomers and protein-protein interactions using hydrogen deuterium exchange mass spectrometry. In studying the large protein complexes (>100 kDa) at the peptide level, separation of peptide spectra has been a major hurdle because of the short LC gradients used and the spectral overlap that was observed after deuteration. In our research we implemented a new dimension of separation using ion mobility spectrometry to ease the crowded spectral regions. In theory HDX-MS has no limitation in studying the large protein complexes, however until recently data analysis has been the major bottleneck in making it a reality. With recent developments in new software tool, like DynamX 2.0 and HDExaminer 1.0, data analysis was simplified. Combing all the advanced techniques and tools, we have been able to successfully study the large protein complexes at the peptide level. This research demonstrates the impact of: (i) a single point mutation on the long range allosteric communications in larger protein-protein complexes; (ii) the sensitivity towards overoxidation of peroxiredoxins studied using a conformational perspective; and (iii) covalent modification of large protein complexes by neddylation. At this point, the applied HDX-MS workflow cannot provide single amino acid resolution data for large protein complexes.

6.1 Conclusions of the conformational studies on *Salmonella typhimurium* AhpC

Peroxiredoxins are important antioxidant enzymes that reduce H_2O_2 in cells and remove alkylhydroperoxides by undergoing a catalytic cycle consisting of the following steps: (a) peroxidation;

(b) resolution; (c) recycling; (d) overoxidation (side reaction step). We conducted comprehensive HDX-MS analyses of *Salmonella typhimurium*, *St*AhpC on related single point mutants. Our research showed that HDX-MS is a suitable approach for studying the redox-dependent oligomerization and active site loop mobility of peroxiredoxins. The isotopic labeling method coupled with acidic proteolytic digestion and LC-ESI-MS analysis provided insights into the conformational dynamics of specific regions of the peroxirdoxins studied. The differential deuterium uptake of the disulfide-bound wild-type protein $Wt_{S\text{-}S}$ (locally unfolded form) *versu*s the thiol-containing reduced form Wt_{SH} (fully folded form) underscored loss of conformational mobility at the active site loop and the C-terminal end in thiolate form of the protein upon disulfide reduction. The other parts of the protein seem to gain conformational plasticity in the absence of the disulfide bond. Our HDX-MS results support the concept of structure and activity correlation in which peroxidatic cysteine sensitivity towards hyperoxidation depends on the conformational flexibility of the active site loop.

HDX-MS experiments were also conducted on two single point mutants T77V and T77I of StAhpC in their oxidized and reduced forms. These mutations are at the dimer-dimer interface of the Prxs. Our HDX-MS results have confirmed that the T77V mutant enhances the conformational stability of the interfacial region thereby promoting decamer formation. However, the T77I mutant studies revealed that this mutatation increased the conformational flexibility at the interfacial regions which was in accord with a decreased tendency to form decamers. Our HDX-MS results of the single point mutants also showed that higher motility was observed in the active site loop of the T77V mutant, whereas higher rigidity was observed for the same region in the T77I mutant. Our HDX-MS results highlight the allosteric effects of the single point mutations that are not apparent in the X-ray structures. In this context, the HDX-MS studies provided insights on the modulation of conformational properties of robust peroxiredoxins. The detection of allosteric changes caused by point mutations in large protein complexes is not easily accessible with other protein analysis techniques.

6.2 Conclusion of comparative conformational studies of robust and sensitive peroxiredoxins

Peroxiredoxins (Prxs) are ubiquitous thiol-based antioxidant proteins that regulate the intracellular peroxide levels and are present universally in most of the organisms. The catalytic cycle involves three major steps: peroxidation, resolution, recycling and overoxidation as a side step reaction. Peroxidatic active site loop should undergo a conformational rearrangement to result in resolution. Depending on their propensity towards overoxidation Prxs are labeled as sensitive or robust. Human Prx2 represent a sensitive peroxiredoxin and whereas most of the bacterial Prxs belong to the robust Prxs. In sensitive Prxs, the characteristic YF motif at the C-terminal helix and the loop containing GGLG mofit prevents the active site CP loop from undergoing a conformational rearrangement. This hinders the resolution step and drives the overoxidation of peroxidatic cysteine.

Our comparative HDX-MS studies focused on for human Prx2, the bacterial *St*AhpC, and the C46S mutant of *St*AhpC. Comparison of deuterium levels of the peptic peptides observed for C46S mutant and the wild-type StAhpC revealed noticeable differences in deuterium incorporation levels for the peptides covering the active site loop 44-50 and the partial sequence 68-89, which is involved in forming the decamer-building (dimer-to-dimer) A-interface. In the C46S mutant, we observed for peptide 44-50 lower deuterium incorporation levels compared to the corresponding peptide in the wild-type protein indicating increase exchange protection and reduced solvent accessibility in this region for the mutant protein compared to the oxidized form of the wild-type protein. Also, the peptide 68-89 showed lower deuterium incorporation levels in the C46S mutant compared to the wild-type protein in accord with the higher decamer-building ability observed for the reduced forms of the robust Prxs. The reduced deuterium incorporation levels observed for the C46S peptide, 68-89, implies that the dimer-

dimer interface region in the C46S mutant is folded and has higher protection against exchange-in in conjunction with reduced solvent accessibility compared to the wild-type Prx. Due to allosteric effects some regions, like 123-132 and 148-156, in the C46S mutant exhibited higher deuterium incorporation compared to the wild-type Prx. Taken together, our HX-MS studies emphasize a reduced solvent accessibility of the region encompassing the active site loop in the reduced-like mutant C46S and, thus, the HDX-MS data complements the X-ray structural analysis of the C46S mutant indicating that, indeed, this region is in its fully folded conformation.

The eukaryotic Prx are considered as sensitive peroxiredoxins. As part of this thesis we conducted HDX-MS studies of the human Prx2 for investigating the conformational properties of a sensitive Prx. The C-terminus region encompassing the peptide 182-194 exhibited the highest deuterium incorporation (i.e., higher flexibility and less protection) and the peptides encompassing 130-140, 156-163 exhibited the lowest deuterium incorporation levels (i.e., low flexibility and high protection) among all the peptides in human Prx2. The peptides 28-40, 74-84 exhibited medium deuterium incorporation, whereas rest of the peptides (2-15, 16-27, 42-48, 56-64, 65-73, 74-84, 85-104, 105-114, 115-130, 141-155 and 164-181) exhibited moderately higher deuterium incorporation levels in human Prx2. Online digestion integrated with the MSE approach provided sufficiently high spatial resolution to enable us to zoom into the important conserved motifs of human Prx2. The conserved YF motif in the C-terminus region exhibited very high deuterium incorporation compared to other parts of the Prx2 protein.

As the human Prx2 studied was in its reduced form, we attempted to conduct a comparative interpretation of the HDX-MS data to the C46S AhPC mutant which mimicks the reduced form of *St*AhpC featuring the conformational properties of a fully folded robust peroxiredoxin. The peptides encompassing the active site regions Cys46 and Cys165 in the C46S mutant exhibited higher deuterium incorporation whereas the peptide containing the Cys172 in the C-terminal region of the human Prx2

exhibited moderately high deuterium incorporation. The peptide encompassing the interfacial region T77 in C46S mutant exhibited low deuterium incorporation where as the one in human Prx2 exhibited medium deuterium incorporation levels. By comparing the deuterium incorporation levels to the B-factors from the respective crystal structures, it was evident that the B-factor values of human Prx2 were relatively lower compared to the B factor values observed for the wild-type ($Wt_{S\text{-}S}$) protein and the C46S mutant of *St*AhpC. Overall, the current HDX-MS results complement the B-factor values and recapitulate that the human Prx2 attains a relatively closed and solvent protected form compared to the bacterial counterparts. We may suggest for future research to focus on a comparative HDX-MS studies involving the oxidized Prx2 in order to further decipher the conformational properties that govern the propensity of peroxiredoxins to hyperoxidaton.

6.3 Conclusion on NEDD8ylation induced conformational changes in Cullin scaffold protein

Culling-RING ubiquitin ligases (CRLs) are the largest family of E3 ligases in all eukaryotes that ubiquitinate protein substrates in various cellular processes. CRLs are multisubunit E3s assembled around a cullin scaffold protein that embraces an extended structure to allow substrate receptor binding via adaptor proteins on the N-terminal domain (NTD) and binding of a RBX RING protein to the C-terminal domain (CTD). The cullin-CTD binds to E2 ubiquitin through the RBX RING subdomain which enables the ubiquitin transfer to the 50 ^{o}A far substrate connected to the substrate receptor. Covalent attachment of ubiquitin-like proteins, such as NEDD8, to a lysine in the cullin (CTD) changes the CRL confirmation and stimulates the ubiquitin transfer from the E2 to the substrate thereby enhancing ubiquitination and proteasomal degradation.

HDX-MS experiments were performed on Cullin1-Rbx1 with and without nedd8ylation, and the Nedd8Q40E-modified Cullin1-Rbx1 protein complex. The Cul1-Rbx1-Nedd8 complex is a very large complex comprised AA in Cul1 (776 AA, 89.6 kDa), AA RBX1 (108 AA, 12.2 kDa) and Nedd8 (76AA, - 9.5 kDa). The Q40E mutant of Nedd8 was used to study the effect of Nedd8 modification by a bacterial effector protein, which is known to deamidate the amino acid Q40 of the host protein Nedd8 conjugate. It is thought that Nedd8 Q40E modification leads to down regulation of the host cullin-RING E3 complex activities. When the HDX-MS results of Nedd8-modified and unmodified Cul1 proteins were compared a major increase in the deuterium uptake was observed in the Nedd8-modified protein indicating higher conformational flexibility for the Nedd8-modified Cul1 protein. Major increase in the deuterium uptake was observed in the CTD of the Nedd8-modified Cul1 whereas the Cul1-NTD exhibited fewer uptake.

Similar changes were also observed among the peptides of Nedd8Q40Emodified Cul1 protein compared to the unmodified Cul1 protein. When the HDX-MS results of Nedd8-, Nedd8 Q40E-modified Cul1 were compared the C-terminal region containing the peptide 755-762 exhibited a major increase in the deuterium uptake for the Nedd8 Q40E-modified Cul1 and very few minimal changes were observed in the rest of the protein. The identical behavior of Cul1-Rbx1 modified by Nedd8 and Q40E Nedd8 mutant suggests that Nedd8 modification does not change the structure of the complex but likely its surface properties for binding Ub-charged E2. RBX1 protein also exhibited an increase in the deuterium uptake at the 37-53 loop region upon neddylation.

Taken together, these finding suggest that nedd8ylation seems to significantly enhance the conformational flexibility in the C-terminal region of Cul1 and the loop region of RBX1. We may speculate that their gain in conformational flexibility upon need8ylation may enable a more flexible positioning of the ubiquitin E2 ligase thereby leading to stimulation of CRL activity.

6.4 Future Direction

The future of the HDX-MS technique is bright. We are confident that some of the current limitations of HDX-MS techniques can be overcome. The increased availability of UPLC and high resolution accurate mass instrumentation has enabled the application of HDX-MS to large protein complexes. Advancement in separation and mass spectrometry technologies is vast and we envision the application of HDX-MS to large protein machines in the near future. Increasing the spatial resolution of the exchange-information to the single residue levels will depend critically on adopting “top down” approaches combined with non-ergodic fragmentation processes such as electron capture dissociation (ETD) or electron transfer dissociation (ECD). Developing the data analysis tools that can handle the ETD and ECD data will be critically important to ensure full use of the HDX-MS methodology in industrial and academic laboratories.